LINEAR PREDICTION FOR SINGLE SNAPSHOT MULTIPLE TARGET DOPPLER ESTIMATION UNDER POSSIBLY MOVING RADAR CLUTTER

A THESIS SUBMITTED TO
THE GRADUATE SCHOOL OF NATURAL AND APPLIED SCIENCES
OF
MIDDLE EAST TECHNICAL UNIVERSITY

BY

BAHA BARAN ÖZTAN

IN PARTIAL FULFILLMENT OF THE REQUIREMENTS
FOR
THE DEGREE OF MASTER OF SCIENCE
IN
ELECTRICAL AND ELECTRONICS ENGINEERING

JULY 2008

Approval of the thesis:

LINEAR PREDICTION FOR SINGLE SNAPSHOT MULTIPLE TARGET DOPPLER ESTIMATION UNDER POSSIBLY MOVING RADAR CLUTTER

submitted by **BAHA BARAN ÖZTAN** in partial fulfillment of the requirements for the degree of **Master of Science in Electrical and Electronics Engineering Department, Middle East Technical University** by,

Prof. Dr. Canan Özgen _____
Dean, Graduate School of **Natural and Applied Sciences**

Prof. Dr. İsmet Erkmen _____
Head of Department, **Electrical and Electronics Engineering**

Prof. Dr. Yalçın Tanık _____
Supervisor, **Electrical and Electronics Engineering Dept., METU**

Examining Committee Members:

Prof. Dr. Mete Severcan _____
Electrical and Electronics Engineering Dept., METU

Prof. Dr. Yalçın Tanık _____
Electrical and Electronics Engineering Dept., METU

Assoc. Prof. Dr. Sencer Koç _____
Electrical and Electronics Engineering Dept., METU

Assist. Prof. Dr. Arzu Tuncay Koç _____
Electrical and Electronics Engineering Dept., METU

Dr. Mert Serkan _____
Radar SMM – REHİS, ASELSAN

Date: 30.07.2008

I hereby declare that all information in this document has been obtained and presented in accordance with academic rules and ethical conduct. I also declare that, as required by these rules and conduct, I have fully cited and referenced all materials and results that are not original to this work.

Name, Last name : Baha Baran ÖZTAN

Signature :

ABSTRACT

LINEAR PREDICTION FOR SINGLE SNAPSHOT MULTIPLE TARGET DOPPLER ESTIMATION UNDER POSSIBLY MOVING RADAR CLUTTER

Öztan, Baha Baran

M.S., Department of Electrical and Electronics Engineering

Supervisor : Prof. Dr. Yalçın Tanık

July 2008, 104 pages

We have devised a processor for pulsed Doppler radars for multi-target detection in same folded range under land and moving clutter. To this end, we have investigated the estimation of parameters, i.e., frequencies, amplitudes, and phases, of complex exponentials that model target echoes under radar clutter characterized by antenna scanning modulation with observation limited to single snapshot, i.e., one burst. The Maximum Likelihood method of estimation is presented together with the bounds on estimates, i.e., Cramér-Rao bounds. We have analyzed linear prediction, together with its efficient implementation invented by Tufts & Kumaresan, and compared its performance to other high resolution frequency estimation algorithms all modified to run under clutter. The essential part of the work is that line spectra estimation techniques model the clutter process also as a complex exponential. In addition, linear prediction combined with linear time–invariant maximum Signal to Interference Ratio (SIR) processor is analyzed. A technique to determine the model order, which is required by the frequency estimation algorithms, is presented that does not distinguish between targets and clutter. Clutter region concept is introduced to identify targets from clutter. The possibility to use these algorithms for target

classification is briefly explained after providing a literature survey on helicopter echoes.

Keywords: Linear Prediction, Radar Clutter, Single Snapshot, Frequency Estimation.

ÖZ

DOĞRUSAL ÖNGÖRÜNÜN TEK GÖZLEM VE HAREKETLİ OLABİLEN RADAR KARGAŞASI ALTINDA BİRDEN FAZLA HEDEFİN DOPPLER KESTİRİMİ İÇİN KULLANILMASI

Öztan, Baha Baran

Yüksek Lisans, Elektrik ve Elektronik Mühendisliği Bölümü

Tez Yöneticisi : Prof. Dr. Yalçın Tanık

Temmuz 2008, 104 sayfa

Darbeli Doppler radarlarında aynı katlanmış menzildeki birden çok hedefi, kara kargaşası ve hareketli kargaşa altında tespit edecek bir yapı geliştirilmiştir. Bu kapsamda radar tarafından tespit edilen hedefleri modelleyen birden fazla karmaşık üstel işaretin frekans, genlik ve fazlarının kestirimi, bir darbe grubunu kapsayan tek gözlem altında ve anten taraması kiplenimi ile şekillenen radar kargaşası varlığında incelenmiştir. En büyük olabilirlik kestirimi yöntemi belirtilmiş ve frekans ile genlik ve fazdan oluşan karmaşık çarpan için Cramér-Rao yansız kestirim değişinti alt sınırları çıkartılmıştır. Doğrusal öngörü yöntemi, Tufts & Kumaresan tarafından geliştirilen verimli uygulanışı ile birlikte, diğer yüksek çözünürlüklü frekans kestirimi yöntemleri ile karşılaştırılarak ve radar kargaşası için gerekli değişiklikler yapılarak analiz edilmiştir. Çalışmamızın önemli özelliği, kullanılan yüksek çözünürlüklü çizgisel spektrum kestirim yöntemlerinin radar kargaşasını da bir karmaşık üstel işlev olarak modellemesidir. Doğrusal öngörü yönteminden önce uygulanabilecek sinyalin kargaşa ve gürültüden oluşan toplam enterferansa olan güç oranını (SIR) en yüksek değere çıkartan doğrusal zamanda değişmez filtrenin başarımı ortaya konmuştur. Algoritmalara girdi olarak verilen model derecesini

bulmak için hedef ve kargaşa ayrımı yapmayan bir teknik geliştirilmiştir. Kargaşa bölgesi kavramı, hedefleri kargaşadan ayırmak için oluşturulmuştur. İncelenen algoritmaların hedef sınıflandırma probleminde kullanımı, helikopter ekosu ile ilgili literatür incelemesi verildikten sonra kısaca aktarılmıştır.

Anahtar Kelimeler: Doğrusal Öngörü, Radar Kargaşası, Tek Gözlem, Frekans Kestirimi.

To My Parents

ACKNOWLEDGMENTS

The author wishes to express his deepest gratitude to his supervisor Prof. Dr. Yalçın Tanık for his guidance, advice, criticism, encouragement, and insight throughout the research.

The author would like to thank the members of the Radar Signal Processing Research Team at METU supported by ASELSAN Inc. for their contribution in establishing the author's background in the area. The technical discussions with Prof. Dr. Yalçın Tanık, Prof. Dr. Mete Severcan, Prof. Dr. Fatih Canatan, Assoc. Prof. Dr. Sencer Koç, Assist. Prof. Dr. Ali Özgür Yılmaz, Assist. Prof. Dr. Çağatay Candan, and Dr. Ülkü Çilek Doyuran are gratefully acknowledged. The author appreciates the opportunity presented by ASELSAN Inc. for him to become a member of the aforementioned research team. For her suggestions and comments, Dr. Ülkü Çilek Doyuran is particularly appreciated.

The author would also like to thank for the scholarship received from the Scientific and Technological Research Council of Turkey (TÜBİTAK) during the course of master's studies.

Lastly, the author believes that the support of his parents and the friendship of his colleague Gökhan Muzaffer Güvensen have to be honored.

TABLE OF CONTENTS

LIST OF TABLES

TABLES

LIST OF FIGURES

FIGURES

CHAPTER 1

INTRODUCTION

Radar research mainly attracts researchers from the electromagnetics and signal processing areas. Algorithm development for achieving certain tasks is one of the main roles of the signal processing and communications oriented researchers. Determination of targets, their number, radial velocity and if possible, their types under strong radar clutter, received echoes from the natural environment land, sea, and weather, have been the major concern of radar designers. Conventional methods like MAXimum Signal to Interference Ratio (MAXSIR) and Moving Target Indicator (MTI) processors, which are in fact clutter suppression filters followed by Discrete Fourier Transformation (DFT), are developed with the aim of clutter elimination, but they suffer from limited resolution capability when used on the radar echo containing multiple targets in the same folded range. This is detailed in Chapter 3 where one can find the literature survey on the conventional radar processors.

In this work, we will study the applicability of Linear Prediction and high resolution frequency estimation methods to the specified problem for land based radars. The aforementioned methods were originally developed to run under Additive White Gaussian Noise (AWGN). The main difference between the usual use of these algorithms and their use in radar problem is the presence of clutter in the radar echo in contrast to operation under AWGN. The clutter elimination is curial for the success of radars and whether these algorithms can also model clutter and how to supply these algorithms the total number of targets and clutter components are the questions to be answered. Consequently, the high resolution frequency estimation algorithms need certain modifications to be used for the multi-target Doppler tone detection under radar clutter. Although separate works investigating the use of some of the high resolution algorithms for different kinds of radars can be found in the

literature, they deserve a unified treatment, possibly including modifications, with all versions of the selected frequency estimation algorithms concerned. Yet there remains the task of distinguishing targets from clutter since the algorithms to be used will treat the clutter and the targets in the same fashion not knowing their origin. This thesis is conducted to find feasible answers to the aforementioned problems.

In this thesis work, we have thoroughly analyzed the use of Linear Prediction, together with its efficient implementation invented by Tufts & Kumaresan [1], and some other high resolution frequency estimation methods, namely, various versions of MUltiple SIgnal Classification (MUSIC) and Estimation of Signal Parameters via Rotational Invariance Techniques (ESPRIT) in radar processing, where the data is corrupted with possibly multiple sources of clutter.

The core of the work is that line spectra estimation techniques can be used to model the clutter as a sum of complex exponential terms, just as they model the targets.

We will be analyzing the estimation of parameters, i.e., frequencies, amplitudes, and phases, of complex exponentials that model target echoes under radar land and possibly moving clutter characterized by the antenna scanning modulation effect. The observation will be limited to a single snapshot, i.e., one burst. Optimal method of estimation, which is the Maximum Likelihood technique, will be presented in its various forms together with the bounds on estimates, i.e., Cramér-Rao bounds. These bounds will serve as the ultimate performances of the algorithms we will test.

A technique to determine the model order required by all of the high resolution frequency estimation methods will be presented that does not distinguish between the targets and the clutter. The proposed clutter region concept is then used to identify the targets from the clutter.

In addition, linear predictor combined with Linear Time–Invariant (LTI) maximum Signal to Interference Ratio (*SIR*) filter is investigated.

Lastly, a literature survey on helicopter echoes and detection is provided to access the possibility to use Linear Prediction (LP) for target classification.

We have published our preliminary works in [2]. The literature survey on various parts of the work in relation to the radar problem will be presented after the explanation of the corresponding parts.

We present the signal model in Chapter 2; conventional radar processors will be presented followed by the optimum nonrandom parameter estimation technique of Maximum Likelihood and derived Cramér-Rao bounds in Chapter 3. Chapter 4 focuses on linear prediction and Tufts-Kumaresan algorithm together with their use in radars. Chapter 5 deals with the modification of selected line spectra estimation algorithms to be used in radars and a different implementation of Maximum Likelihood technique that needs to be preceded by a high resolution frequency estimation algorithm. Determination of amplitudes and phases of targets will be discussed in Chapter 6, where a brief comparison of the algorithms is also presented. The clutter region concept first introduced in Chapter 4 will be further elaborated together with the model order determination procedure in Chapter 7. We will develop the LTI MAXSIR filter that can precede a high resolution spectra estimation algorithm under scenarios containing land clutter in Chapter 8. In Chapter 9, we present the performances of the algorithms through Monte-Carlo simulations. In Chapter 10, the concepts developed are extended to moving clutter problem, where the only difference assumed is the center frequency shift of the clutter. Target classification based on LP and other high resolution frequency estimation algorithms is also included in this chapter.

1.1. Nomenclature

In this section notations and some of the conventions used throughout the thesis will be given.

$\mathbf{A}$ denotes a matrix, $\mathbf{a}$ denotes a vector, $\mathbf{A}_{:,j}$ denotes the j^{th} column of matrix $\mathbf{A}$, $\mathbf{A}_{k,j}$ denotes the element at the k^{th} row and j^{th} column of matrix $\mathbf{A}$ and $\mathbf{a}_j$ denotes the j^{th} element of vector $\mathbf{a}$. $E\{\bullet\}$ is the expectation operator. Some of the upper-right corner signs and their meanings are as follows:

*: conjugation,

$'$: derivative,

^{T} : transpose,

^{H} : hermitian, and

$^{\#}$: pseudoinverse operator.

“Signal” can both mean the complete signal model explained in the following chapter, or, the part modeling the targets, which will be clear from the context.

Throughout this thesis work it is assumed that eigenvalues of all matrices are ordered in decreasing order.

CHAPTER 2

SIGNAL MODEL

In this chapter the model of the radar echo that will be used in target detection and high resolution velocity estimation will be explained in detail.

Let $x_c(t)$ be the complex valued continuous time base-band signal received from the targets and the environment. $\mathbf{x}$ consists of uniformly spaced samples of $x_c(t)$ at a sampling rate equal to the pulse repetition interval (PRI). They are called slow time samples in radar literature [3]. t_o denotes, in mod PRI, the time between the pulse is transmitted, reflected from a certain range of interest, and received by the radar, i.e., round trip delay time in mod PRI. N is the number of radar pulses, whose echoes contain the same number of targets that are in the same folded range when considered in mod$(cPRI/2)$. Here, c denotes the speed of light. Then, the observation vector $\mathbf{x}$ can be expressed as:

$$\begin{aligned} x_c(t_o + mPRI) &= x_m, \quad m = 0,\ldots,N-1 \\ \mathbf{x} &= \begin{bmatrix} x_0 & \cdots & x_{N-1} \end{bmatrix}^T \end{aligned} \quad . \tag{2.1}$$

One can observe that total observation time $\mathbf{x}$ spans is

$$T_{obs} = N \times PRI \, . \tag{2.2}$$

The resolution of a pulsed Doppler radar is given by [3]

$$\Delta R = \frac{c}{2\beta} \tag{2.3}$$

where β is the bandwidth of the radar waveform. Samples obtained from radar measurements can be grouped in a matrix [3]. Each row of this matrix consists of the vector $\mathbf{x}^T$ corresponding to a certain t_o and consecutive rows have t_o values differing by $1/\beta$. The elements of each row are called slow time samples and they

are separated by PRI. The samples along a column are named as fast time samples, which are the samples of the echo of a single radar pulse. We will be focusing on the processing that needs to be done for each t_o separately and thus focus on a single row of the explained matrix.

Doppler shift or Doppler frequency is the frequency deviation in the received echo signal caused by the radial velocity of the observed target and is given by [3], [4]

$$F_D = \frac{2v_{radial}}{\lambda_{RadarTX}} \tag{2.4}$$

where v_{radial} is the radial velocity difference between the radar and the target (positive for approaching targets, negative for receding ones), and $\lambda_{RadarTX}$ is the transmitted wavelength. One can unambiguously observe a Doppler frequency interval of $1/PRI$ [3], which is called the pulse repetition frequency (PRF). This means that one can observe F_D in mod PRF.

When M target echoes are present in the data vector $\mathbf{x}$, it has the following explicit form

$$\mathbf{x} = \sum_{i=1}^{M} a_i \mathbf{V}_{:,i} + \mathbf{n} \tag{2.5}$$

where [3]

$$\mathbf{V}_{:,i} = \begin{bmatrix} 1 & e^{j\omega_i} & \cdots & e^{j(N-1)\omega_i} \end{bmatrix}^T \tag{2.6}$$

and

$$\mathbf{n} = \begin{bmatrix} n_0 & \cdots & n_{N-1} \end{bmatrix}^T \tag{2.7}$$

where $\mathbf{n}$ models the effects of noise and various forms of clutter. a_i is the complex coefficient, or equivalently complex multiplier, that contains the magnitude and phase of the i^{th} target and ω_i can be expressed as

$$\omega_i = 2\pi f_i \tag{2.8}$$

where

$$f_i = \frac{2PRIv_{radial}}{\lambda_{RadarTX}} \tag{2.9}$$

Note that, in equation (2.9), v_{radial} is given in $\mathrm{mod}\left(\lambda_{RadarTX}/2PRI\right)$. Our aim is to decide on M and to estimate a_i and f_i for each target.

a_i has a random phase which is uniformly distributed in $[0,2\pi)$. $|a_i|$ is another random variable with a proper distribution. Note that, with this notation we have implicitly assumed that a_i attains the same value from pulse-to-pulse and can change from scan-to-scan. This corresponds to Swerling models of 1 or 3 depending on the distribution of $|a_i|^2$ one uses to model target echoes [3].

In our work, the phases of the targets are modeled by taking them as independent identically distributed random variables with $\angle a_i$, phase of a_i, being a uniformly distributed random variable in $[0,2\pi)$. $|a_i|$ is considered as an unknown parameter (nonrandom, i.e., its probability distribution is not known). The necessary derivations will include the cases of $\angle a_i$ being nonrandom and being random although the latter is used in the simulations to obtain numerical results.

One can obtain the results for various values of $|a_i|, i=1,\ldots,M$ to obtain the conditional probability density function of a desired quantity z, which can be a frequency or complex multiplier estimate, as $p\left(z\middle||a_1|\cdots|a_M|\right)$ and the generalization to the random magnitude case is trivial with the integral

$$p(z)=\int p\left(z\middle||a_1|\cdots|a_M|\right)p\left(|a_1|\cdots|a_M|\right)\mathrm{d}|a_1|\cdots\mathrm{d}|a_M| \tag{2.10}$$

where $p\left(|a_1|\cdots|a_M|\right)$ is the probability density function one decides to use for the magnitudes of the targets and $p(z)$ is the probability density function of the desired quantity z under this condition.

In summary, throughout this work, the assumed probability density function of a_i in polar coordinates is

$$p_{a_i}(r)=\frac{1}{2\pi|a_i|}\delta\left(r-|a_i|\right). \tag{2.11}$$

The normalized frequency of a target f_i is also taken as a nonrandom parameter.

Noise and clutter together can be treated as a colored noise and **n** is the corresponding vector modeling complex Gaussian white noise with identically distributed real and imaginary parts and the clutter components. Clutter components can be of two types: land clutter and moving (weather etc.) clutter. The composite clutter is assumed to be of complex circularly symmetric Gaussian distribution. This makes sense since radar echoes from individual resolution volumes are the superposition of scattered echoes by a large number of particles, forming a Gaussian random process [5]. The governing equations for **n** are

$$E\{\mathbf{n}\} = \mathbf{0} \tag{2.12}$$

$$\mathbf{R}^n = \sigma_{WN}^2 \left(\mathbf{I}_{NxN} + \frac{\sigma_{LC}^2}{\sigma_{WN}^2} \mathbf{R}^C \right) \tag{2.13}$$

where

$$\mathbf{R}_{k,l}^n = E\left\{ \mathbf{n}_k \mathbf{n}_l^* \right\}. \tag{2.14}$$

σ_{WN}^2 and σ_{LC}^2 are the powers of the white noise and land clutter components, respectively. $\mathbf{R}^C$ is the total clutter autocorrelation matrix and includes land clutter and optionally moving clutter components (normalized matrices $\mathbf{R}^{LC}$ and $\mathbf{R}^{MC}$, respectively).

$$\mathbf{R}^C = \mathbf{R}^{LC} + \frac{\sigma_{MC}^2}{\sigma_{LC}^2} \mathbf{R}^{MC} \tag{2.15}$$

where σ_{MC}^2 is the power of the moving clutter. Elements of $\mathbf{R}^{LC}$ are obtained considering antenna scanning modulation effect [6], [4]. Due to angular motion of the antenna in a mechanically scanned system, the radar does not receive echoes from the identical patches of scatterers from consecutive pulses. This causes degradation of the pulse-to-pulse clutter correlation. This effect can also be explained in the following way. Due to finite time on clutter scatterers, the clutter spectrum widens, i.e., loss of correlation is observed. The longer the time on clutter patch, the less will be the spread in the clutter spectrum.

If the two-way antenna power pattern is approximated as a Gaussian pattern, one obtains a Gaussian shaped clutter power spectrum [6] with the autocorrelation

matrix entries found using the fact that Fourier Transformation of a Gaussian function is also Gaussian and given by

$$\mathbf{R}_{k,l}^{LC} = \exp\left[-\frac{\sigma_w^2 \left((k-l)\, PRI \right)^2}{2} \right] \tag{2.16}$$

where σ_w is the standard deviation of the clutter power spectrum and given by [6]

$$\sigma_w^2 = \left[\frac{\left(\theta_{2WHP}^{\circ} \right)^2}{72\alpha^2 \ln 2} \right]^{-1} . \tag{2.17}$$

In equation (2.17), θ_{2WHP}° is the two way half power beamwidth of the radar antenna and α is the rotation rate of the radar antenna in units $revolutions/minute$ and rpm will be used to denote the value of α.

$\mathbf{R}^{MC}$ is obtained through the equations

$$\mathbf{R}^{MC} = \mathbf{D}^{MC} \mathbf{R}^{LC} \left(\mathbf{D}^{MC} \right)^H \tag{2.18}$$

$$\mathbf{D}_{k,k}^{MC} = e^{j2\pi f_c (k-1)}, \quad k = 1, \ldots, N \tag{2.19}$$

where $\mathbf{D}^{MC}$ is a diagonal matrix and f_c is the moving clutter center frequency.

The equations (2.15), (2.18), and (2.19) are valid up to one moving clutter source. For cases containing more than one moving clutter source the extension is trivial. Until Chapter 10, it will be assumed that the only source of clutter is land clutter.

As a final remark on the received signal model, note that clutter, noise, and target components of the received signal are all taken as independent.

We will choose our SNR definition in a way such that it reflects the effect of N and thus in comparison with previous works, one may need to be careful about different conventions. SNR for each target is defined as the SNR when the other target is not present and is given by

$$SNR_i = 10 \log \left(\frac{|a_i|^2 N}{\sigma_{WN}^2} \right). \tag{2.20}$$

CNR will refer to land clutter to white noise power ratio, i.e., σ_{LC}^2 to σ_{WN}^2, and *MCCR* to moving clutter to land clutter power ratio, i.e., σ_{MC}^2 to σ_{LC}^2.

In some equations although the autocorrelation matrix may appear as defined in this chapter, it may refer to a submatrix of the one defined in this chapter. It will have an appropriate size, which will become clear from the equations.

For figures presented, please consult section 9.1. for further details on used parameters.

CHAPTER 3

RADAR DETECTORS, DOPPLER PROCESSORS AND OPTIMAL APPROACH

3.1. Conventional Radar Processors

Optimum Doppler processor in terms of Signal to Clutter plus Noise Ratio (*SCNR*) or equivalently *SIR* maximization is the Hsiao filter, or MAXSIR filter, when the Doppler frequency of the target is known a-priori [7]-[9]. The explicit form of the filter is given by

$$\mathbf{w} = \left(\mathbf{R}^n\right)^{-1} \mathbf{V}_{:,i} \tag{3.1}$$

where $\mathbf{R}^n$ is defined in equation (2.14) and $\mathbf{V}$ in equation (2.6). This formula uses both clutter statistics, thus a proper filter shape is designed accordingly, and at the same time performs coherent integration of the target signal. In practice, a bank of filters is necessary, together with a technique to estimate $\mathbf{R}^n$. This bank of filters can be implemented with windowed DFT operation.

In Figure 1 we have plotted an instance of the spectrum of the observed data, following the MAXSIR processing. The scenario used consists of two targets having frequencies $\begin{bmatrix} f_1 & f_2 \end{bmatrix} = \begin{bmatrix} 0.2813 & 0.3563 \end{bmatrix}$ with $SNR = 24dB$ and $CNR = 45dB$. The instance in Figure 1 clearly shows that resolution capability of MAXSIR operation for two targets is limited although it is successful at clutter suppression. Zero-padding is used in obtaining the figure to approximate Discrete Time Fourier Transform (DTFT). Although quadratic interpolation for fine frequency estimation [3] can be employed, this is suitable for single target cases.

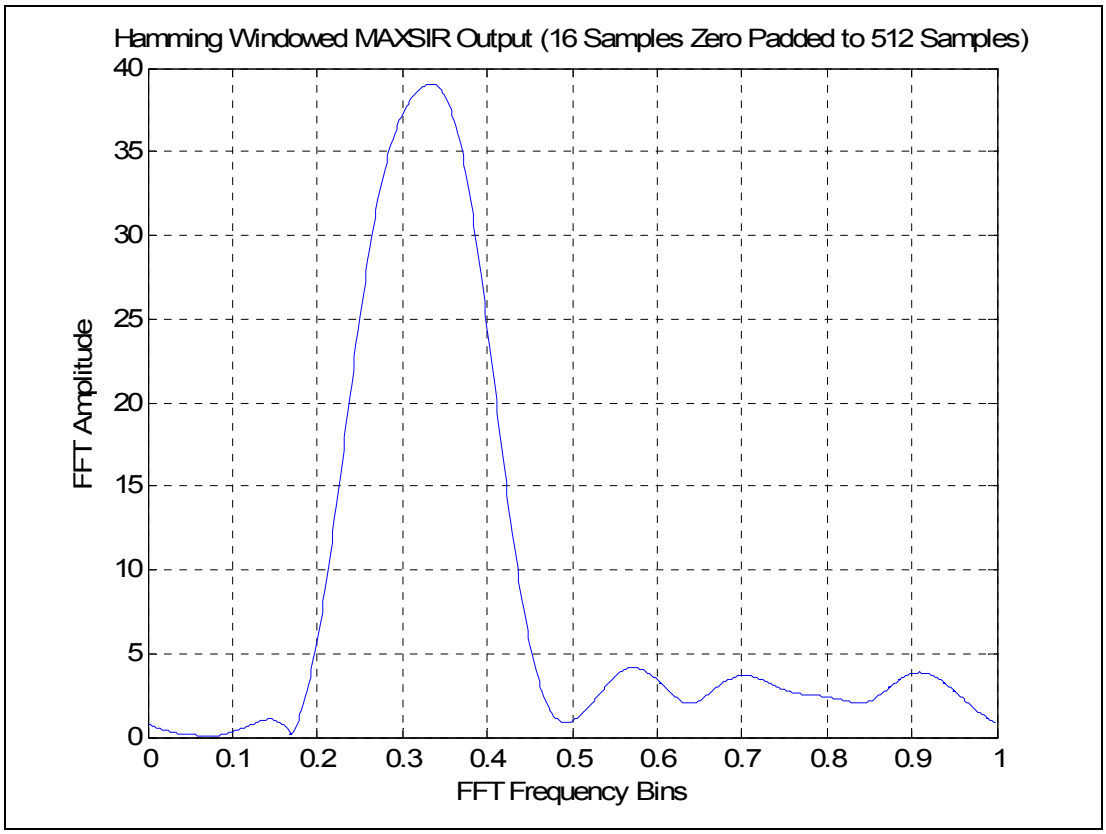

Figure 1 Resolution capability of windowed MAXSIR operation

A sub-optimal alternative is to use Moving Target Indicator (MTI) followed by windowed DFT [3], [7], [9]. MTI pulse cancellers are high pass filters whose coefficients are obtained from the binomial series. Through weighted subtraction and addition of the echoes from consecutive samples, one aims to achieve clutter suppression since land clutter has a Doppler around zero and multiple pulse canceller filters have a notch at zero frequency. On the other hand, target components with nonzero Doppler frequency will be observed at the filter output with possible attenuation in their magnitudes. The pass-band narrows for larger filter orders. In MTI processors one loses both from not using the actual clutter correlation and being only matched to the DFT frequencies.

The results of three different MTI processors are presented in section 9.2. In the double pulse canceller, consecutive pulses are canceled and useable number of

output samples is one less than the number of input samples. This version is named as HWMTI_11, where HW letters are added for Hamming Windowing after MTI operation. Another version presented combines three samples with the coefficients 1, -2, and 1 and called HWMTI_121. In this version, useable number of output samples is two less than the number of input samples. In the third alternative, we use all the output samples and use a combination of two and three pulse canceller. The input vector is processed by the matrix

$$\begin{bmatrix} -1 & 1 & 0 & \cdots & \cdots & 0 \\ 1 & -2 & 1 & 0 & \cdots & 0 \\ 0 & \ddots & \ddots & \ddots & 0 & 0 \\ 0 & 0 & \ddots & \ddots & \ddots & 0 \\ 0 & \cdots & 0 & 1 & -2 & 1 \\ 0 & \cdots & \cdots & 0 & 1 & -1 \end{bmatrix}_{NxN} . \tag{3.2}$$

This last version is named as HWMTI.

3.2. Maximum Likelihood (ML) Technique

The generally accepted best procedure of frequency estimation is based on the Maximum Likelihood (ML) method. If an unbiased estimator that attains the Cramér-Rao bound (to be defined in the next section) exists, it is ML. For large N, ML estimator has asymptotic properties of being unbiased, efficient, and Gaussian distributed [10].

Let us derive the ML equations for our problem of targets in radar clutter. Assuming that $\mathbf{R}^n$ is perfectly known, the conditional probability density function of $\mathbf{x}$ is [10]

$$p\left(\mathbf{x} \mid a_1,\ldots,a_M,\omega_1,\cdots,\omega_M\right) = \frac{1}{\pi^N \det \mathbf{R}^n} \exp\left(-\left(\mathbf{x}-E\{\mathbf{x}\}\right)^H \mathbf{Q}\left(\mathbf{x}-E\{\mathbf{x}\}\right)\right) \tag{3.3}$$

where

$$\mathbf{Q} = \left(\mathbf{R}^n\right)^{-1} \tag{3.4}$$

and

$$E\{\mathbf{x}\} = \sum_{i=1}^{M} a_i \mathbf{V}_{:,i} + E\{\mathbf{n}\} . \tag{3.5}$$

The ML estimates of a_i's and ω_i's can be obtained through the maximization of equation (3.3), or equivalently

$$\min_{a_1,\ldots,a_M,\omega_1,\ldots,\omega_M} \left(\mathbf{x}-E\{\mathbf{x}\}\right)^H \mathbf{Q}\left(\mathbf{x}-E\{\mathbf{x}\}\right). \tag{3.6}$$

Note that with expression (3.6), we have converted our cost function from p to $-\ln(p)$ and maximization to minimization.

The problem considered here is referred to as deterministic maximum likelihood [11] in contrast to the case where the complex multipliers of the complex exponentials are treated not as parameters, but as random variables. The latter approach is called stochastic maximum likelihood [11].

Theorem [12]: Let $\ln\left(p\left(\mathbf{z},\mathbf{z}^*\right)\right)$ be a real-valued function of the complex vectors $\mathbf{z}$ and $\mathbf{z}^*$. The vector pointing in the direction of the maximum rate of change of $\ln\left(p\left(\mathbf{z},\mathbf{z}^*\right)\right)$ is $\nabla_{\mathbf{z}^*}\ln\left(p\left(\mathbf{z},\mathbf{z}^*\right)\right)$.

The scalar version of the complex gradient is given by [11]

$$\nabla_{z^*}\ln\left(p\left(z,z^*\right)\right)=\frac{1}{2}\left(\frac{\partial\ln(p)}{\partial z_{real}}+j\frac{\partial\ln(p)}{\partial z_{imaginary}}\right) \tag{3.7}$$

where

$$z = z_{real} + jz_{imaginary}. \tag{3.8}$$

When one uses the given definition of derivatives in solving the minimization expression (3.6), the following governing equations are obtained from the minimization with respect to a_k's

$$-\mathbf{V}_{:,k}^H\mathbf{Q}\mathbf{x}+\sum_{l=1}^{M}\mathbf{V}_{:,k}^H\mathbf{Q}a_l\mathbf{V}_{:,l}=0,\quad k=1,\ldots,M \tag{3.9}$$

and from the minimization with respect to ω_p's

$$2\,\mathrm{Re}\left\{\sum_{i=1}^{M}a_i^*a_p\mathbf{V}_{:,i}^H\mathbf{Q}\mathbf{V}_{:,p}^{'}\right\}-2\,\mathrm{Re}\left\{a_p\mathbf{x}^H\mathbf{Q}\mathbf{V}_{:,p}^{'}\right\}=0,\quad p=1,\ldots,M \tag{3.10}$$

where

$$\mathbf{V}_{:,p}^{'}=\begin{bmatrix}0 & je^{j\omega_p} & \cdots & j(N-1)e^{j(N-1)\omega_p}\end{bmatrix}^T. \tag{3.11}$$

Although the general model can be developed assuming a nonzero mean for the clutter and noise (together treated as a colored noise), in the subsequent parts we

will assume a zero mean since generally there is no reason to assume a nonzero mean for the colored noise part of a radar observation.

One can observe that the ML estimates for a_i's and ω_i's are unbiased by taking the expected values of both sides of the equations (3.9) and (3.10). In other words, expected values of estimates are found to be equal to their actual values.

Now, let us examine if there occurs any change in equations (3.9) and (3.10), for the situation involving random target phases. There will be no change since for any given parameter vector $\boldsymbol{\varphi}$, one will do the maximization of the following function

$$\begin{aligned} p(\mathbf{x},\boldsymbol{\varphi}) &= p(\mathbf{x}\,|\,\boldsymbol{\varphi})\,p(\boldsymbol{\varphi}) \\ \ln p(\mathbf{x},\boldsymbol{\varphi}) &= \ln p(\mathbf{x}\,|\,\boldsymbol{\varphi}) + \ln p(\boldsymbol{\varphi}) \end{aligned} \tag{3.12}$$

and

$$\nabla_{\boldsymbol{\varphi}}\left[\ln p(\boldsymbol{\varphi})\right] = \mathbf{0} \tag{3.13}$$

for uniform distribution on $\boldsymbol{\varphi}$.

Note that ML equations (3.9) and (3.10) are such that given ω_i's, a_i's can be solved. Thus one can do the minimization only with respect to ω_i's. Defining

$$\mathbf{a} = \begin{bmatrix} a_1 & \cdots & a_M \end{bmatrix}^T \tag{3.14}$$

the minimization problem (3.6) can be expressed as

$$\min_{f_1,\cdots,f_M,\mathbf{a}} \left\| \mathbf{Q}^{1/2}(\mathbf{x} - \mathbf{V}\mathbf{a}) \right\|^2 \tag{3.15}$$

where

$$\mathbf{V}_{:,k} = \mathbf{v}_k\,. \tag{3.16}$$

The minimization with respect to $\mathbf{a}$ is obtained by

$$\mathbf{a} = \left(\mathbf{Q}^{1/2}\mathbf{V}\right)^{\#} \mathbf{Q}^{1/2}\mathbf{x}\,. \tag{3.17}$$

Substituting (3.17) in equation (3.15), we obtain

$$\min_{\omega_1,\ldots,\omega_M} \left(\mathbf{x} - \mathbf{V}\left(\mathbf{Q}^{1/2}\mathbf{V}\right)^{\#} \mathbf{Q}^{1/2}\mathbf{x}\right)^H \mathbf{Q}\left(\mathbf{x} - \mathbf{V}\left(\mathbf{Q}^{1/2}\mathbf{V}\right)^{\#} \mathbf{Q}^{1/2}\mathbf{x}\right). \tag{3.18}$$

Similar derivations can be found in literature [13], [14], [11].

The downside of ML method is that it requires a global optimization procedure in order not to stick to a local minimum. It requires an initial condition in the vicinity of the global optimum.

3.3. Cramér-Rao Bound

Cramér-Rao (CR) expressions which form the lower bound for variances of unbiased estimates [15] can be obtained for the observation **x** (nonrandom case) as follows [11], [15]: One defines and calculates the expressions

$$\mathbf{s} = \nabla_{\boldsymbol{\theta}} \left[-\left(\mathbf{x} - E\{\mathbf{x}\}\right)^H \mathbf{Q} \left(\mathbf{x} - E\{\mathbf{x}\}\right) \right] \tag{3.19}$$

$$\boldsymbol{\theta} = \left[\mathbf{g}_1 \quad \cdots \quad \mathbf{g}_M\right]^T, \mathbf{g}_i = \left[a_i^* \quad \omega_i\right]^T \tag{3.20}$$

$$\mathbf{J} = E\left\{\mathbf{s}\mathbf{s}^H\right\}. \tag{3.21}$$

$\mathbf{J}$ is the Fisher information matrix with the entries given by

$$\mathbf{J}_{k,l} = \mathbf{V}_{:,k}^H \mathbf{Q} \mathbf{V}_{:,l}, \quad k,l = 1,3,\ldots,2M-1 \tag{3.22}$$

$$\mathbf{J}_{k,l} = 2\,\mathrm{Re}\left\{a_k a_l^* \left(\mathbf{V}_{:,l}'\right)^H \mathbf{Q} \mathbf{V}_{:,k}'\right\}, \quad k,l = 2,4,\ldots,2M \tag{3.23}$$

$$\mathbf{J}_{k,l} = a_l \mathbf{V}_{:,k}^H \mathbf{Q} \mathbf{V}_{:,l}', \mathbf{J}_{kl} = \mathbf{J}_{lk}^*, \quad k = 1,3,\ldots,2M-1, \quad l = 2,4,\ldots,2M. \tag{3.24}$$

For the random case the following changes are to be observed in the above equations, which are obtained by taking expectations over the random and uncorrelated phases $\angle a_k$ and $\angle a_l$ for $k \neq l$

$$\mathbf{J}_{k,k} = 2\left|a_k\right|^2 \left(\mathbf{V}_{:,k}'\right)^H \mathbf{Q} \mathbf{V}_{:,k}', \quad k = 2,4,\ldots,2M \tag{3.25}$$

$$\mathbf{J}_{k,l} = 0, \quad k \neq l, \quad k,l = 2,4,\ldots,2M \tag{3.26}$$

$$\mathbf{J}_{k,l} = 0, \mathbf{J}_{l,k} = 0, \quad k = 1,3,\ldots,2M-1, \quad l = 2,4,\ldots,2M. \tag{3.27}$$

Cramér-Rao lower bounds for unbiased estimates are obtained via

$$\mathrm{var}\left(a_k\right) \geq \mathbf{J}_{2k-1,2k-1}^{-1}, \quad k = 1,2,\ldots,M \tag{3.28}$$

$$\mathrm{var}\left(\omega_p\right) \geq \mathbf{J}_{2p,2p}^{-1}, \quad p = 1,2,\ldots,M. \tag{3.29}$$

Alternatively, square root of the bounds can be used to obtain lower bound on standard deviations.

CHAPTER 4

LINEAR PREDICTION AND THE TUFTS–KUMARESAN METHOD

4.1. Motivation

Maximum Likelihood (ML) estimation of the frequencies is effective yet requires a difficult multidimensional search. Consequently, one resorts to suboptimum, but practical algorithms.

Radar clutter can be modeled quite accurately as a relatively low order autoregressive (AR) process [16], a process generated by filtering white noise with an all-pole filter [12], so it can be modeled by the zeros of or, if required, canceled by a FIR filter. This is not only true for land clutter, but also for weather and bird clutter [16].

First we will investigate the hypothetical case of known $\mathbf{R}^x$ defined by

$$\mathbf{R}^x = \sum_{k=1}^{M} |a_k|^2 \mathbf{V}_{:,k} \mathbf{V}_{:,k}^H + \mathbf{R}^n \tag{4.1}$$

which is the autocorrelation of the data vector $\mathbf{x}$ under uniform and uncorrelated target phases. Note that for nonrandom case, $\mathbf{R}^x$ is not stationary. We will not investigate it in our work. In this chapter, Linear Prediction (LP) and its relation to AR processes will be shown. Then Tufts-Kumaresan method (TK) [17], [1], [18], which is a practical implementation of LP when $\mathbf{R}^x$ is not known, will be investigated. After the explanation of the specified topics, literature survey on their use in radar problem will be given. It is believed that after the topics have been covered, it will be easier to follow the literature survey.

4.2. Linear Prediction

The aim of Linear Prediction is to minimize the prediction error variance σ_e^2 by linearly combining the L samples of the sequence $x[n]$ to estimate another sample of it [11], [12]. This is summarized in Figure 2.

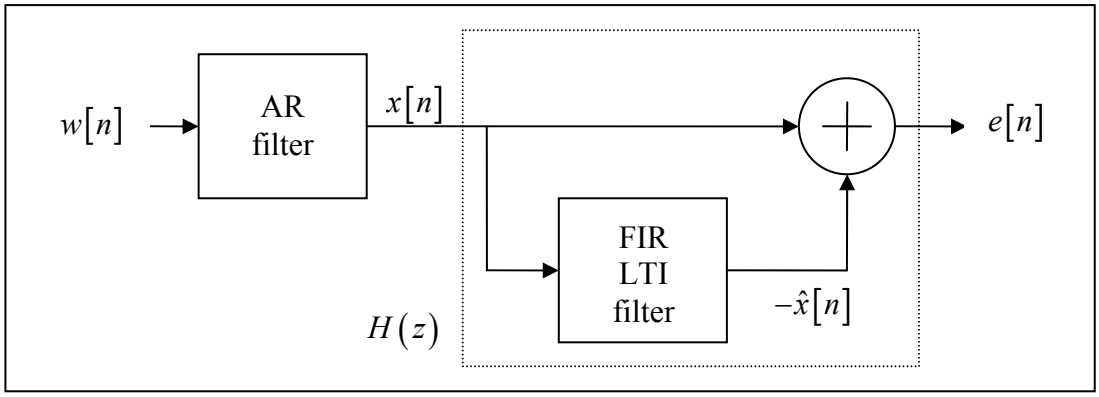

Figure 2 Linear prediction block diagram

Forward LP (FLP) corresponds to using L samples to predict the next sample, while backward LP (BLP) corresponds to using L samples to predict the next earlier sample [11] as shown in Figure 3.

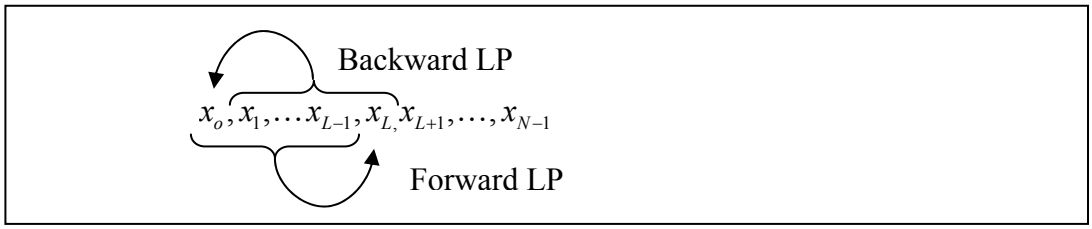

Figure 3 Forward and backward linear prediction

The main equation for FLP is

$$\hat{x}[n] = \sum_{k=1}^{L} -g_k^* x[n-k] \tag{4.2}$$

where $1, g_1^*, \ldots, g_L^*$ are the coefficients of the prediction-error filter $H(z)$ (PEF) shown in Figure 2. The coefficients can be found by satisfying the orthogonality principle which states that [11]

$$E\left\{x[n-i]e^*[n]\right\} = 0, \quad i = 1, \ldots, L. \tag{4.3}$$

Using this principle the equations obtained, under the assumption that $x[n]$ is Wide Sense Stationary (WSS), are

$$H^{Ideal}(z) = 1 + \sum_{k=1}^{L} \left(\mathbf{g}_k^{Ideal}\right)^* z^{-k} \tag{4.4}$$

where

$$\mathbf{g}^{Ideal} = \left[\left(\mathbf{R}^x_{(1:L),(1:L)}\right)^T\right]^{\#} \left(-\mathbf{R}^x_{1,(2:L+1)}\right). \tag{4.5}$$

These equations are *Ideal* in the sense that perfect knowledge of $\mathbf{R}^x$ is assumed. It is well known that [11] if $x[n]$ is an AR process generated by passing white noise $w[n]$ through the filter

$$\frac{1}{D(z)} = \frac{1}{1 + \sum_{k=1}^{L} b_k z^{-k}} \tag{4.6}$$

then

$$\left(g_i^{Ideal}\right)^* = b_i. \tag{4.7}$$

In other words, as long as a linear predictor has order L larger than or equal to that of the AR process, which is P,

$$g_i^{Ideal} = 0, \quad L \geq i > P \tag{4.8}$$

and

$$H(z) = D(z) \tag{4.9}$$

as shown in Figure 4.

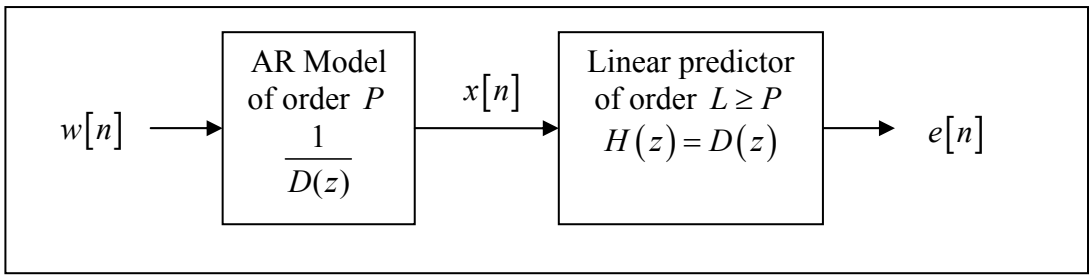

Figure 4 Relationship between linear prediction and AR processes

This means that parameters of any AR model can be found by LP. It is also true that when PEF is inverted and driven by white noise, the resulting random process will have the same statistical characteristics as $x[n]$. Consequently, as long as clutter can be considered as an AR process, LP with finite order L can be used to model it.

As for the BLP, the main equation is

$$\hat{x}[n-L] = -\sum_{k=1}^{L} c_k^* x[n-L+k] \tag{4.10}$$

with the orthogonality condition given by [11]

$$E\left\{x[n-L+i]e_b^*[n-L]\right\} = 0, \quad i = 1,\ldots,L \tag{4.11}$$

where

$$e_b[n-L] = x[n-L] - \hat{x}[n-L]. \tag{4.12}$$

In BLP, $\sigma_{e_b}^2$ is minimized.

It has been shown that [11]

$$\mathbf{g}_i^{Ideal} = c_i^*. \tag{4.13}$$

BLP can be associated with an anticausal AR model.

4.2.1. Further Remarks on Linear Prediction

In LP, although it is possible to obtain filters recursively for increasing values of L [11], we will concentrate on the fixed order case.

Other important properties of LP may be listed as follows [11], [12]:

1. If a fixed, but reasonably high order PEF is used, $e[n]$ will have approximately constant variance terms that are orthogonal to each other. This means that $e[n]$ is white noise. Thus PEF is a whitening filter.
2. For FLP, $H(z)$ is causal and minimum phase, which means that it is a causal stable filter with a causal stable inverse. In other words, all of its zeros are inside the unit circle.
3. For BLP, $H(z)$ is an anticausal and maximum phase polynomial.

4.3. Modified Tufts-Kumaresan Method

4.3.1. Overview of Tufts-Kumaresan Method

A practical way of implementing LP, when $\mathbf{R}^x$ needs to be estimated from an extremely limited number of observations is due to the methods developed by Tufts and Kumaresan (TK) [17], [1], [18] for detecting complex exponentials in AWGN.

Tufts & Kumaresan's method (TK method) brings performance improvement to LP based frequency estimation methods at low *SNR* by using the prior knowledge about the rank M of the signal correlation matrix. TK method estimates are comparable to ML estimates and its performance is close to Cramér-Rao (CR) bound, even when the data consists of closely spaced frequencies. Also, the value of *SNR* at which the accuracy of the frequency estimates departs drastically from the CR bound, the threshold *SNR* value, is brought much closer to that of ML by the use of TK method.

Estimated correlation matrix is replaced by an estimated signal matrix in the AWGN case. For the pulsed Doppler radar problem, the estimated correlation matrix is replaced by an estimated signal and clutter correlation matrix, which is a necessary modification to the TK method under scenarios containing clutter in addition to the AWGN. This means filtering out some portion of the noise. Equivalently, the forward-backward (FB) data matrix $\mathbf{A}$ can be approximated by a lower rank $\breve{M}$ matrix where the FB data matrix $\mathbf{A}$ is given by

$$\mathbf{A}=\begin{bmatrix} x_{L-1} & x_{L-2} & \cdots & x_0 \\ x_L & x_{L-1} & \cdots & x_1 \\ \vdots & \vdots & & \vdots \\ x_{N-2} & x_{N-3} & \cdots & x_{N-L-1} \\ x_1^* & x_2^* & \cdots & x_L^* \\ x_2^* & x_3^* & \cdots & x_{L+1}^* \\ \vdots & \vdots & & \vdots \\ x_{N-L}^* & x_{N-L+1}^* & \cdots & x_{N-1}^* \end{bmatrix} \tag{4.14}$$

and tends to be full rank in the noisy case. Let $\tilde{\mathbf{A}}$ be the reduced rank FB data matrix corresponding to the actual FB data matrix $\mathbf{A}$ and $\tilde{\mathbf{R}}$ be the reduced rank version of the estimated correlation matrix $\hat{\mathbf{R}}^x$ of the signal, clutter, and noise. The relations between the specified matrices are as follows:

$$\begin{aligned} \hat{\mathbf{R}}^x &= \mathbf{A}^H\mathbf{A} \\ \tilde{\mathbf{R}} &= \tilde{\mathbf{A}}^H\tilde{\mathbf{A}} \end{aligned}. \tag{4.15}$$

This procedure is called principal components approximation [11], a method of preserving signal subspace only.

4.3.2. Tufts-Kumaresan Algorithm Details

The TK algorithm has the following structure. Basically, the solution of equation

$$\mathbf{Ag}=-\mathbf{b} \tag{4.16}$$

is sought, where

$$\mathbf{b}=\begin{bmatrix} x_L & x_{L+1} & \cdots & x_{N-1} & x_0^* & x_1^* & \cdots & x_{N-L-1}^* \end{bmatrix}^T \tag{4.17}$$

is the data vector and

$$\mathbf{g}=\begin{bmatrix} g_1 & \cdots & g_L \end{bmatrix}^T \tag{4.18}$$

is the impulse response of the prediction filter of order L. Equation (4.16) is solved for $\mathbf{g}$ in the least squares sense; i.e., one minimizes

$$\left\|-\mathbf{b}-\mathbf{Ag}\right\|^2. \tag{4.19}$$

The transfer function of the prediction-error filter $H(z)$ is given by

$$H(z)=1+\sum_{k=1}^{L} g_k z^{-k}. \tag{4.20}$$

For deterministic signals not corrupted by noise, the degree L of the prediction-error filter polynomial $H(z)$ should satisfy [18]

$$\breve{M} \le L \le \left(N - \text{round}\left(\frac{\breve{M}}{2} \right) \right) \tag{4.21}$$

in order to have $\breve{M}$ zeros associated with signal and clutter when using the FBTK method (TK method with the FB data matrix), where $\breve{M}$ equals M plus the number of zeros required to model clutter. Besides $L - \breve{M}$ extraneous zeros, zeros at positions

$$e^{j2\pi f_i}, \quad i = 1, \ldots, \breve{M} \tag{4.22}$$

are observed when used on a data consisting of undamped complex exponentials, which is consistent with our signal model as explained in the next paragraph.

Targets can be modeled by complex exponentials and as can be seen from the above explanation, TK is suitable in this aspect. Since clutter is an AR process, we expect it to be modeled by one or more, $\breve{M} - M$, complex exponentials just as the targets. We have observed that if the radar antenna is not rotating, i.e., working condition is zero rpm , it is modeled by one complex exponential, and, increasing the rpm and/or CNR results in more poles being required in the AR model. Although a table of number of poles needed to model the clutter can be obtained depending on the operating conditions, it is not necessary as we will explain in Chapter 7. An algorithm will be developed to decide on $\breve{M}$ and then the targets will be identified based on clutter regions. Under these circumstances, TK is suitable in radar signal modeling as a whole, since it is one of the most successful high resolution frequency estimation techniques.

For the FTK or BTK methods, the condition becomes [18]

$$\breve{M} \le L \le \left(N - \breve{M} \right) \tag{4.23}$$

and one uses the upper or the lower half of the matrix $\mathbf{A}$ in the calculations, thus the name FTK or BTK, respectively.

If the prediction filter coefficients are selected to have minimum Euclidean norm and the first coefficient is taken to be unity, the $L - \breve{M}$ extraneous zeros of the

filter polynomial are approximately uniformly distributed inside the unit circle [18], [11]. To observe this fact, one can factor $H(z)$ as

$$H(z) = H_1(z) H_2(z) \tag{4.24}$$

where $H_1(z)$ has $\breve{M}$ zeros modeling the signal and the clutter; and $H_2(z)$ has $L - \breve{M}$ zeros, which are the extraneous zeros. The polynomial $H_2(z)$ can be associated with a prediction-error filter operating on the data-sequence defined by the coefficients of $H_1(z)$ and yielding the error sequence, which are the coefficients of $H(z)$. Minimizing the Euclidean norm of $H(z)$, while keeping its first coefficient at unity in order to prevent a zero solution, is identical to minimizing the error energy in the autocorrelation method of linear prediction. It is a known fact that the prediction-error filter is minimum phase [11] and its zeros have magnitude less than unity, thus proving that $L - \breve{M}$ extraneous zeros of $H(z)$ fall in the unit circle.

The above observation is necessary to identify the two groups of zeros: those related to signal and clutter, and the extraneous or spurious zeros. By using the Moore-Penrose pseudoinverse [19] of $\mathbf{A}$ in calculating $\mathbf{g}$, we satisfy the minimum Euclidean norm condition on $\mathbf{g}$.

However, when the data is noisy, the extraneous zeros can lie closer to or outside the unit circle. Rank reduction alleviates this problem by effective *SNR* enhancement. The best lower rank of $\breve{M}$ approximation (in term of Frobenius norm) to a given matrix can be found based on Singular Value Decomposition (SVD), by setting all but $\breve{M}$ of its largest singular values to zero [17], [1].

The solution to equation (4.16), satisfying the two constraints, is

$$\mathbf{g} \approx \tilde{\mathbf{g}} = \tilde{\mathbf{A}}^{\#} (-\mathbf{b}) \tag{4.25}$$

where $\tilde{\mathbf{A}}^{\#}$ is the reduced rank pseudoinverse of $\mathbf{A}$. To find an explicit form of equation (4.25), we start by finding the SVD of $\mathbf{A}$

$$\mathbf{A} = \mathbf{U}^A \mathbf{S}^A \left(\mathbf{V}^A\right)^H \tag{4.26}$$

where the columns of $\mathbf{U}^A$ are eigenvectors of $\mathbf{A}\mathbf{A}^H$, the columns of $\mathbf{V}^A$ are eigenvectors of $\mathbf{A}^H\mathbf{A}$, and the singular values on the diagonal of $\mathbf{S}^A$ are the square

roots of the nonzero eigenvalues of both $\mathbf{A}\mathbf{A}^H$ and $\mathbf{A}^H\mathbf{A}$. Once the SVD of $\mathbf{A}$ is obtained, its Moore-Penrose pseudoinverse $\mathbf{A}^{\#}$ is given by $\mathbf{V}^A\left(\mathbf{S}_I^A\right)^T\left(\mathbf{U}^A\right)^H$ where $\mathbf{S}_I^A$ is obtained from $\mathbf{S}^A$ by replacing each nonzero diagonal entry by its reciprocal. Using only $\breve{M}$ singular values instead of the matrix $\mathbf{S}_I^A$ to achieve rank reduction, $\mathbf{g}$ in equation (4.25) is obtained as

$$\mathbf{g} \approx \tilde{\mathbf{g}} = -\sum_{i=1}^{\breve{M}} \frac{\left(\mathbf{U}_{:,i}^A\right)^H \mathbf{b}\mathbf{V}_{:,i}^A}{\mathbf{S}_{i,i}^A}. \tag{4.27}$$

$\tilde{\mathbf{g}}$ does not minimize the prediction-error energy, but is an approximation of the noiseless situation.

Lastly, the angle (in radians) between each of the $\breve{M}$ zeros of $H(z)$ closest to the unit circle and the positive real axis in the complex plane when divided by 2π gives the frequency estimates. The target frequency estimates f_i's are found after eliminating $\breve{M} - M$ of the obtained frequency estimates that model the clutter and thus fall in one of the clutter regions to be defined. A pictorial representation of the zeros of $H(z)$ is given in Figure 5 where $L = 9, M = 2$ and $\breve{M} = 4$.

TK method modified with truncation control, i.e., rank reduction to values other than $\breve{M}$, selecting more zeros closer to the unit circle than a threshold and eliminating them from their magnitude is investigated in [20], [21].

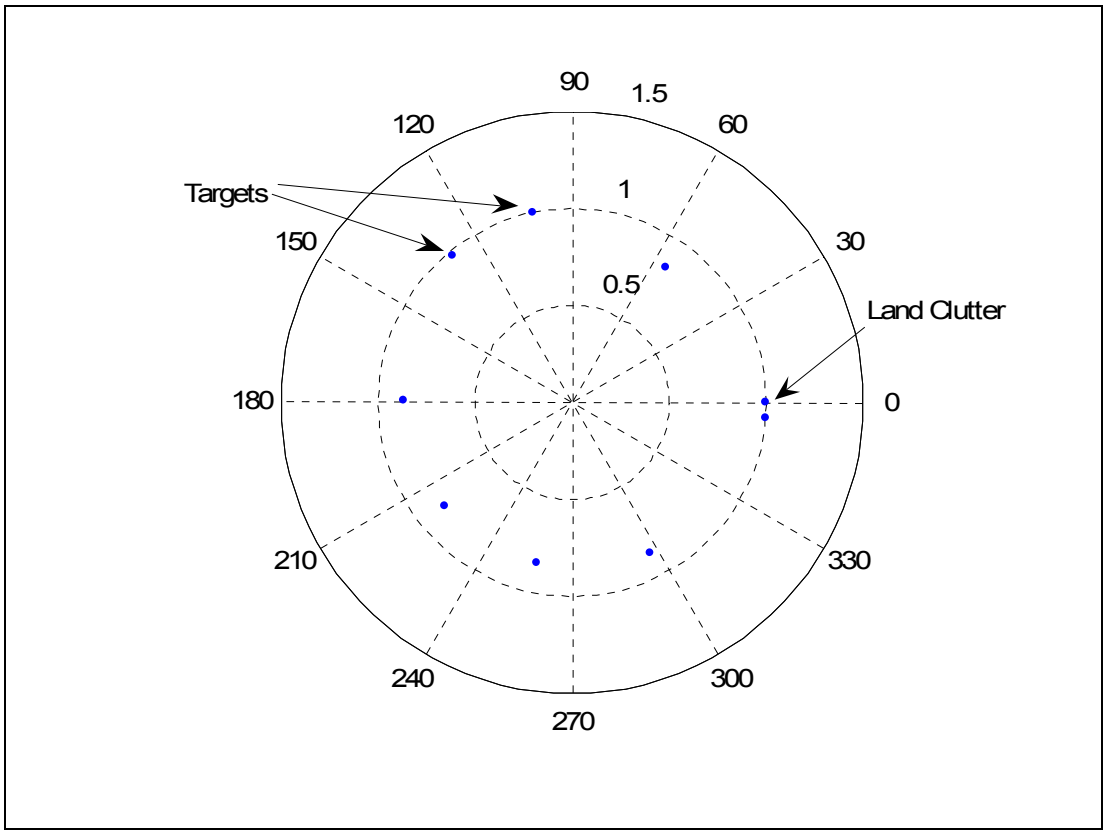

Figure 5 Zeros of prediction-error filter

4.3.3. FBTK, FTK vs. BTK in Modeling Clutter

In FTK, zeros are in their actual positions [22]. If the zeros of clutter tend to fall outside the unit circle, this would make them easily separable from the extraneous zeros. For the BTK case, they fall at positions $e^{-s_k^*}$ [22] and need to be reflected inside the unit circle to positions e^{s_k} 's to find the actual frequency components. This method would be suitable for processes that actually have zeros inside the unit circle so that its zeros would be separable from the extraneous ones by the BTK modeling. However, we have observed that radar clutter component with the specified model in Chapter 2 does not exhibit a behavior suitable to either FTK or BTK modeling.

4.3.4. FBTK Noise Reduced Data Vector Version

We have devised a version of FBTK by also reducing the effect of noise in the data vector (4.17). We form the concatenation of the data matrix and the data vector as

$$\begin{bmatrix}\mathbf{b} & \mathbf{A}\end{bmatrix} \tag{4.28}$$

and retaining $\breve{M}$ of the singular values of this matrix, re-obtain the noise reduced versions of **b** and **A** from the corresponding positions of the same size, but rank reduced concatenated matrix. All the other steps are the same with the FBTK algorithm after this step. The performance and necessity of this modification are discussed during the simulations under the algorithm name 'FBTK, NRDV,' where NRDV stands for noise reduced data vector.

4.4. Distinguishing Clutter and Targets: the Concept of Clutter Region

In works found in the literature, land clutter is distinguished from its velocity being nearest to zero [5]. However, we cannot distinguish it from the large power of its singular value, since depending on *CNR* this condition may not be true. For a given set of radar parameters, we performed simulations to specify clutter regions, one for each source of clutter. If a frequency estimate falls in a clutter region, it is identified as a clutter component resulting in separation of the frequencies of targets and clutter.

With this technique, clutter spread observed in its power spectrum is not always modeled by a single DC term, but it can be modeled by more than one prediction-error filter zeros falling in the clutter region near location at zero frequency with a certain width, i.e., land clutter region, or around any other frequency with the same width for moving clutter case. Further explanation will be provided in Chapter 7.

4.5. Linear Predictor as a Radar Processor

When using LP in a radar detector a filter bank is unnecessary, since the processor is not designed based on specific target frequencies. In other words, a single LP processor is sufficient. It can be designed as a linear prediction-error filter by using the a priori knowledge on clutter. When there is a target its output is

expected to consist of a target component plus suppressed clutter. However, we point out that although LP can be used to filter the radar echo in order to get rid of clutter followed by target detection, it is also possible and requires less computation to include both the targets and the clutter, possibly both land and moving weather clutter, in its design. In this way we can achieve clutter filtering (including weather clutter), multiple target detection and high resolution velocity estimation with a single processor. Also using LP in a way to estimate other samples than the next or the previous sample is studied [8].

LP in slow time samples can be used as an efficient tool to estimate Doppler frequencies, in addition to some other methods, but not in its FB version and for mean Doppler frequency estimation of weather radar signal in the presence of single clutter source which is the ground clutter in [5] with L fixed at 2 and the estimated frequency further from zero corresponding to weather clutter and that near zero frequency corresponding to ground clutter. In this work the frequency range not affected by clutter is reported to be $[0.2, 0.8]$ with RMSE ≤ 0.04. After separating the target and the clutter, LP is used to cancel clutter in [23]. It is used to model both the ship echo and Bragg lines in [24]. The Bragg lines are the scattering from surface waves which have wavelength equal to one half of the radar wavelength and move directly away or towards the receiving radar. A sea clutter whitening preprocessing is also developed based on multiple bursts in [24].

Our approach of using LP as a clutter filter can be seen to have some similarities with [24]. However, there are major differences such as Coherent Integration Time's (CIT) required. For the given work, under favorable conditions CITs of 2s. are reported for ships and under normal conditions for aircrafts, whereas our observation time for a typical $PRF = 10KHz$ is in the order of ms. One reason for this difference may be the fact that we applied the similar processor to a different scenario where Bragg scattering of the ocean surface is not the major source of clutter. Continuing with the differences observed in our work, our radar is a land based one with multiple clutter sources due to weather clutter and can perform target discrimination. We analyzed its performance depending on the various parameters used and compared with other high resolution spectrum estimation algorithms. We also use a different method to find the number of frequencies, which is explained in

Chapter 7, since Akaike Information Criterion (AIC) [25] used in [24] is not a suitable method for short data lengths [12] and non-Gaussian data, which is the case for our observations under the assumption of random target phases. We intentionally did not assume a distribution for the target magnitude in order to be able to generalize results to arbitrary distributions after obtaining results at different amplitude values of complex multipliers.

CHAPTER 5

OTHER HIGH RESOLUTION LINE SPECTRA ESTIMATION TECHNIQUES

In this chapter DTFT, MUSIC and ESPRIT algorithms as applied to target detection in radar clutter will be studied. A literature survey on the use of MUSIC in radar problem will be provided after the descriptions of the algorithm. Lastly, it will be made clear why ML algorithm requires the output of one of the defined high resolution frequency estimation algorithms in order to function properly.

5.1. Can Pure DFT Be an Alternative?

The DTFT of a sample vector $\mathbf{x}$ defined in equation (2.5) (obtained by zero-padded DFT) is shown in Figure 6. Although two targets at frequencies $[f_1 \quad f_2] = [0.2813 \quad 0.3563]$ under strong clutter are present, even the presence of two targets cannot be detected As a result, one can conclude that without clutter suppression or pre-whitening a promising result cannot be obtained with Fourier Transformation approach to frequency estimation. We have also observed, as explained in section 3.1., that MAXSIR or MTI type methods that suppress clutter do not provide the required resolution to differentiate two targets.

Although, when noise is not present, three samples are enough to distinguish a complex exponential from another including phase and magnitude, especially if the samples do not cover an integer number of periods of the Doppler tone from a target in a pulsed Doppler radar (periodic extension of this waveform determines the signal being processed [26]), DFT suffers from the sidelobes of complex exponentials burying nearby complex exponential peaks. In other words, spectral lines widen in frequency domain [3]. In this case larger DFT lengths with zero-padding do not help. With DFT, frequency resolution is inversely proportional to the number of data

points, although the best resolution achievable from the discrete samples as observed via DTFT is limited by the inverse of the observation time [26]. As a result, one can conclude that the resolution of the DFT processing is limited when the frequencies of the sinusoids are more closely spaced than the reciprocal of the observation time [1], in case of multiple targets.

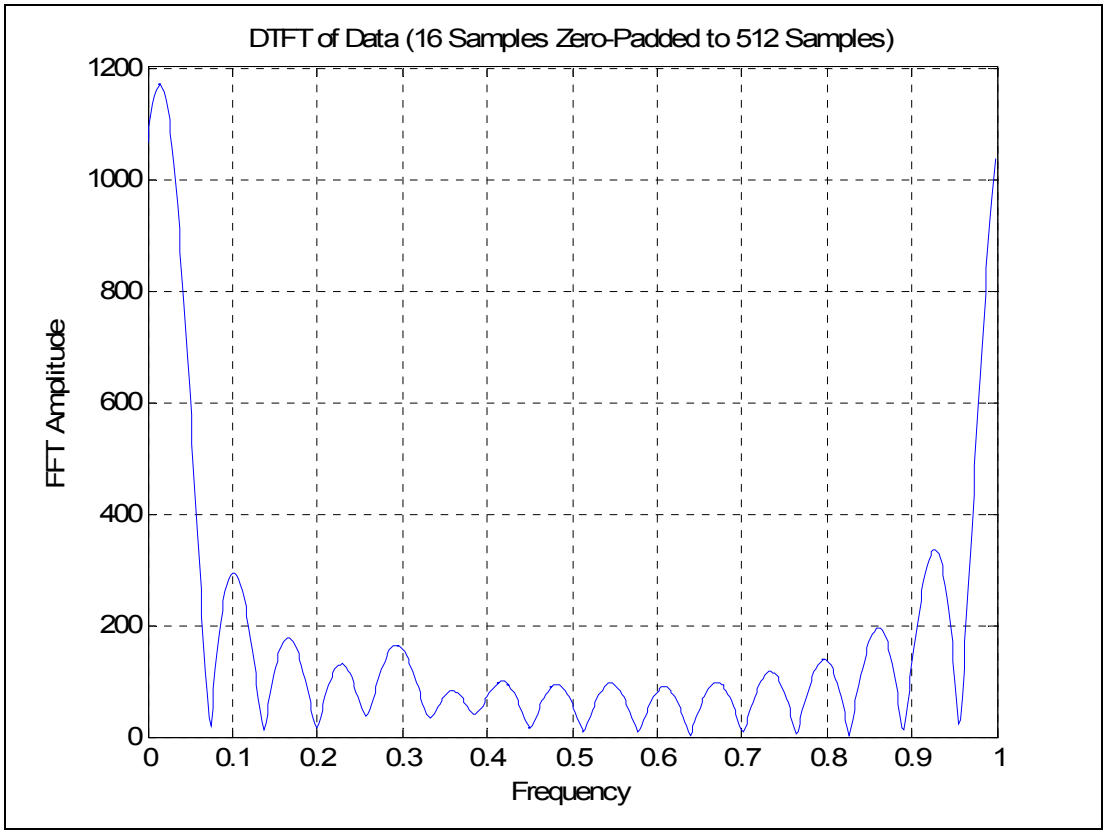

Figure 6 DTFT analysis of input data

As DFT cannot be used to perform multiple target detection it cannot be a feasible alternative to TK. Modern high resolution spectral estimation techniques are used under high *SNR* conditions for a better frequency resolution compared to DFT when the number of samples is small. As TK is a high resolution frequency

estimation technique suitable for signals possessing line components like target echoes, other well known algorithms such as MUSIC [12], [11] and ESPRIT [11] with their various suggested versions that we will review are also applicable. These algorithms are not originally developed for radar scenarios under clutter, but they are basically designed for data corrupted in AWGN. To use them for modeling clutter, we will make the necessary modifications as we did for TK and analyze their performance in comparison with TK's. One can say that line component estimation techniques are not suitable for an arbitrary clutter plus noise covariance matrix. Only when clutter can be modeled as a group of targets, the above mentioned algorithms are suitable.

5.2. MUSIC Algorithm

In this section original MUSIC algorithm will be explained followed by its implementation under single snapshot observation and the necessary modifications needed in order to apply it to our problem of detection multiple targets under radar clutter. The last sub-section will also detail various versions of the MUSIC algorithm applied to our problem.

5.2.1. Basic MUSIC Algorithm

In this sub-section the observation $\mathbf{x}$ will be assumed to be free of clutter to explain the basic version of the MUSIC algorithm. If the eigenvalues of the actual correlation matrix of the data $\mathbf{x}$ containing M complex exponentials of unknown amplitude, phase, and frequency, $\mathbf{R}^x$, are arranged in decreasing order, largest M of them will correspond to signal subspace with the rest belonging to the noise subspace [12], [11]. For a Hermitian matrix $\mathbf{R}^x$, its eigenvectors will be orthogonal resulting in the above defined subspaces to be orthogonal [12]. Thus, one over the magnitude square of DTFT of the noise subspace eigenvectors will have peaks at the frequencies of the complex exponential signals present in $\mathbf{x}$. Equivalently, noise subspace eigenfilters formed by the z-Transformation of the eigenvectors corresponding to the noise will have M of its roots lying on the unit circle at the frequencies of the complex exponential signals [12]. The frequency estimates can be obtained from the angles of these roots. However, other zeros of this polynomial can

also be located near the unit circle making it hard to distinguish them from signal zeros. Also, when an estimate of $\mathbf{R}^x$, $\hat{\mathbf{R}}^x$, is used, signal zeros may not remain on the unit circle. These effects are reduced and spurious roots are moved away from the unit circle by means of averaging used in the algorithm called MUltiple SIgnal Classification (MUSIC).

Let $\mathbf{E}^x_{:,k}$, $k = M+1,\ldots,L$ denote the noise subspace eigenvectors of an estimated autocorrelation matrix $\hat{\mathbf{R}}^x$ of the data with size $L \times L$. These are distinguished from signal subspace eigenvectors by having the smallest $L-M$ eigenvalues. One then forms the polynomial

$$D(z) = \sum_{l=M+1}^{L} E_l(z)\left(E_l\left(1/z^*\right)\right)^* \tag{5.1}$$

where

$$E_l(z) = \sum_{k=1}^{L} \mathbf{E}^x_{:,k} z^{-(k-1)}, \quad l = M+1,\ldots,L. \tag{5.2}$$

The last step is to choose $2M$ roots of the polynomial in equation (5.1) that are closest to the unit circle and, eliminating double roots, select M of them whose angles (in radians) will provide the frequency estimates.

We have focused on the root-MUSIC algorithm since otherwise there is the task of peak detection to find the signal frequencies from one over equation (5.2) evaluated at $z = e^{j2\pi f}$.

Note that TK and MUSIC involve nonlinear operations and their performance analysis is not simple, so simulation will be used as a tool to evaluate the performances.

5.2.2. Estimation of the Autocorrelation Matrix from Single Snapshot Observation

Usually $\hat{\mathbf{R}}^x$ is estimated from multiple observations. The use of MUSIC technique under cases involving single snapshot is justified in [27].

The main rationale behind estimating the autocorrelation matrix of the observation from a single burst of observation is to partition the data into pieces to create more virtual instances of the observation instead of directly using $\mathbf{x}\mathbf{x}^H$ as the

estimated autocorrelation matrix. The partitioning of the data can be done in one direction or in both directions as will be explained next.

Defining

$$\mathbf{X}^{cov} = \begin{bmatrix} x_{L-1} & \cdots & x_0 \\ \vdots & \ddots & \vdots \\ x_{N-L} & \cdots & x_{L-1} \\ \vdots & \ddots & \vdots \\ x_{N-1} & \cdots & x_{N-L} \end{bmatrix}, \tag{5.3}$$

one can form the expression for a possible estimate of the autocorrelation matrix of the observation as

$$\hat{\mathbf{R}}^{x,cov} = \left(X^{cov}\right)^H X^{cov}. \tag{5.4}$$

For this autocorrelation matrix estimate, partitions of the data are formed in a single direction. MUSIC algorithm resulting from such an autocorrelation estimate will be called simply MUSIC algorithm, in contrast to the 'MUSIC, FB' resulting from using

$$\mathbf{X}^{mod} = \begin{bmatrix} x_{L-1} & \cdots & x_0 \\ \vdots & \ddots & \vdots \\ x_{N-L} & \cdots & x_{L-1} \\ \vdots & \ddots & \vdots \\ x_{N-1} & \cdots & x_{N-L} \\ x_0^* & \cdots & x_{L-1}^* \\ \vdots & \iddots & \vdots \\ x_{L-1}^* & \cdots & x_{N-L}^* \\ \vdots & \iddots & \vdots \\ x_{N-L}^* & \cdots & x_{N-1}^* \end{bmatrix} \tag{5.5}$$

to estimate the autocorrelation matrix of the observation as

$$\hat{\mathbf{R}}^{x,mod} = \left(\mathbf{X}^{mod}\right)^H \left(\mathbf{X}^{mod}\right) \tag{5.6}$$

where pieces of the data are used in both directions to obtained the autocorrelation matrix estimate.

5.2.3. MUSIC Algorithm as Applied to Our Problem

For the basic MUSIC algorithm explained in sub-section 5.2.1, there was no clutter, hence no clutter region, but only AWGN.

We perform the eigendecomposition of $\hat{\mathbf{R}}^{x}$ (either $\hat{\mathbf{R}}^{x,cov}$, $\hat{\mathbf{R}}^{x,mod}$). If $\hat{\mathbf{R}}^{x,mod}$ is used there will be the letters 'FB' in naming of the algorithms. Two cases will be investigated: performing whitening with the matrix $\mathbf{R}^{n}$ when it is known, or, omitting this step. The first case is further classified into two: Clutter can be counted as targets after whitening or only target frequencies can be sought.

First let us explain the whitened version of MUSIC [28], [11]: We define the generalized eigenvalue problem to be satisfied by the noise subspace (if clutter still needs to be associated with target subspace after whitening it will be named as 'M, W (Clutter Counted as Target)' or 'M, WFB (Clutter Counted as Target)' otherwise just 'M, W' or 'M, WFB'):

$$\hat{\mathbf{R}}^{x}\mathbf{E}^{x}_{:,k} = \lambda^{x}_{k}\mathbf{R}^{n}\mathbf{E}^{x}_{:,k}\,. \tag{5.7}$$

Here $\mathbf{E}^{x}_{:,k}$ is orthogonal to signal subspace and our aim is to find these vectors. A method to accomplish this task is by performing Cholesky decomposition of $\mathbf{R}^{n}$ as

$$\mathbf{R}^{n} = \mathbf{C}^{H}\mathbf{C}\,. \tag{5.8}$$

Next one performs the operation

$$\hat{\mathbf{R}}^{x,whitened} = \mathbf{C}^{-H}\hat{\mathbf{R}}^{x}\mathbf{C}^{-1}\,. \tag{5.9}$$

The eigendecomposition of equation (5.9) is given by

$$\hat{\mathbf{R}}^{x,whitened}\mathbf{V}^{x,whitened} = \mathbf{V}^{x,whitened}\mathbf{D}^{x,whitened} \tag{5.10}$$

where $\mathbf{V}^{x,whitened}$ has the eigenvectors of $\hat{\mathbf{R}}^{x,whitened}$ as its columns and $\mathbf{D}^{x,whitened}$ is a diagonal matrix of eigenvalues. Comparing equation (5.11), which is written by inserting equation (5.9) into equation (5.10) and multiplying both sides by $\mathbf{C}^{H}$ form right,

$$\hat{\mathbf{R}}^{x}\mathbf{C}^{-1}\mathbf{V}^{x,whitened} = \mathbf{R}^{n}\mathbf{C}^{-1}\mathbf{V}^{x,whitened}\mathbf{D}^{x,whitened} \tag{5.11}$$

with equation (5.7), one can obtain

$$\mathbf{E}^{x}_{:,k} = \mathbf{C}^{-1}\mathbf{V}^{x,whitened}_{:,k} \tag{5.12}$$

and form the polynomial

$$E_{l}(z) = \sum_{k=1}^{L}\mathbf{C}^{-1}\mathbf{V}^{x,whitened}_{k,l}z^{-(k-1)}, \quad l = \tilde{M}+1,\ldots,L\,. \tag{5.13}$$

If $\tilde{M} = \breve{M}$ is used, we have the '(Clutter Counted as Target)' version of the algorithm, otherwise $\tilde{M} = M$ is used after whitening.

As a final step, one forms and chooses $2\tilde{M}$ roots of the polynomial

$$D(z) = \sum_{l=\tilde{M}+1}^{L} E_l(z)\left(E_l\left(1/z^*\right)\right)^* \tag{5.14}$$

that are closest to the unit circle and, eliminating double roots, selects $\tilde{M}$ of them whose angles (in radians) will provide the frequency estimates. For the '(Clutter Counted as Target)' case we have the clutter region concept, otherwise this concept is not used after whitening. For all $\tilde{M}$ groupings of $2\tilde{M}$ frequency estimates, we have calculated the minimum of the distances between all possible two pairs of $\tilde{M}$ frequency estimates in mod 1. We have selected $\tilde{M}$ of the roots such that they have the maximum of the calculated minimum distance. As a result, we eliminate frequencies that are originating from the same frequency and do not count them twice.

Non-whitened MUSIC uses the same algorithm as above, with the only change that $\mathbf{R}^n$ in equation (5.8) is taken as $\mathbf{I}$ having the same size assuming clutter as targets and $\tilde{M} = \breve{M}$. An instance of the MUSIC spectrum for the non-whitened case for two targets at frequencies $\begin{bmatrix} f_1 & f_2 \end{bmatrix} = \begin{bmatrix} 0.2813 & 0.3563 \end{bmatrix}$ is given in Figure 7, which is obtained by evaluating one over the equation (5.14) at $z = e^{j2\pi f}$. The presence of two peaks near the target frequencies reveals the resolution capability of MUSIC and its applicability to our problem.

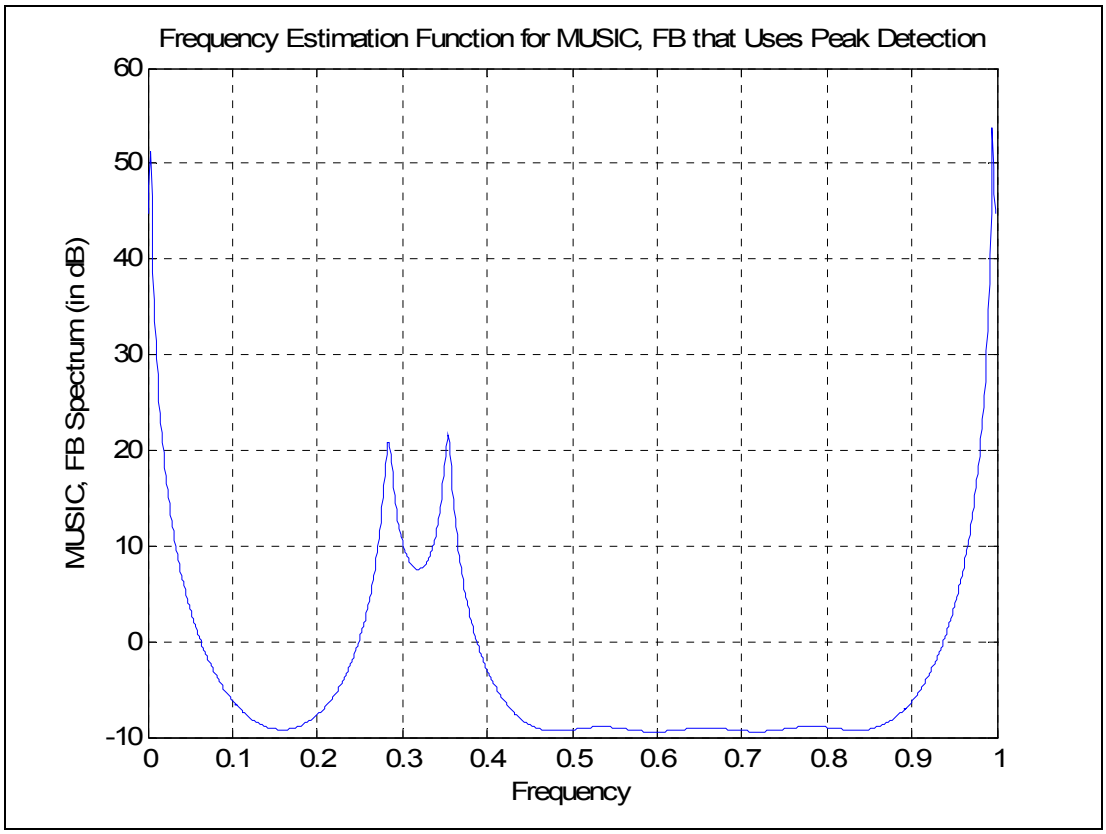

Figure 7 MUSIC spectrum

5.3. Use of MUSIC Technique in the Literature

In the literature, MUSIC is used in a vast range of applications that include modeling vessel wall motion and blood flow components in ultrasound flow measurements [29]. It has been suggested to estimate Doppler frequency as part of a signal processing unit of a radar in [30]. It is used in sea clutter suppressed version by eliminating largest singular values of the Hankel matrix formed from the data in [31]; in pre-whitened version employed in HF Surface Wave Radar in [28]. Its FB version is analyzed in [32].

5.4. Total Least Squares ESPRIT Algorithm

5.4.1. Basic Total Least Squares ESPRIT Algorithm

The essence of the basic ESPRIT algorithm [11] will be explained in this subsection.

Firstly, one obtains the M signal subspace eigenvectors of $\hat{\mathbf{R}}^x$ and forms the matrix $\mathbf{B}$ by placing them as the columns. Assume there is a hypothetical matrix $\breve{\mathbf{V}}$ having the sought complex exponential signals placed at its columns. Since the columns of matrices $\mathbf{B}$ and $\breve{\mathbf{V}}$ span the same subspace, a nonsingular transformation can be defined between them:

$$\mathbf{B}\Upsilon = \breve{\mathbf{V}} . \tag{5.15}$$

One can observe that due to the special nature of matix $\breve{\mathbf{V}}$,

$$\breve{\mathbf{V}}_{(2:end),:} = \breve{\mathbf{V}}_{(1:end-1),:}\mathbf{\Phi} \tag{5.16}$$

can be written where $\mathbf{\Phi}$ is a diagonal matrix with entries:

$$\mathbf{\Phi}_{k,k} = e^{j\omega_k} . \tag{5.17}$$

Using equation (5.16) in equation (5.15), the following equations can be obtained

$$\begin{aligned} \mathbf{B}_{(1:end-1),:}\Upsilon &= \breve{\mathbf{V}}_{(1:end-1),:} \\ \mathbf{B}_{(2:end),:}\Upsilon &= \breve{\mathbf{V}}_{(1:end-1),:}\mathbf{\Phi} \end{aligned} \tag{5.18}$$

that can be combined to get

$$\mathbf{B}_{(1:end-1),:}\mathbf{\Psi} = \mathbf{B}_{(2:end),:} \tag{5.19}$$

where

$$\mathbf{\Psi} = \Upsilon\mathbf{\Phi}\Upsilon^{-1} . \tag{5.20}$$

Equation (5.19) can be solved in total least squares sense [11] to obtain $\mathbf{\Psi}$. The angles of the eigenvectors of $\mathbf{\Psi}$ will yield the signal frequency estimates as can be seen from equations (5.20) and (5.17).

5.4.2. Total Least Squares ESPRIT Algorithm as Applied to Our Problem

Similar to the MUSIC algorithm, two versions of the Estimation of Signal Parameters via Rotational Invariance Techniques (ESPRIT) algorithm [11] will be investigated: One that employs pre-whitening with its two versions and the other one

that treats clutter components as targets and assumes operation under AWGN. Autocorrelation matrix of the data vector can be estimated in two different ways as pointed out in MUSIC algorithm, resulting in ESPRIT or 'ESPRIT, FB'. There is no difference between these two versions except the mentioned step.

Let us now explain the algorithm. First we need to obtain the eigenvectors of $\hat{\mathbf{R}}^x$ corresponding to non-noise subspace. Similar to MUSIC algorithm, when matrix $\mathbf{R}^n$ is used in the calculations instead of the matrix $\mathbf{I}$, clutter can be counted still in the signal subspace, '(Clutter Counted as Target)' version that requires clutter region definition, or can be included in the noise subspace with no need for clutter region. We define the whitening transformation

$$\mathbf{y} = \left(\mathbf{R}^n\right)^{-1/2} \mathbf{x} . \tag{5.21}$$

One needs the signal subspace eigenvectors and eigenvalues in the whitened domain in order to obtain the corresponding eigenvectors of $\hat{\mathbf{R}}^x$. Defining $\hat{\mathbf{R}}^y = E\left\{\mathbf{y}\mathbf{y}^H\right\}$,

$$\hat{\mathbf{R}}^y \mathbf{V}^y = \mathbf{V}^y \mathbf{D}^y \tag{5.22}$$

is the equation satisfied in whitened interference domain. Multiplying both sides of equation (5.22) from the left by $\left(\mathbf{R}^n\right)^{1/2}$ after inserting $\hat{\mathbf{R}}^y = \left(\mathbf{R}^n\right)^{-1/2} \hat{\mathbf{R}}_x \left(\mathbf{R}^n\right)^{-1/2}$ in equation (5.22), one obtains

$$\hat{\mathbf{R}}^x \mathbf{V}^{g,x} = \mathbf{R}^n_{(1:L),(1:L)} \mathbf{V}^{g,x} \mathbf{D}^{g,x} \tag{5.23}$$

where

$$\begin{aligned} \mathbf{V}^{g,x} &= \left(\mathbf{R}^n\right)^{-1/2} \mathbf{V}^y \\ \mathbf{D}^{g,x} &= \mathbf{D}^y \end{aligned} . \tag{5.24}$$

As a result, eigenvectors of $\hat{\mathbf{R}}^x$ related to the target, and possibly, clutter subspace are

$$\mathbf{B} = \mathbf{R}^n_{(1:L),(1:L)} \mathbf{V}^{g,x}_{:,\left(1:\tilde{M}\right)} . \tag{5.25}$$

Here $\tilde{M}$ can be M or $\breve{M}$, similar to the case in MUSIC method, depending on the algorithm. Since the columns of $\mathbf{B}$ and $\breve{\mathbf{V}}$ span the same subspace

$$\mathbf{B}\Upsilon = \breve{\mathbf{V}} \tag{5.26}$$

can be written, where $\breve{\mathbf{V}}$ is a hypothetical matrix that contains target, and possibly clutter echoes depending on the version of the algorithm, expressed in complex exponentials and placed at the columns of this matrix.

Lastly, one finds the TLS solution of equation (5.19) which is given as [11]

$$\left[\mathbf{B}_{(1:end-1),:}\mathbf{B}_{(2:end),:}\right]=\mathbf{U}^{B}\mathbf{S}^{B}\left(\mathbf{V}^{B}\right)^{H} \tag{5.27}$$

$$\mathbf{\Psi}=-\mathbf{V}^{B}_{(1:\tilde{M}),(\tilde{M}+1:end)}\left(\mathbf{V}^{B}_{(\tilde{M}+1:end),(\tilde{M}+1:end)}\right)^{-1}. \tag{5.28}$$

The frequency estimates are then obtained as

$$\mathbf{\Psi}=\mathbf{V}^{\Psi}\mathbf{D}^{\Psi}\left(\mathbf{V}^{\Psi}\right)^{H} \tag{5.29}$$

$$\omega_k=\angle\mathbf{D}^{\Psi}_{k,k},\quad k=1,\ldots,\tilde{M}\,. \tag{5.30}$$

Note that although we have taken into account the non-white autocorrelation of clutter plus noise, it will be seen in section 9.2. that as in the case of MUSIC it gives more reliable results to run the algorithm for $\breve{M}$, rather than for M and then use frequency elimination based on clutter region for obtaining target frequencies.

Another alternative way of implementing ESPRIT can be based on assuming $\mathbf{R}^{n}$ as matrix $\mathbf{I}$ and doing the same derivations. One then obtains total number of $\breve{M}$ target and clutter frequencies by selecting $\tilde{M}=\breve{M}$.

5.5. High Resolution Methods Combined with ML

Estimates obtained from high resolution line component estimations techniques can be improved in an optimal sense. Since the likelihood function possesses lots of valleys, one needs a good initial guess of the optimal point for convergence to the global optimum if not using a difficult multidimensional search. Otherwise, the ML algorithm will stuck to a local optimum point. The aim of the TK, MUSIC or ESPRIT can be to form the aforementioned initial point [11], if further reduction of variance and unbiasedness is desired.

Log-Likelihood function (defined in equation (3.6)) as a function of f_1 and f_2 is plotted in Figure 8 by finding the optimal complex coefficients for each frequency using equation (3.17) under the presence of two targets having frequencies $\left[f_1 \quad f_2\right]=\left[0.2813 \quad 0.3563\right]$. Likelihood function, whose minimum is sought, has

two minima differing by the order of the frequencies and a line in between where the function value is dramatically large. This is the result of taking two frequencies the same, i.e., assuming that the number of targets is one. If high resolution techniques result in poor estimates of parameters, it is improbable for the ML to improve these estimates without employing a global optimization procedure due to the presence of valleys and surface being not convex or concave.

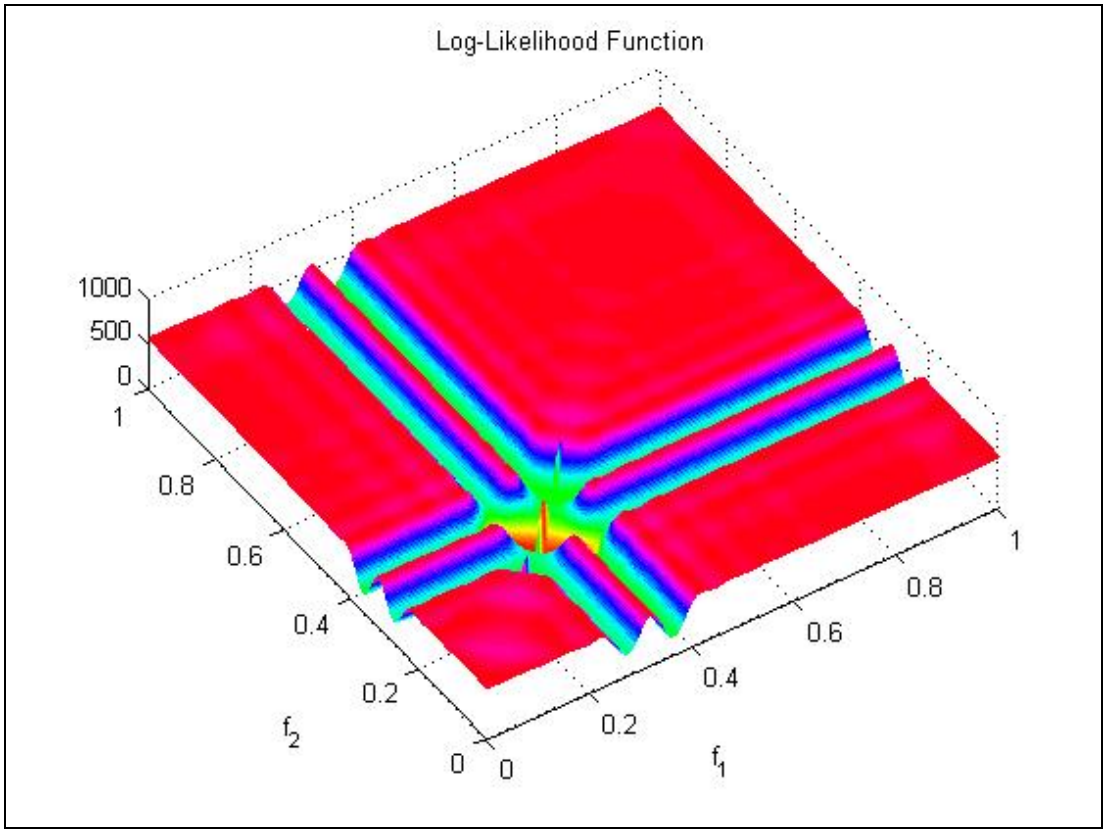

Figure 8 Log-likelihood function for a sample data for CNR=50dB

CHAPTER 6

DETERMINATION OF AMPLITUDES AND PHASES

Finding complex amplitudes after the frequency estimates are obtained can be realized via two different techniques: Least Squares Estimation or Maximum Likelihood technique. Their application to radar observations corrupted with clutter will be explained in this chapter followed by a brief comparison of high resolution line spectra estimation algorithms.

6.1. Least Squares Estimator

This method uses the fact that radar clutter can be modeled as a sum of complex exponentials. Obtaining frequency estimates, one can form the matrix **F** with entries [10]

$$\mathbf{F}_{k,p} = \exp\left(j\omega_p \left(k-1\right)\right), \quad k = 1,\ldots,N, \quad p = 1,\ldots,\breve{M} \tag{6.1}$$

as an intermediate step for obtaining the amplitudes and phases as follows:

$$\left[a_1 \quad \cdots \quad a_{\breve{M}} \right]^T = \left(\mathbf{F}^H \mathbf{F} \right)^{-1} \mathbf{F}^H \mathbf{x} \, . \tag{6.2}$$

Note that we have obtained $\breve{M}$ complex coefficients although only M of them are associated with targets as seen in equation (2.5). Using the fact that clutter is contained in a clutter region with a known mean (D.C. frequency for land clutter), one can distinguish the M complex exponentials of the targets. If the version of the high resolution frequency estimation algorithm yields only target frequencies, a complex exponential signal with a frequency of zero should be associated with land clutter and $\breve{M}$ in equations (6.1) and (6.2) should be selected as $M+1$.

In cases where clutter is modeled with complex exponentials differing very little in frequency, inverse operation in (6.2) can be replaced by pseudoinverse.

6.2. Maximum Likelihood Derivative Equations

Here, we make the assumption that $\mathbf{R}^n$ is known and after frequencies of the targets have been determined use equations (3.9), which are repeated here for convenience,

$$-\mathbf{V}_{:,k}^H \mathbf{Q}\mathbf{x} + \sum_{l=1}^{M} \mathbf{V}_{:,k}^H \mathbf{Q} a_l \mathbf{V}_{:,l} = 0, \quad k = 1,\ldots,M \tag{6.3}$$

to find the amplitudes and phases of the targets.

6.3. Comparison of Techniques

Methods can be classified based on the use of noise autocorrelation matrix: It can be the actual one or the estimated one. ML, whitened versions of MUSIC, HWMAXSIR, and versions of ESPRIT that require $\mathbf{R}^n$ are somewhat ideal in the sense that actual version of this matrix is supplied to the algorithms although there would be estimation errors in practice. Other algorithms do not require this matrix. If one uses ML derivative equations to obtain complex coefficients in the model, it is again assumed that actual $\mathbf{R}^n$ is known. On the other hand, the least squares estimator does not use $\mathbf{R}^n$.

Computational complexity of the algorithms can be accessed by comparing the required operations detailed in the explanation of the algorithms and the time the desired processor spends to perform these tasks. A careful study of this issue has not been performed yet.

CHAPTER 7

CLUTTER REGIONS AND DETERMINATION OF THE NUMBER OF SIGNAL PLUS CLUTTER ZEROS

The number of complex exponentials that comprise targets and the clutter can be determined by various methods: observing the sharp fall in the magnitudes of the eigenvalues of the estimated autocorrelation matrix of observation, $\hat{\mathbf{R}}^x$, or in the magnitudes of the singular values of matrix $\mathbf{A}$ defined in equation (4.14) [1], which fails when the frequencies to be estimated are close to each other; using CFAR hypothesis tests employing multiple thresholds on the noise subspace energy found by the sum of squares of the corresponding singular values [33]; applying Akaike Information Criterion (AIC), Minimum Description Length (MDL) criterion [25] etc.

It is also possible that the number of targets M is provided by another block of the system and one focuses on the high precision velocity estimation of the targets that are in the same folded range. For this case, $\breve{M} - M$ can be changed depending on *CNR* and *rpm* which dictate clutter spreading, or it can be chosen as the maximum value under the specified operational conditions. We have observed that at zero *rpm*, the clutter is modeled just like a single target for all *CNR*. However, as *rpm* increases for different *CNR* levels, clutter can be thought of as a group of targets having similar Doppler frequencies. On the other hand, targets at all *rpm*'s and *SNR*'s are modeled by one zero. When the largest possible $\breve{M} - M$ value is chosen, this covers possible lower values since the estimates beyond the actual number of signal plus clutter estimates will have very small magnitudes. In this method, with the assumption that number of signals, equivalently the number of targets in the same folded range, is provided, zeros falling in the clutter region are eliminated and if the remaining number of zeros is larger than the number of signal

zeros, additional zeros starting with smallest magnitude and outside the clutter region are eliminated. The lastly defined zero could have been caused from the interactions of the clutter and noise with the targets. However, we will not be using the procedure defined in this paragraph, since we propose a better one that does not require the knowledge of M.

Our motivation for the remaining of the chapter will be to develop the model order selection algorithm; show that it functions successfully and allows us to select the total number of targets plus clutter components. Any further increase in the model order corresponds to adding components due to AWGN. Also, the determination of the width of the clutter region is outlined.

We have used a method that depends on the estimated magnitudes of the detected complex exponential signals. For a radar system, number of pulses N, rpm, and the filter order L to be used are generally predetermined and depending on the measured σ_{WN}^2 and CNR, we vary the threshold which one should compare the estimated magnitudes to, in order to achieve a fixed probability of false alarm (P_{FA}), which is defined outside the clutter region. It is the probability of occurrence of one or more detections when there are no targets present and in radar systems it is tried to be kept fixed. Under constant P_{FA}, two conditional probabilities measured outside the clutter regions are of interest: Given that there are M targets, the probability that at least one detection occurs (P_D), called probability of detection, and under the same condition the probability that the exact number of target detections (M) are made (P_C), called probability of correct number of detections. In Chapter 9, the events contributing to P_C are considered in obtaining the estimate variances and means. The aim of any method should be to maximize P_D and/or P_C under constant P_{FA}.

Let us now explain the details of the algorithm that makes a threshold comparison of the estimated magnitudes: Starting from an estimate of $\breve{M}$ being 1 and increasing it up to L, one makes threshold comparison for estimated amplitudes to find the total number of targets and clutter components. We stop when there is an amplitude estimate below the threshold for the first time and decrease the assumed number of complex exponentials of that try by 1 to find $\breve{M}$. Note that the maximum

number of targets allowed in the data, the maximum M value, is limited such that $\breve{M} \leq L$ should be satisfied. We do not start the test by assuming $\breve{M}$ to be L in order to achieve noise reduction at each step.

A set of design graphs for our selected parameters are presented in Figure 9 - Figure 18. In Figure 9- Figure 14, there are no targets and CNR is varied. For Figure 15 - Figure 18, there are two targets with frequencies $[f_1 \quad f_2] = [0.2813 \quad 0.3563]$ are present and their SNR is changed at $CNR = 50dB$. Let us now detail how these figures are obtained:

1. FBTK algorithm is used (any other algorithm can also be used) and run with the assumption of the specified number of complex exponentials $\breve{M}$ indicated in Figure 9 - Figure 18. In fact, it will be clear that the assumed $\breve{M}$ values in Figure 9 - Figure 18 are greater than the actual $\breve{M}$ values by 1.

2. Each simulation yields frequency and associated amplitude estimates. The number of these pairs is equal to the assumed number of complex exponentials.

3. These pairs resulting from each simulation run are sorted based on amplitude estimates. Thus, frequency estimates are ordered in such a way that their associated amplitude estimates follow a sorted order.

4. Sorted results of all simulations, when combined, form groups of estimates. Each of these groups of frequency or amplitude estimates is plotted with another sorting through the simulations. This sorting is done separately for amplitude and frequency estimates. Thus, the link between the frequency and amplitude estimates of a single simulation run is destroyed, but the aforementioned grouping establishes a link among the highest amplitude estimates of all simulations; a different link among the frequency estimates associated with the highest amplitude estimates; a different one among the lowest amplitude estimates of all simulations; a different one among the frequency estimates associated with the lowest amplitude estimates, and so on.

Interpretation of Figure 9 - Figure 18 is as follows:

1. In these figures, parts of the graphs where slope is low indicate that there is a large probability of observing the output read from the y-axis. Conversely, parts of the graphs where slope is high indicate that there is a very small probability of observing the output read from the y-axis.

2. When the assumed number of complex exponentials exceeds $\breve{M}$, the estimate having the complex multiplier with the smallest amplitude will separate out. The frequency estimate for this complex multiplier will be approximately uniformly distributed in $(-0.5, 0.5]$ excluding the neighborhood of target frequencies as observed in Figure 9 - Figure 18. This denotes the step where FBTK algorithm is run with $\breve{M}+1$ and thus $\breve{M}$ is found. In the number of complex exponential determination algorithm one can reduce the computational load by not starting the iterations from $\breve{M}=1$, but from a value consistent with the given CNR.

3. The clutter region can be found by determining the width of the region around the frequency of 0 (note that frequencies repeat themselves in mod 1) by observing where frequency estimates are concentrated on the y-axis. It can be observed from the increasing number of frequency estimate graphs indicating frequency values near 0 and increasing number of amplitude graphs indicating large amplitude values in Figure 9 - Figure 18 that as CNR is increased, clutter needs to be modeled by increasing number of complex exponentials, but is confined in an interval called the clutter region. The determination of the clutter region's width is clearly shown in Figure 14. Note that clutter region width is not a parameter to be selected after fixing the system parameters. One should use the corresponding value for it.

4. As a final remark on Figure 9 - Figure 18, these graphs cannot be used to evaluate P_{FA}, P_D, or P_C since all these probabilities are defined outside the clutter windows, or equivalently regions, and the aforementioned figures are used to determine the width of the clutter window and show the rationale behind model order detection algorithm.

The dependence of threshold value on CNR is expected to be a weak one since P_{FA} which is tried to be kept fixed is defined outside the clutter region and it will be shown that clutter region width can be selected to be the same for all CNR values. Once N, rpm, and L are selected, one can determine the clutter region width, which models the spread of clutter frequencies around a mean value, from design figures obtained for all possible operational values of the clutter power.

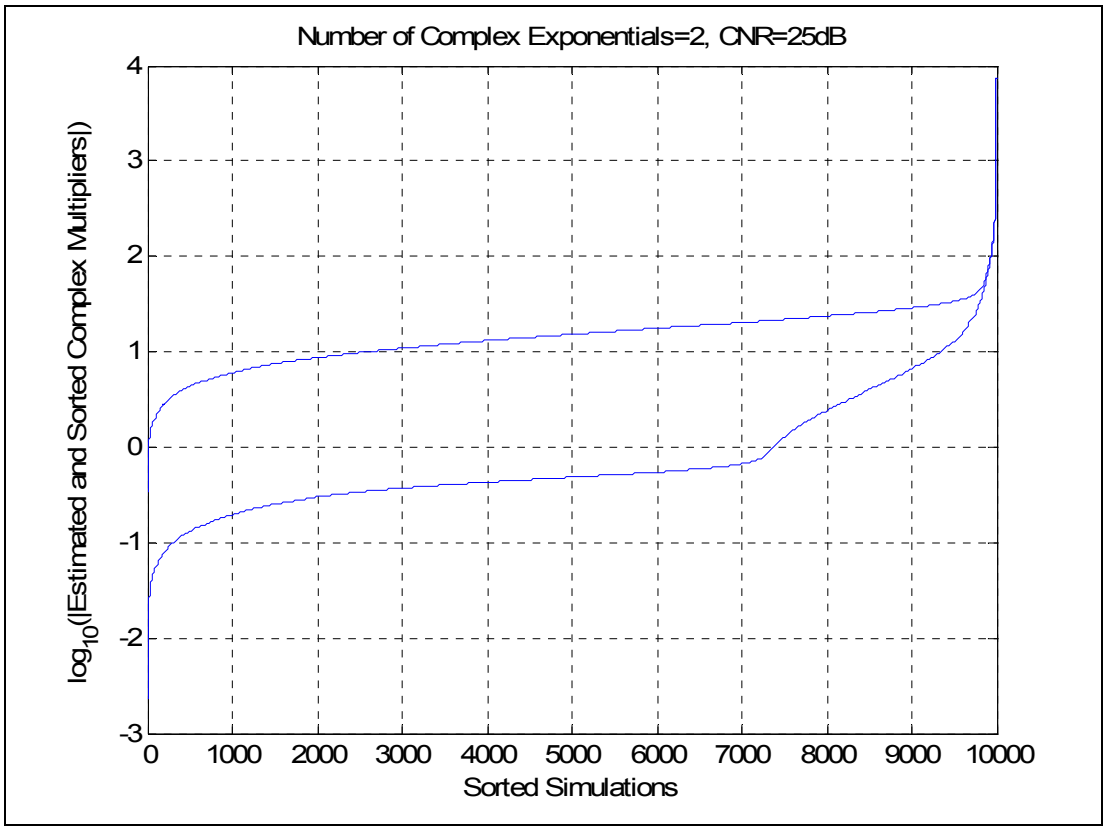

Figure 9 Complex multiplier estimates of FBTK when no targets are present, CNR=25dB

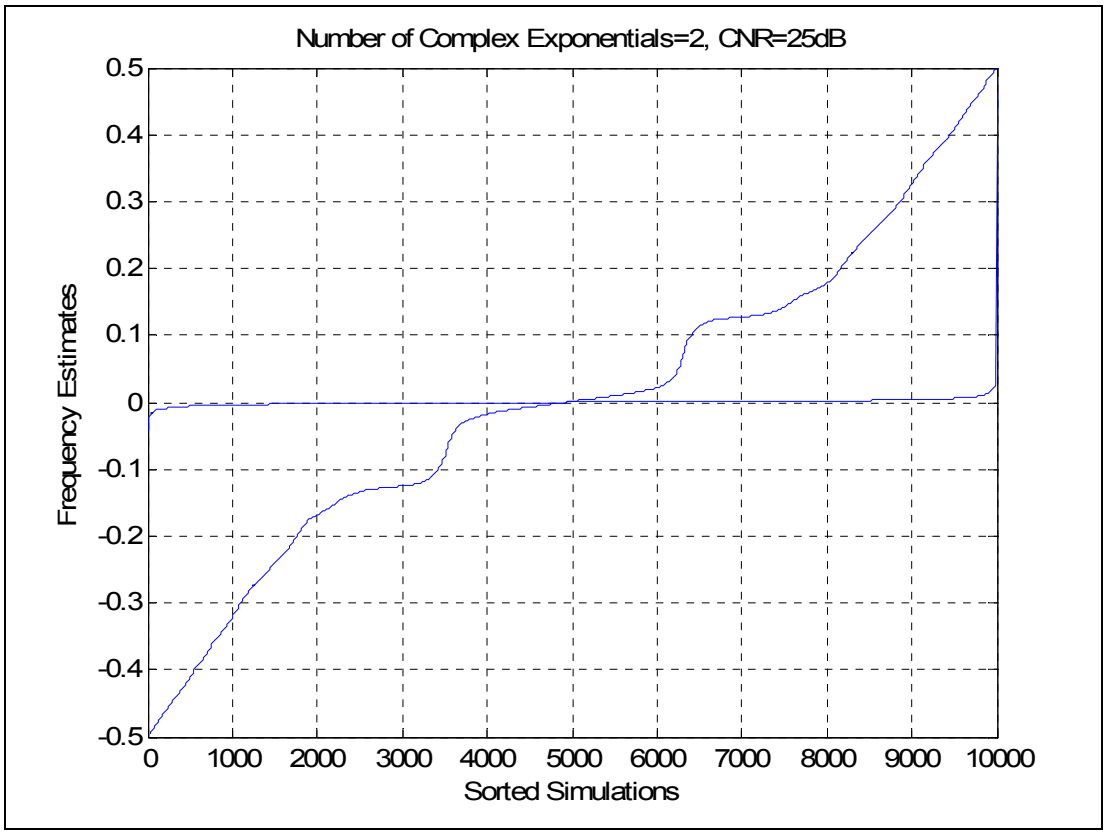

Figure 10 Frequency estimates of FBTK when no targets are present, CNR=25dB

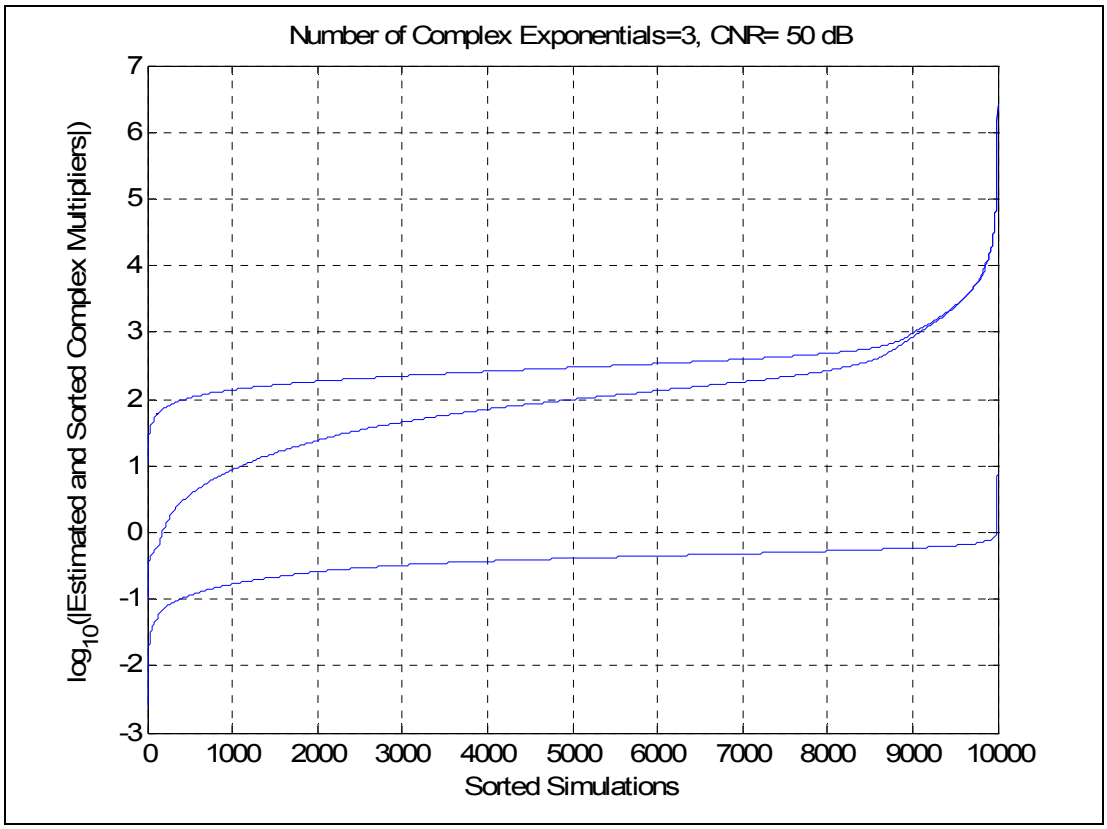

Figure 11 Complex multiplier estimates of FBTK when no targets are present, CNR=50dB

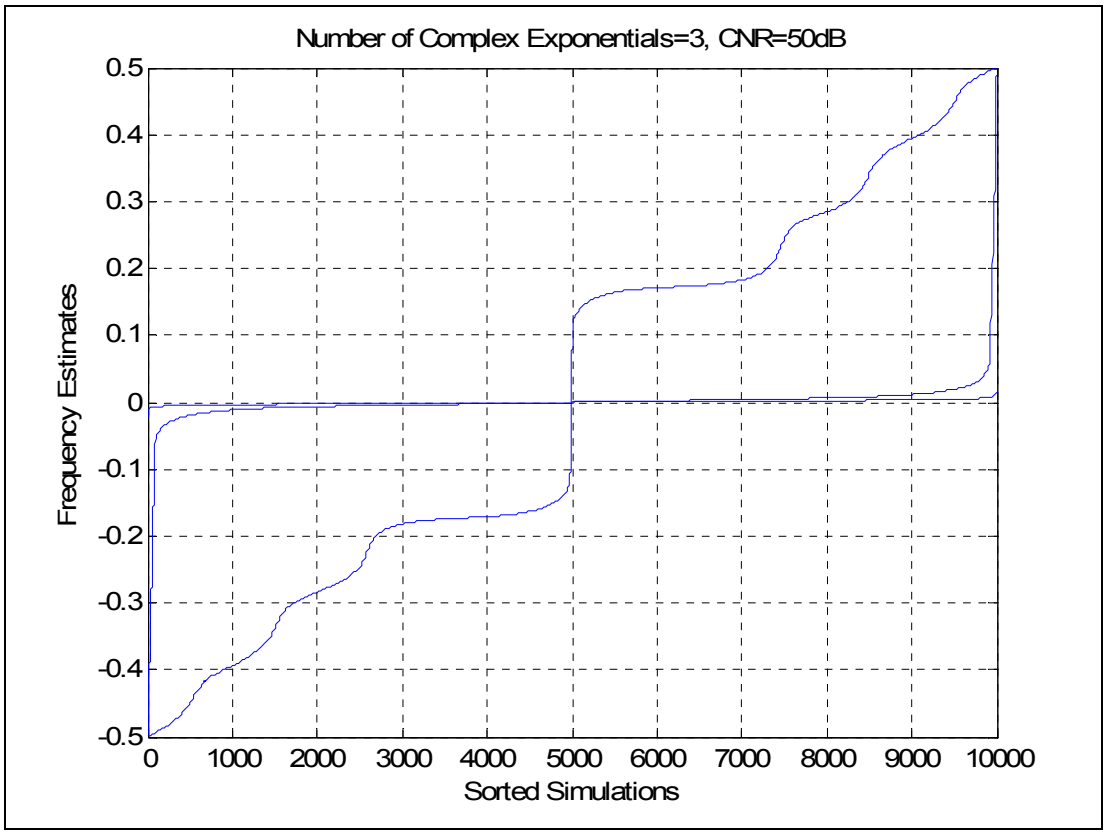

Figure 12 Frequency estimates of FBTK when no targets are present, CNR=50dB

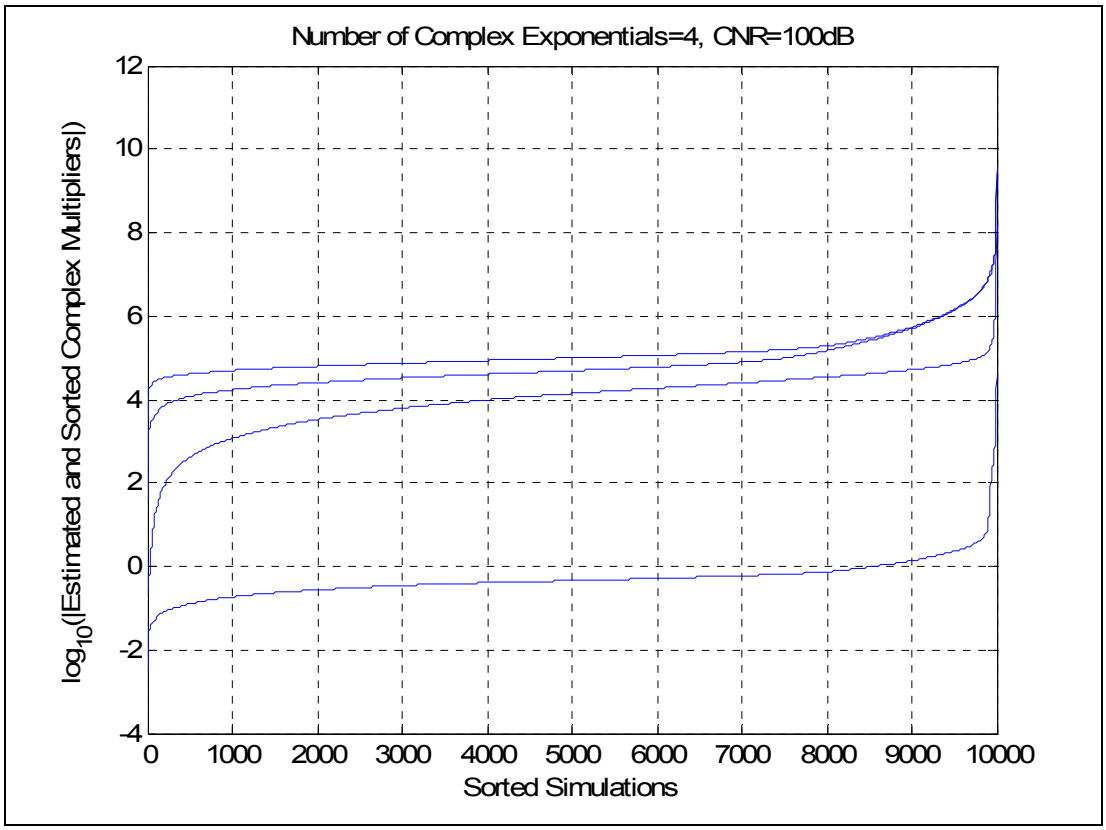

Figure 13 Complex multiplier estimates of FBTK when no targets are present, CNR=100dB

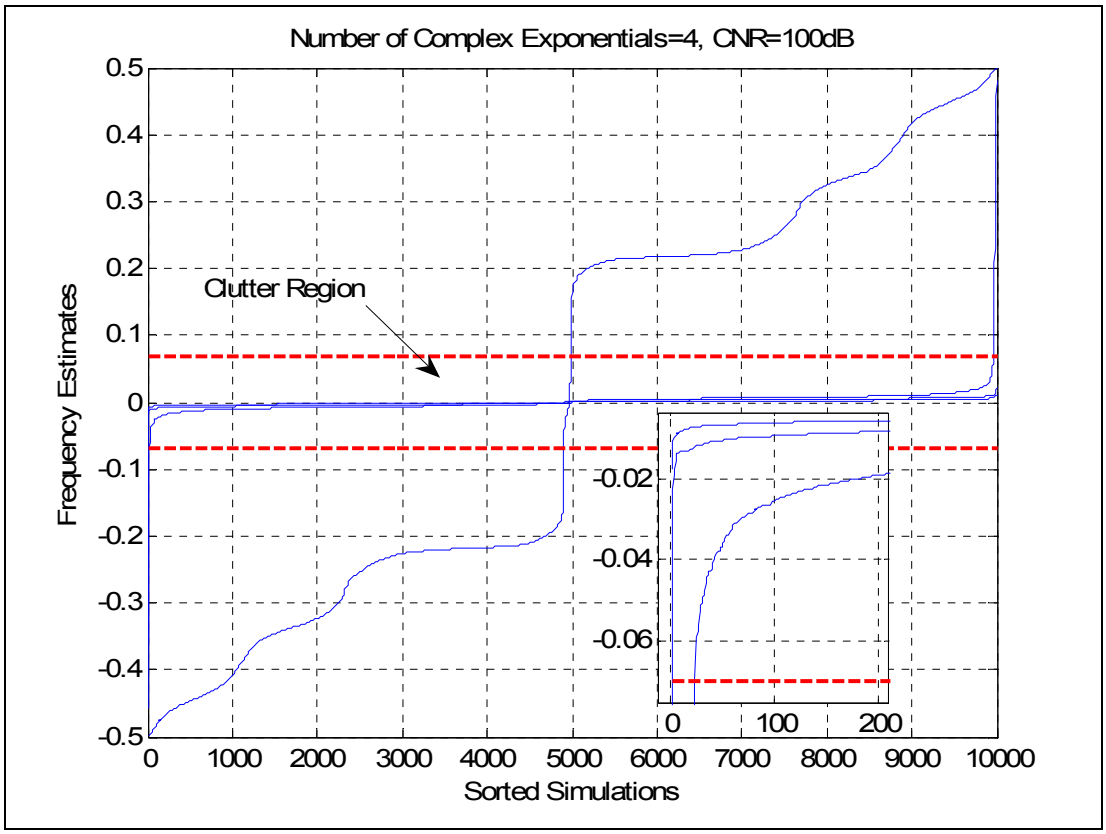

Figure 14 Frequency estimates of FBTK when no targets are present with a zoomed in view provided to show the determination of the clutter region width, CNR=100dB

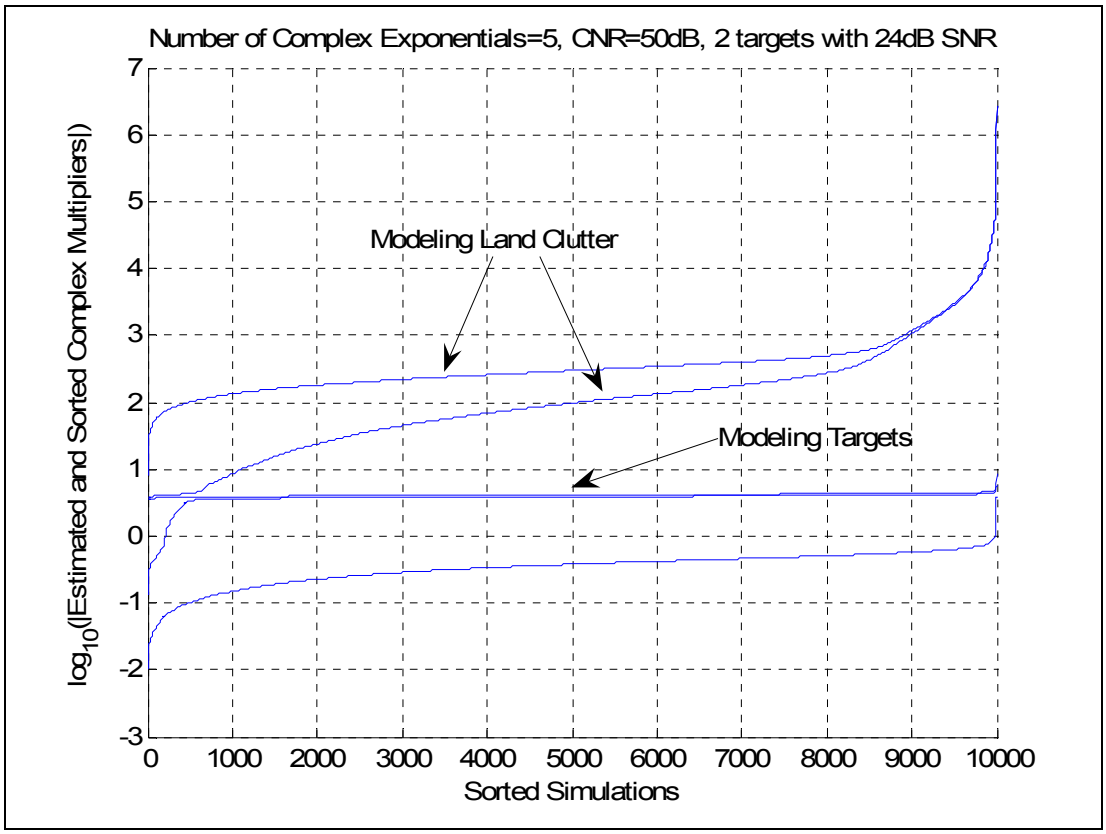

Figure 15 Complex multiplier estimates of FBTK, CNR=50dB, SNR=24dB

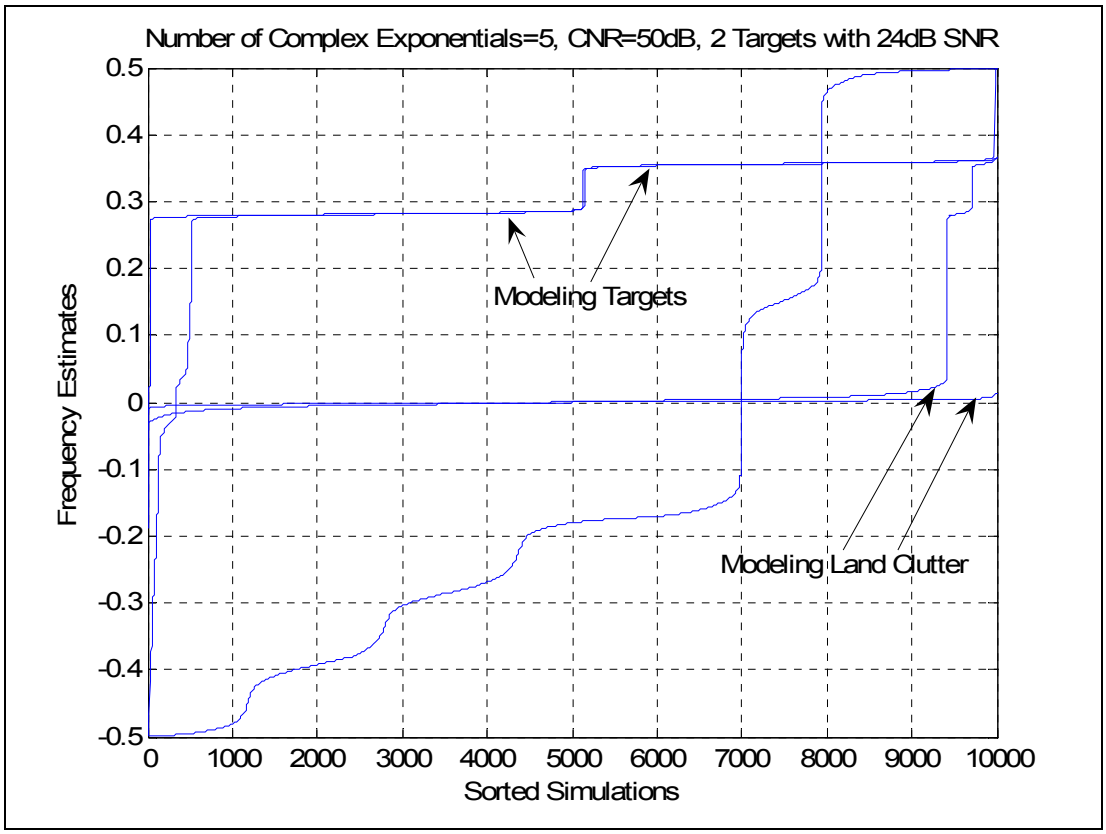

Figure 16 Frequency estimates of FBTK, CNR=50dB, SNR=24dB

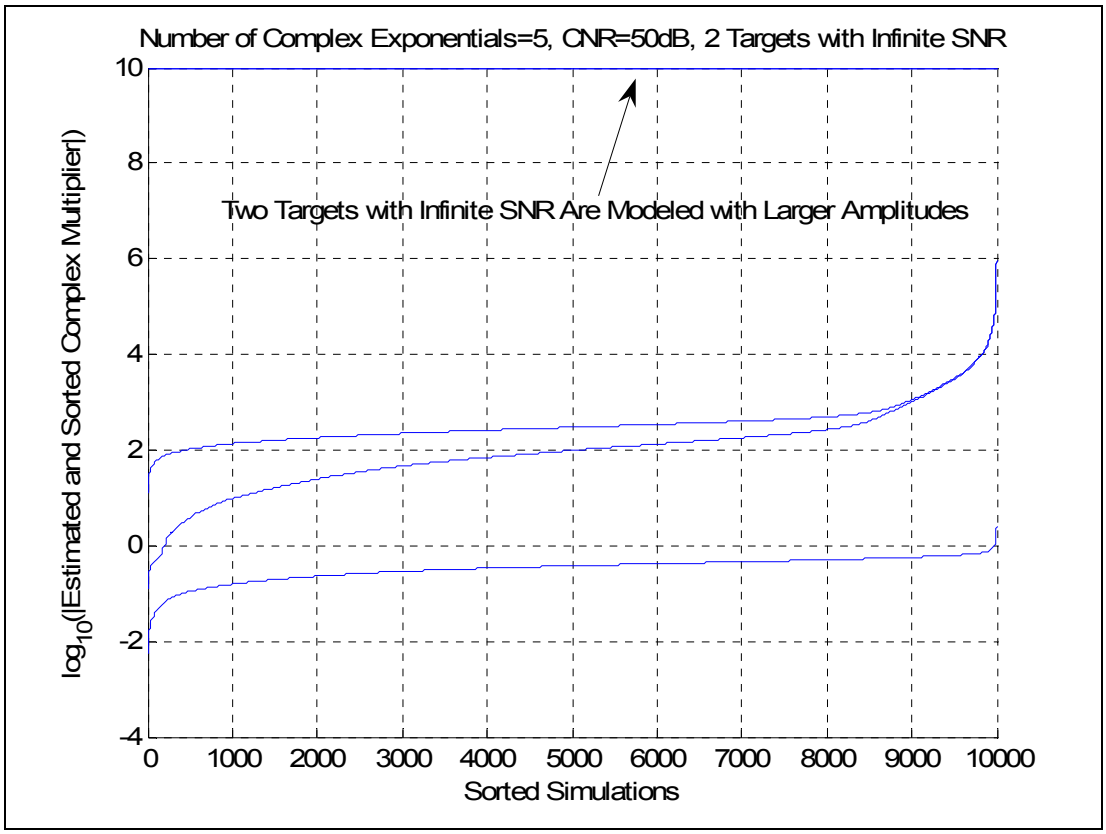

Figure 17 Complex multiplier estimates of FBTK, CNR=50dB, infinite SNR case

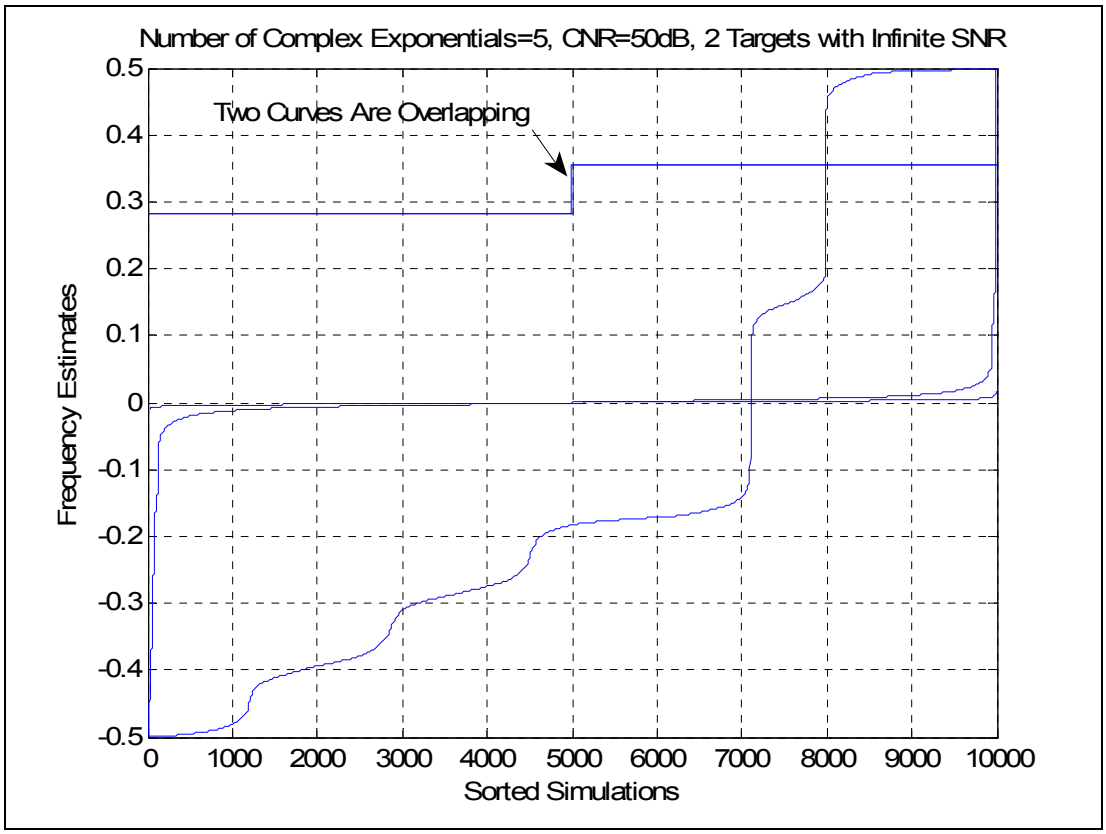

Figure 18 Frequency estimates of FBTK, CNR=50dB, infinite SNR case

We have observed that a logic that also uses the information about the closeness of the zeros to the unit circle is not very reliable since as the assumed $\breve{M}$ value increases during the hypothesis tests, more zeros move towards the unit circle, making it impossible to estimate the actual $\breve{M}$ value. However; it has been observed for the method that uses a threshold based on magnitudes that for 95% of the time, at the last iteration, where $\breve{M}+1$ is tried, the $\left(\breve{M}+1\right)^{st}$ zero is well separated from the first $\breve{M}$ zeros nearer to the unit circle.

The correlation between the two procedures, namely, the observation that frequency components with large magnitudes are located closer to the unit circle, can be used to determine a joint number of target detector logic as a future work. Magnitude elimination method and closeness of zeros to the unit circle differ since a

second or third clutter zero can be the one farthest from the unit circle among the selected zeros, while it results in a large magnitude since very closely spaced complex exponentials result in high amplitude levels when least squares method is used in amplitude determination.

Procedure to decide on M and $\breve{M}$ is not repeated for each high resolution line component estimation technique, but the results obtained from using FBTK are used in other algorithms. This is to ensure same level of noise reduction in all algorithms and compare their effectiveness under given $\breve{M}$.

CHAPTER 8

LTI MAXSIR FILTER DESIGN FOR LAND CLUTTER

In this chapter, we will investigate possibilities on whether there exists pre-processing algorithms that can improve the performance of FBTK algorithm.

When one pre-whitens the data through the transformation

$$\mathbf{y} = \left(\mathbf{R}^n\right)^{-1/2} \mathbf{x}, \tag{8.1}$$

$\mathbf{y}$ with its N samples cannot be processed directly with the FBTK algorithm to obtain the frequencies of the targets because the complex exponential model of $\mathbf{x}$ is not preserved with this transformation.

We will derive the optimal linear time-invariant (LTI) filter in terms of $SCNR$ maximization when the Doppler frequency of the target is known to lie in a certain interval and show that its presence cannot improve the estimation results obtained by LP. We have chosen an LTI filter so that the input frequency components will be observed at the output with possibly amplitude and phase distortion. Since one cannot do much when the target is in the clutter region, the interval in which the frequencies of targets should lie will be chosen as uniform distribution outside the land clutter region.

In order to satisfy the WSS condition, one can use only $N-K+1$ number of samples at the output of the designed filter $\mathbf{u}$, i.e., the transient samples at both ends should be discarded and only the samples resulting from parts of $\mathbf{x}$ and $\mathbf{u}$ fully overlapping should be used. Let us assume that phases of complex multipliers of targets are uncorrelated and uniformly distributed in $(-\pi, \pi]$. Also, complex exponential frequencies ω_i's modeling targets are taken to be uniformly distributed in $\left(-\pi, \frac{-\pi}{\beta}\right) \cup \left(\frac{\pi}{\beta}, \pi\right]$. We define the optimum filter $\mathbf{u}$ as

$$\mathbf{u} = \begin{bmatrix} u_0 & \cdots & u_{K-1} \end{bmatrix}^T \tag{8.2}$$

and, considering equations (2.5) and (3.14), $\mathbf{s}$ as

$$\mathbf{V}\mathbf{a} = \mathbf{s} = \begin{bmatrix} s_0 & \cdots & s_{N-1} \end{bmatrix}^T. \tag{8.3}$$

Output signal energy from the filter is

$$\begin{aligned} &\underset{\omega_1,\ldots,\omega_M,\mathbf{a}}{E}\left\{\sum_{i=K-1}^{N-1}\left|\sum_{k=0}^{K-1}u_k s_{i-k}\right|^2\right\} \\ &= \left(N-K+1\right)\sum_{k=0}^{K-1}\sum_{m=0}^{K-1}u_k u_m^* f_M\left(m-k\right) \end{aligned} \tag{8.4}$$

where

$$f_{M,\beta}\left(m-k\right) = \text{constant}\left(\text{M},\beta\right)\frac{\sin\left(\pi\left(m-k\right)\right)-\sin\left(\frac{\pi}{\beta}\left(m-k\right)\right)}{m-k} \tag{8.5}$$

while the output clutter energy is

$$\begin{aligned} &E\left\{\sum_{i=K-1}^{N-1}\left|\sum_{k=0}^{K-1}u_k n_{i-k}\right|^2\right\} \\ &= E\left\{\sum_{i=K-1}^{N-1}\sum_{k=0}^{K-1}\sum_{m=0}^{K-1}u_k u_m^* n_{i-k} n_{i-m}^*\right\} \\ &= \sum_{i=K-1}^{N-1}\sum_{k=0}^{K-1}\sum_{m=0}^{K-1}u_k u_m^* R^n\left(m-k\right) \end{aligned} \tag{8.6}$$

where $R^n\left(\bullet\right)$ is the autocorrelation sequence of the colored noise.

Passing to the vector-matrix notation, the problem becomes the maximization of the Lagrangian

$$\Lambda\left(\mathbf{u}\right) = \mathbf{u}^H\mathbf{F}^{M,\beta}\mathbf{u} - \lambda\left(\mathbf{u}^H\mathbf{R}^n\mathbf{u} - c\right) \tag{8.7}$$

where

$$\mathbf{F}_{m,k}^{M,\beta} = f_{M,\beta}\left(m-k\right). \tag{8.8}$$

The solution can be obtained as follows:

$$\begin{aligned} \nabla_{\mathbf{u}^*}\Lambda &= \mathbf{0} \\ \mathbf{F}^{M,\beta}\mathbf{u} - \lambda\mathbf{R}^n\mathbf{u} &= \mathbf{0} \\ \left(\mathbf{R}^n\right)^{-1}\mathbf{F}^{M,\beta}\mathbf{u} - \lambda\mathbf{u} &= \mathbf{0} \\ \left(\left(\mathbf{R}^n\right)^{-1}\mathbf{F}^{M,\beta} - \lambda\mathbf{I}\right)\mathbf{u} &= \mathbf{0} \end{aligned} \tag{8.9}$$

From the last equation it is clear that optimal $\mathbf{u}$ is an eigenvector of $\left(\mathbf{R}^n\right)^{-1}\mathbf{F}^{\beta}$, where it is evident that the constant in equation (8.5) is of no importance and thus

dependence of $\mathbf{F}^{M,\beta}$ on M is dropped. Since SCNR is λ and has to be real, one chooses the eigenvector of $\left(\mathbf{R}^{n}\right)^{-1}\mathbf{F}^{\beta}$ corresponding to the largest real eigenvalue.

After finding the frequencies of the targets by using LTI MAXSIR filtering followed by any one of the line spectra estimation algorithms, one still needs to use the data prior to LTI MAXSIR filtering to obtain the amplitudes and phases of the targets by using one of the two methods mentioned in Chapter 6.

K tap filter, due to the fact that signal is modeled outside the clutter region, converges to a conventional pulse canceller as seen in Figure 19. The results of preceding FBTK with the LTI MAXSIR filter developed in this chapter will be shown in section 9.6.

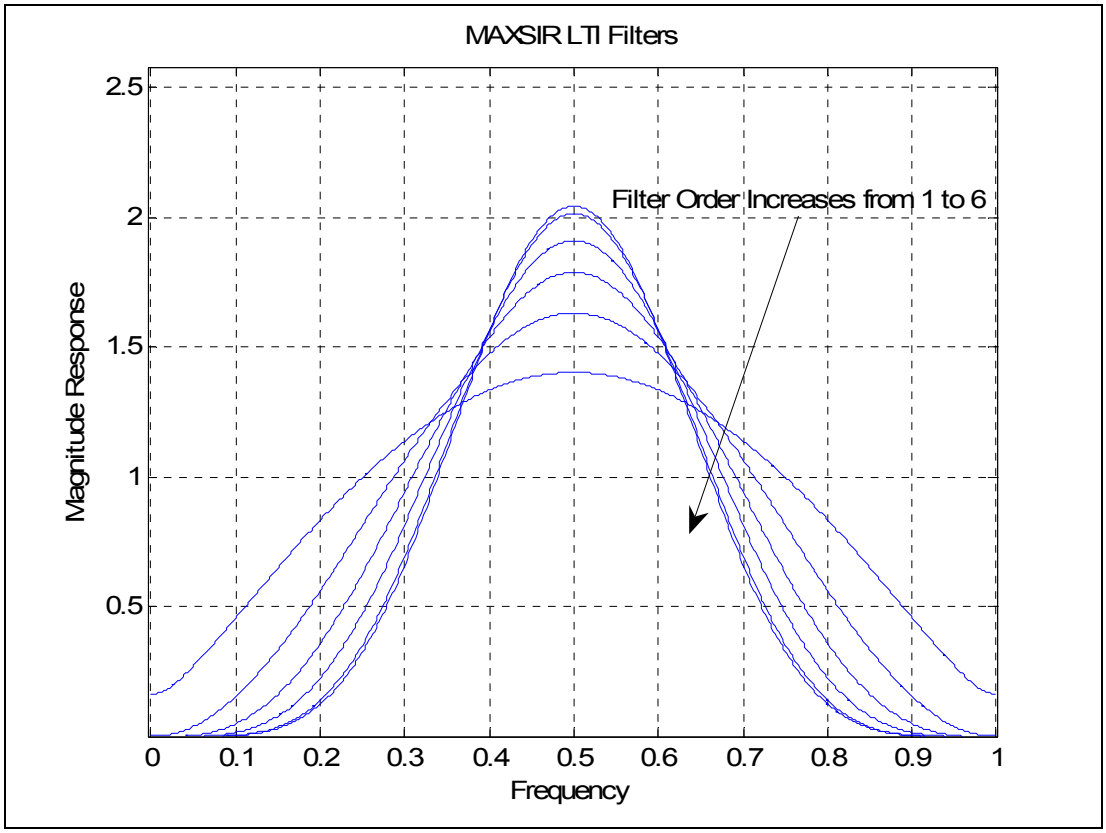

Figure 19 LTI MAXSIR filters of different orders

CHAPTER 9

SIMULATION RESULTS

In this chapter we present the results pertaining to performances of the various algorithms discussed so far. The results have been obtained using Monte-Carlo simulations.

9.1. Simulation Parameters

Unless otherwise stated, the default simulation parameters are as follows: $rpm = 30, \theta^{\circ}_{2WHP} = 1.2728^{\circ}, PRI = 10^{-4}s, N = 16, L = 9, CNR = 45dB, M = 2, SNR = 24dB,$ $\begin{bmatrix} f_1 & f_2 \end{bmatrix} = \begin{bmatrix} 0.2813 & 0.3563 \end{bmatrix}, MCCR = -5dB, f_c = 0.7688$ and number of simulations= 10000. In the simulations the noise power σ^2_{WN} is kept fixed at 1. *SNR* or *CNR* is varied to obtain the necessary graphs. Both of the targets are assumed to have the same fixed *SNR* , thus same fixed amplitude, throughout the simulations and phases of the targets are uniformly distributed in $[0, 2\pi)$ and random phase values are used in each simulation.

Moving clutter will be considered in Chapter 10, so the results in this chapter include only the land clutter. The results are expected to be the same for moving clutter since the only difference in their models (see Chapter 2) is that land clutter is centered at zero frequency.

Clutter region width does not depend on *CNR* or σ^2_{WN} and as can be interpreted from design graphs suited to our selected parameters and depicted in Figure 9 - Figure 18, where all possible clutter powers of interest are considered, taking its width to be ±0.07 around its center is considered to be a good choice for the selected parameters.

Table 1 gives the number of detections of the FBTK method that are outside the clutter region, and thus identified as targets, for various *SNR* levels. $M = 2$ is

assumed except for the row having zero amplitudes for the two targets and depicting $M = 0$ case. For the 10000 simulations performed for each SNR level, the amplitudes of the two targets are taken to be the same.

P_{FA}, P_D and P_C values defined for detections occurring outside the clutter region can be obtained from Table 1. P_{FA}, which is defined for the no target case, can be obtained from the associated row by $1-10^{-4}\times$(the entry of the column associated with zero number of detected targets), where 10^{-4} is one over the number of simulations. P_{FA} is 5×10^{-4} and the corresponding threshold on amplitudes is 1 when σ_{WN}^2 is selected as 1. Simulations can be performed to obtain the threshold levels for all σ_{WN}^2 and CNR values so as to satisfy fixed P_{FA} although CNR is expected to have a small effect on the determination of the threshold. P_D is obtained similarly, but only the rows obtained under the presence of targets can be used, since otherwise P_D is not defined. For an SNR level of $24dB$, P_D is 0.9512. P_C is also defined under the presence of targets, and since $M = 2$ is taken, it is found by 10^{-4} times the entry of the column associated with two detected targets. P_C for an SNR level of $24dB$ is 0.9006.

Table 1 Distribution of number of detections for various SNR levels, CNR=45dB

		Number of Detected Targets					
Amplitude	SNR, dB (see equation (2.20))	0	1	2	3	4	5 or more
0	No Targets	9995	3	2	0	0	0
1	12	3825	4527	1648	0	0	0
2	18	914	683	8395	4	4	0
4	24	488	501	9006	3	2	0
8	30	129	233	9633	3	2	0
16	36	74	25	9898	2	1	0
32	42	17	0	9981	1	1	0

For the simulation results $f_i - \left\langle \hat{f}_i \right\rangle, \left\langle \left| a_i - \hat{a}_i \right| \right\rangle$, which are biases or mean separations, $\sqrt{\mathrm{var}\left(f_i\right)}$, which is standard deviation (stdev), and $\sqrt{\left\langle \left| a_i - \hat{a}_i \right|^2 \right\rangle}$, which is the root mean square (RMS) value of separation, will be presented; where $\langle \bullet \rangle$ operator stands for averaging over the simulations. Estimated frequencies and actual ones are associated in such a way that the total difference between the associated pairs is minimized. If this is equal, the one with the smaller difference between the associated pair differences is selected.

9.2. Selection of the Superior Algorithms

Extended simulations have been performed only for the algorithms that yielded lower standard deviations and biases for their estimates. For this purpose Table 2 is prepared. 'C # TD' stands for correct number of target detections. 'Cov' or 'W' indication means that the algorithm uses the matrix $\mathbf{R}^n$ instead of matrix **I** as explained in previous chapters also listed in Table 2.

The number of target plus clutter zeros are determined by the FBTK method, so no M or $\breve{M}$ values are provided as inputs to any algorithm. However, any other algorithm can also be used instead of FBTK method for the determination of model order. Consequently for the selected case, the results of the algorithms other than FBTK are considered valid only when they are provided with the number of target plus clutter zeros that causes correct decision for the FBTK method. This is done in order to observe the performance of the model order detector and the line spectra estimation algorithms separately since a different block for the determination of the number of targets plus clutter can be employed. It can be seen that it is not the class of the algorithm like TK, MUSIC, and ESPRIT, but the version of it, i.e., 'FB,' 'W,' etc., that determines the correct number of decisions as seen in Table 2.

Table 2 Performance of all the algorithms for the selected operating condition

	f_1 stdev	f_1 bias	f_2 stdev	f_2 bias	C # TD
FTK (see section 4.3.)	2,41E-02	1,67E-03	1,61E-02	-1,01E-03	2810
BTK	1,28E-02	8,42E-04	1,89E-02	-1,09E-03	2802
FBTK	2,73E-03	3,08E-05	2,80E-03	-2,33E-04	9017
FBTK, NRDV	2,74E-03	-4,13E-05	2,82E-03	9,70E-05	9014
FBTK + ML (see sections 3.2., 4.3.)	2,29E-03	-7,77E-05	2,28E-03	2,75E-05	9017
M (see sub-sections 5.2.2., 5.2.3.)	4,27E-03	1,37E-04	1,37E-02	-6,08E-04	3567
M, FB	3,25E-03	-1,28E-04	3,15E-03	1,33E-04	9010
M, W	7,38E-03	-2,50E-05	1,97E-02	-1,22E-03	8617
M, WFB	8,47E-03	-2,08E-05	1,72E-02	-8,04E-04	7721
M, W (Clutter Counted as Target)	4,33E-02	2,74E-01	1,48E-01	1,16E-01	9017
M, WFB (Clutter Counted as Target)	1,25E-01	7,72E-02	3,21E-02	8,50E-03	9017
Esp (see sub-section 5.4.2.)	4,77E-03	-1,99E-04	4,58E-03	2,12E-05	5576
Esp, FB	3,16E-03	-9,80E-05	3,16E-03	1,04E-04	9016
Esp, Cov	2,93E-02	1,85E-03	3,79E-02	-5,78E-03	1056
Esp, Cov FB	3,96E-02	2,84E-03	3,74E-02	-5,69E-03	2963
Esp, Cov (Clutter Counted as Target)	3,21E-02	2,66E-01	1,47E-02	8,35E-03	9017
Esp, Cov FB (Clutter Counted as Target)	6,61E-02	2,40E-01	3,64E-02	2,10E-02	9017
HWMAXSIR (see section 3.1.)	3,04E-02	-7,21E-03	9,49E-03	-1,73E-02	9017
HWMTI	2,88E-02	-1,22E-02	0,00E+00	-1,88E-02	9017
HWMTI_11	1,62E-02	1,04E-02	3,14E-02	6,45E-04	9016
HWMTI_121	3,03E-02	-1,84E-02	2,89E-02	-1,57E-02	9017
CR Bound, ML (see sections 3.2., 3.3.)	8,17E-04	0,00E+00	8,12E-04	0,00E+00	

Standard deviation and mean estimates are obtained from variable number of simulations. We do so because discarding some samples in calculations is not meaningful although this results in variable confidence intervals. We shall note that confidence intervals decrease with the number of considered simulations [34] - [36], i.e., those that yield correct number of target detections. For the results that are

presented, ten thousand simulations are made and only those that yield correct number of target estimations are used in obtaining the figures.

We have used the MATLAB function *fminunc*, which solves unconstrained optimization problems by finding the minimum of the cost functions, without providing Gradient or Hessian information (see Appendix A) except for the cases of low *SNR* or closely spaced complex exponential frequencies. The results are just indicative of the fact that estimates can be improved with ML processing.

Only five of the algorithms presented in Table 2 will be considered for further analysis because they yield the lower biases and standard deviations. Namely, they are FBTK, 'FBTK, NRDV,' 'FBTK + ML,' 'M, FB,' and 'Esp, FB'. We can observe that 'W' or 'Cov' versions of the algorithms require to run with $\breve{M}$ rather than M and employ the clutter region concept for better estimates. However, we can conclude from the simulations that these versions of the algorithms are inferior to the versions that do not use the actual clutter plus noise autocorrelation matrix and consider the clutter as additional number of targets and formulate the problem in white noise.

Considering the computational complexities of the selected algorithms, although not conclusive in any sense, time consumption of the algorithms can be ordered from lowest to highest as 'Esp, FB,' FBTK, 'FBTK, NRDV,' and 'M, FB'.

9.3. Analysis of Linear Prediction and FBTK Algorithm

Linear prediction uses the autocorrelation matrix of the clutter plus noise, not the actual observation vector. Thus, we call it Ideal LP. As a result, the estimates will not have any variation, but only a bias. As can be seen from Figure 20, this bias decreases with the order L of $H^{Ideal}(z)$ in equation (4.4). This bias may result from the zeros of targets, clutter, and noise affecting each other's position.

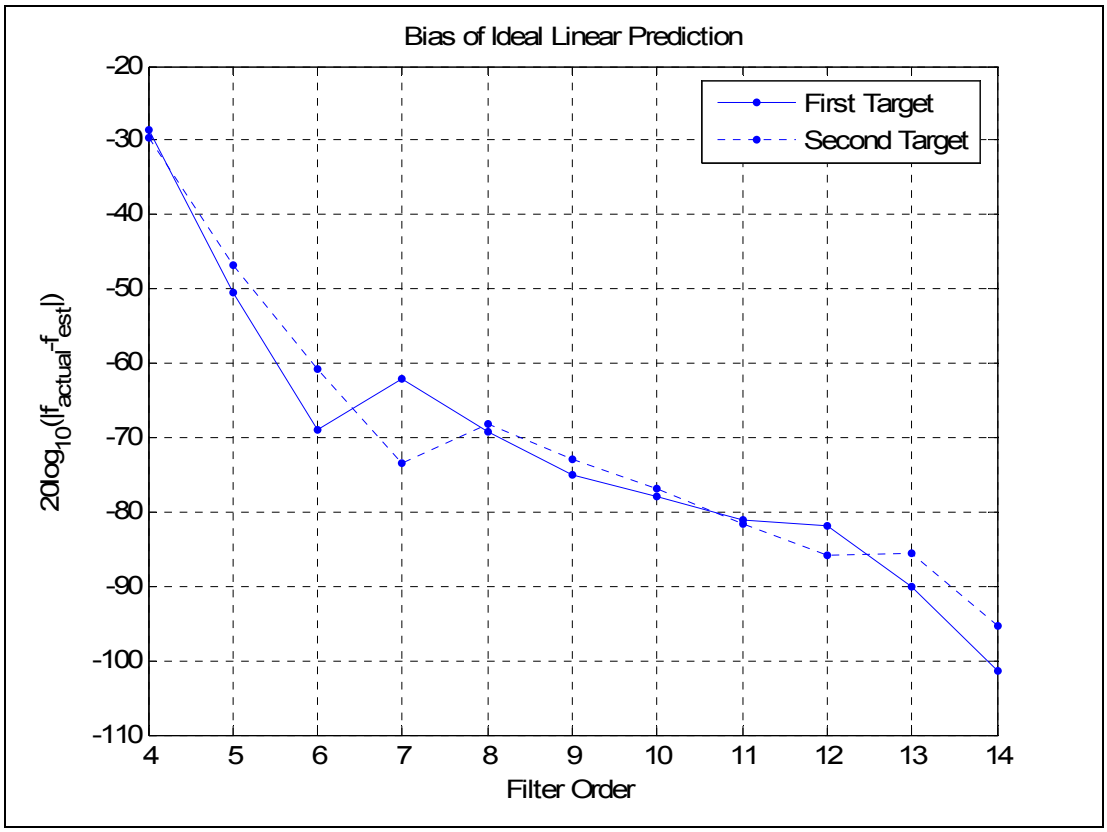

Figure 20 Bias of linear prediction when clutter plus noise autocorrelation is known

Standard deviation and bias of the estimates obtained by the FBTK method under varying L of equation (4.20) are shown in Figure 21 and Figure 22. The reason why we selected L as 9 is clear from the figures. This value is different from the proposed value of $3N/4$ in [1]. The same value of L is used in the other algorithms as well in selecting the size of the estimated autocorrelation matrix of the observation vector (equations (5.4) and (5.6)).

Increased order L of the prediction filter improves the resolution capability of the filter; however, too large values for L results in $L-\breve{M}$ redundant zeros to fluctuate in their locations and move towards the unit circle resulting in spurious zeros. This results from the observation that elements of $\hat{\mathbf{R}}^{x}$ are formed from less number of samples.

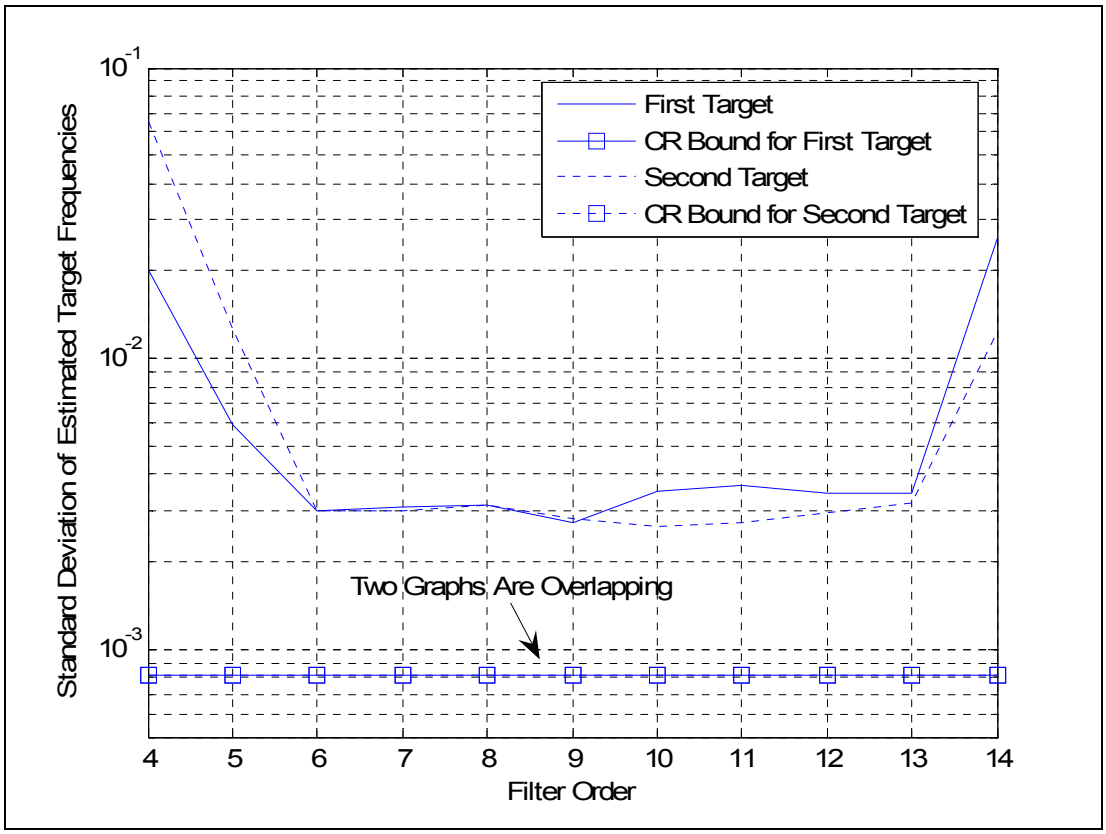

Figure 21 Standard deviation of FBTK frequency estimates for different filter orders, L

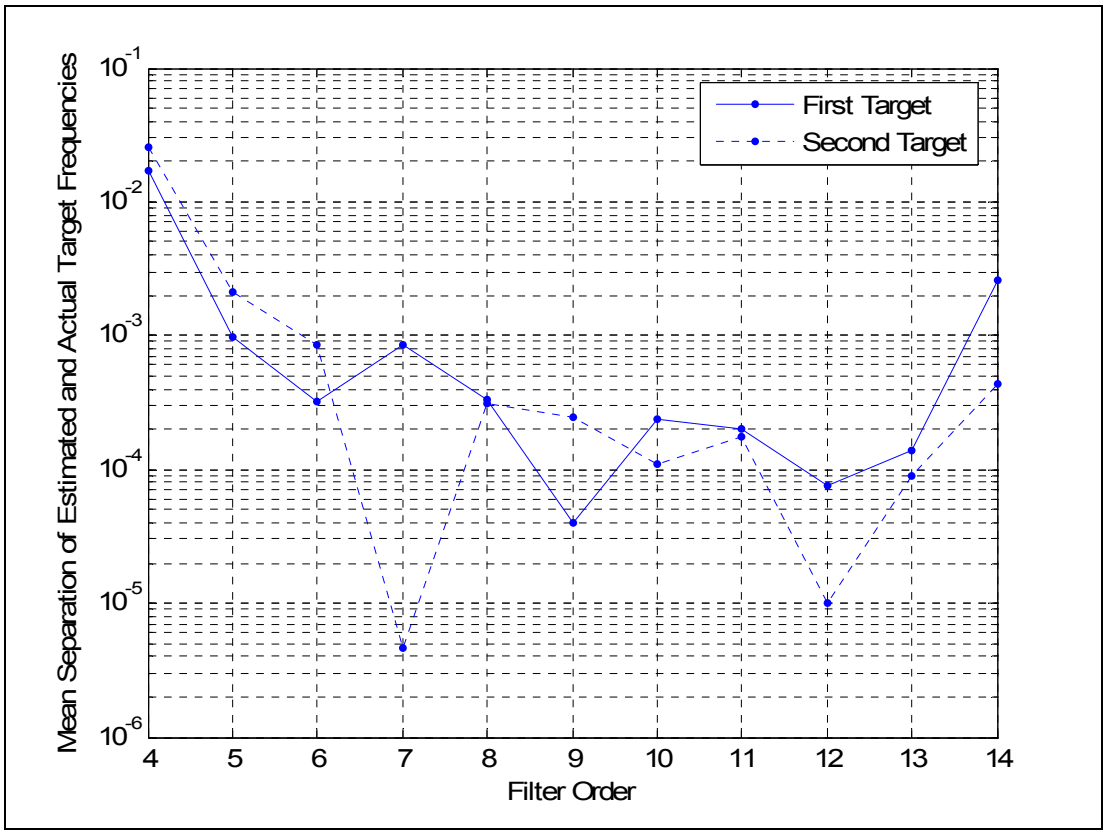

Figure 22 Bias of FBTK frequency estimates for different filter orders, L

The standard deviations of the FBTK frequency estimates decrease with the increased number of samples N as can be seen in Figure 23 and Figure 24. If the magnitude of the complex multipliers of targets are kept fixed during the simulations and SNR is allowed to increase with N as given in equation (2.20), with increasing N one gets frequency estimates with lower standard deviations that are closer to the CR bound curve. However, if SNR is kept fixed by lowering the magnitude of the complex multipliers of targets as N increases, the standard deviation of the estimates does not approach to the CR bound curve.

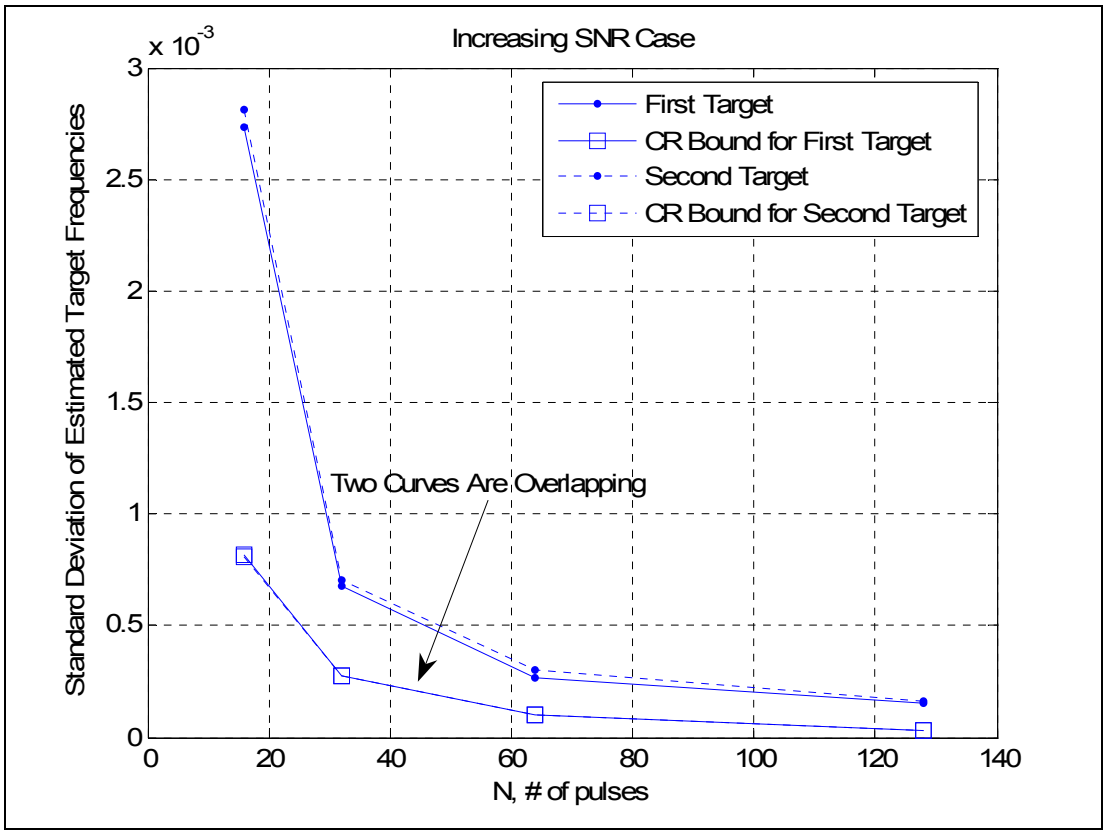

Figure 23 Standard deviation of FBTK frequency estimates in comparison to CR bound for increasing number of samples (SNR increases with increasing number of samples)

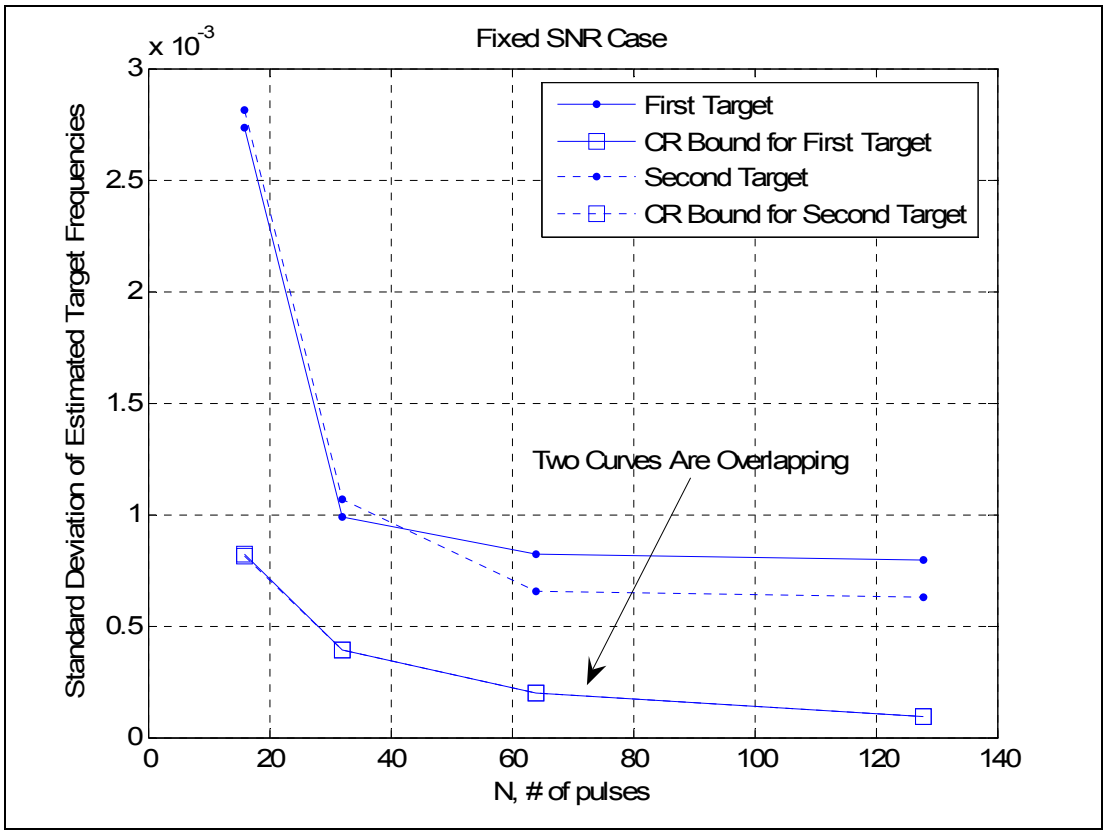

Figure 24 Standard deviation of FBTK frequency estimates in comparison to CR bound for increasing number of samples (SNR is kept fixed)

We have also considered the case where we increased the order L, together with the number of samples N and allowed SNR to increase with N. Note from Figure 25 and Figure 26 that this mode of operation degrades the quality of the estimates as well as increasing the computational load since computational load increases with the order. As a consequence, if one is provided with a larger number of samples, the order L should be kept fixed in order to obtain estimates with standard deviations close to CR bound.

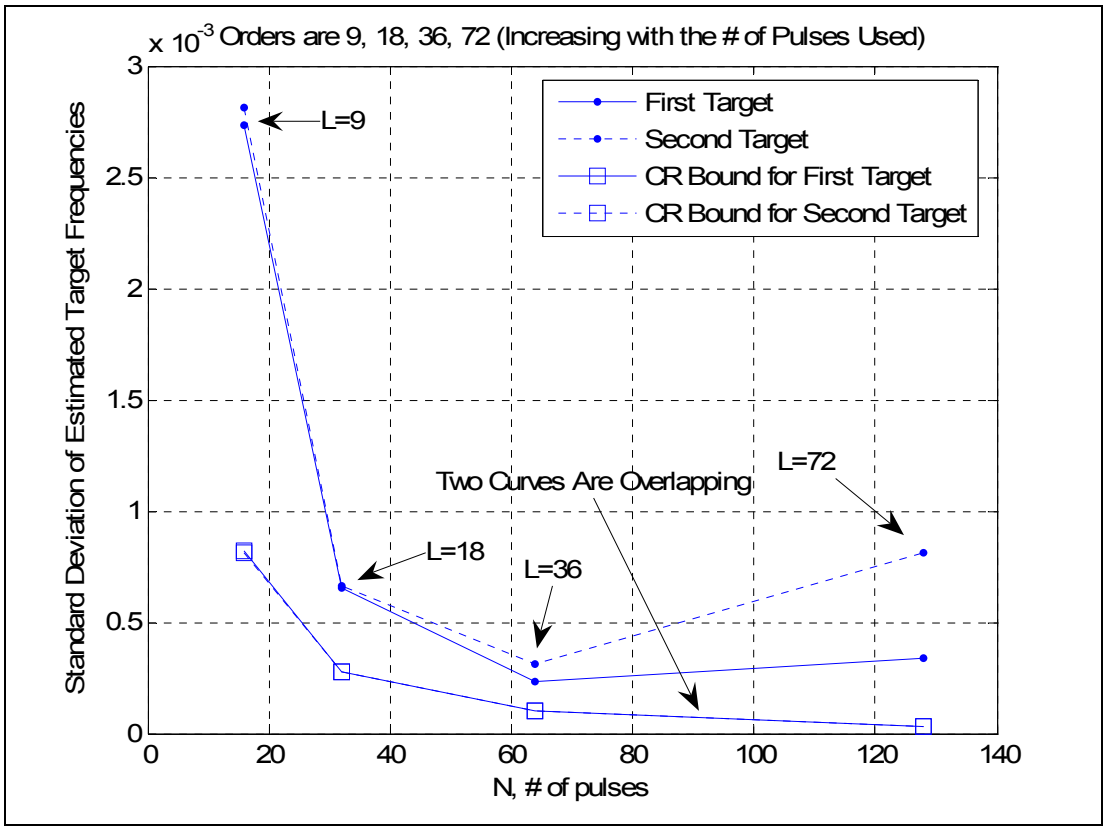

Figure 25 Standard deviation of FBTK frequency estimates as a function of number of samples (Prediction order increases with number of samples as 9, 18, 36, 72).

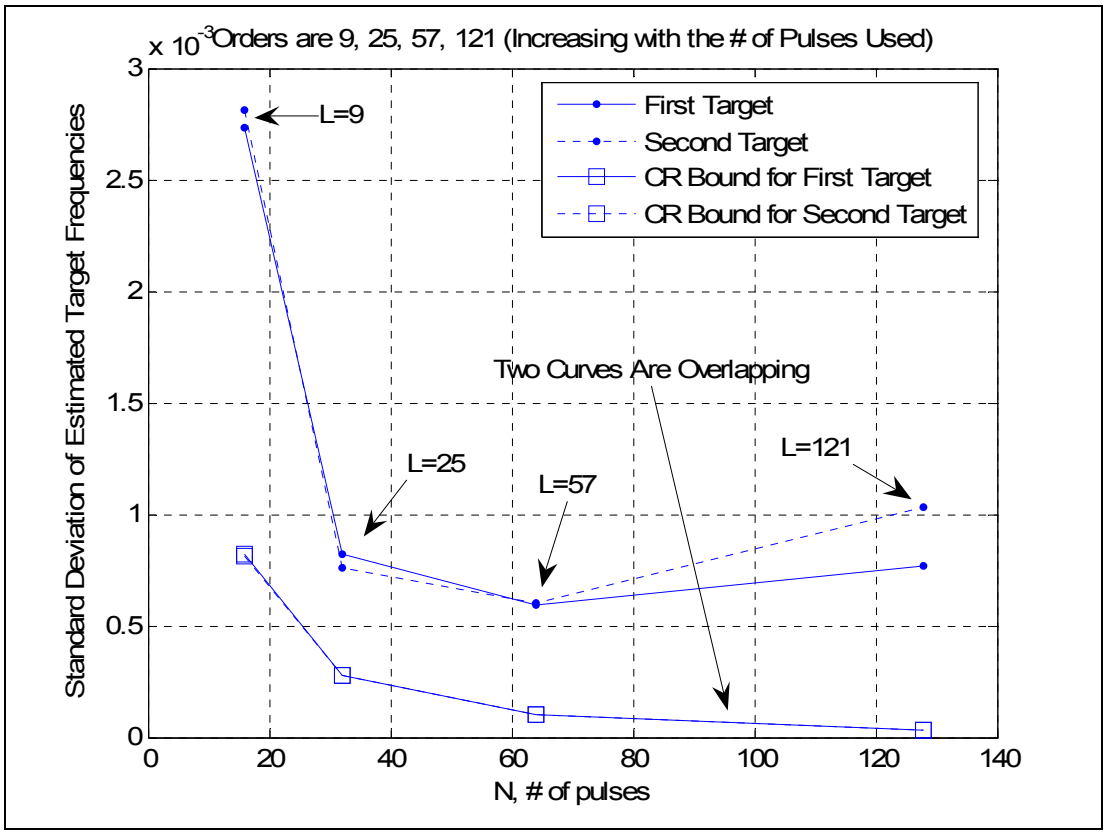

Figure 26 Standard deviation of FBTK frequency estimates as a function of number of samples (Prediction order increases with number of samples as 9, 25, 57, 121).

9.4. Effect of SNR for the Selected Algorithms

The effects of target *SNR* on the quality of the estimates are depicted in Figure 27 - Figure 31. Depicted in the figures are standard deviations and biases of frequency estimates, RMS value of biases for complex coefficients found via techniques presented in Chapter 6 and biases for complex coefficient estimates. Although all of the selected algorithms yield similar performance results, the superiority of the FBTK algorithm in comparison to other algorithms, excluding the obvious improvement achieved with subsequent ML processing, is evident from the figures. Other observations one can make from the figures are that the estimates can

be considered unbiased and there is no improvement achieved with the 'FBTK, NRDV' algorithm.

CR bounds shown in the figures have been derived under the assumption of unbiased estimates and the figures showing the bias of the estimates are given to verify this assumption.

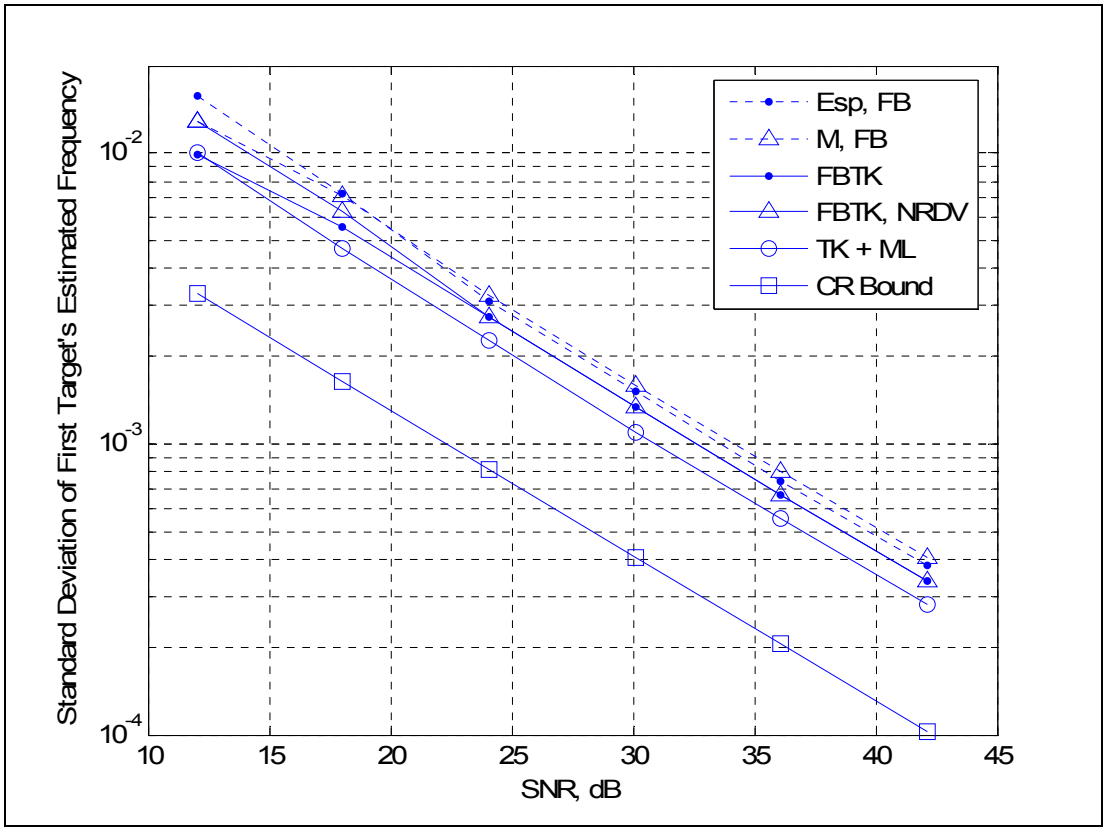

Figure 27 Standard deviation of the first target's frequency estimate of selected methods with SNR

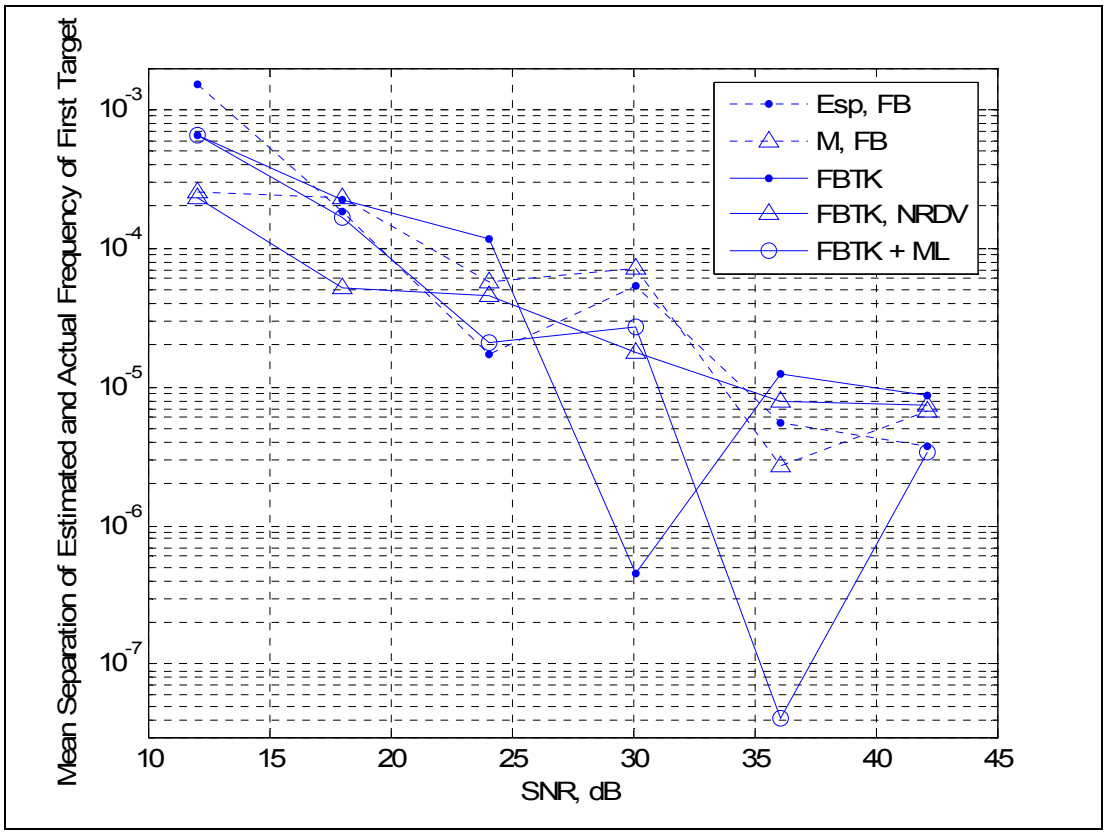

Figure 28 Bias of the first target's frequency estimate of selected methods with SNR

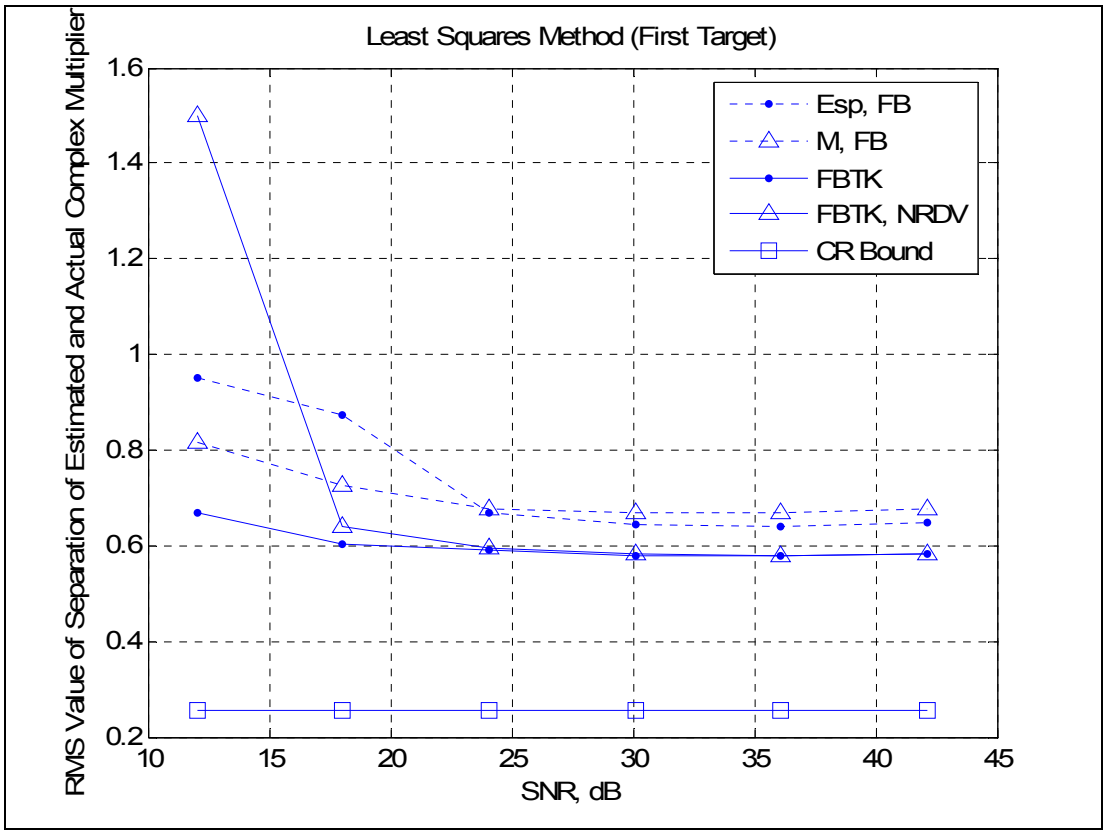

Figure 29 RMS value of separation of the first target's estimated and actual complex multiplier with SNR for selected methods (Least squares method)

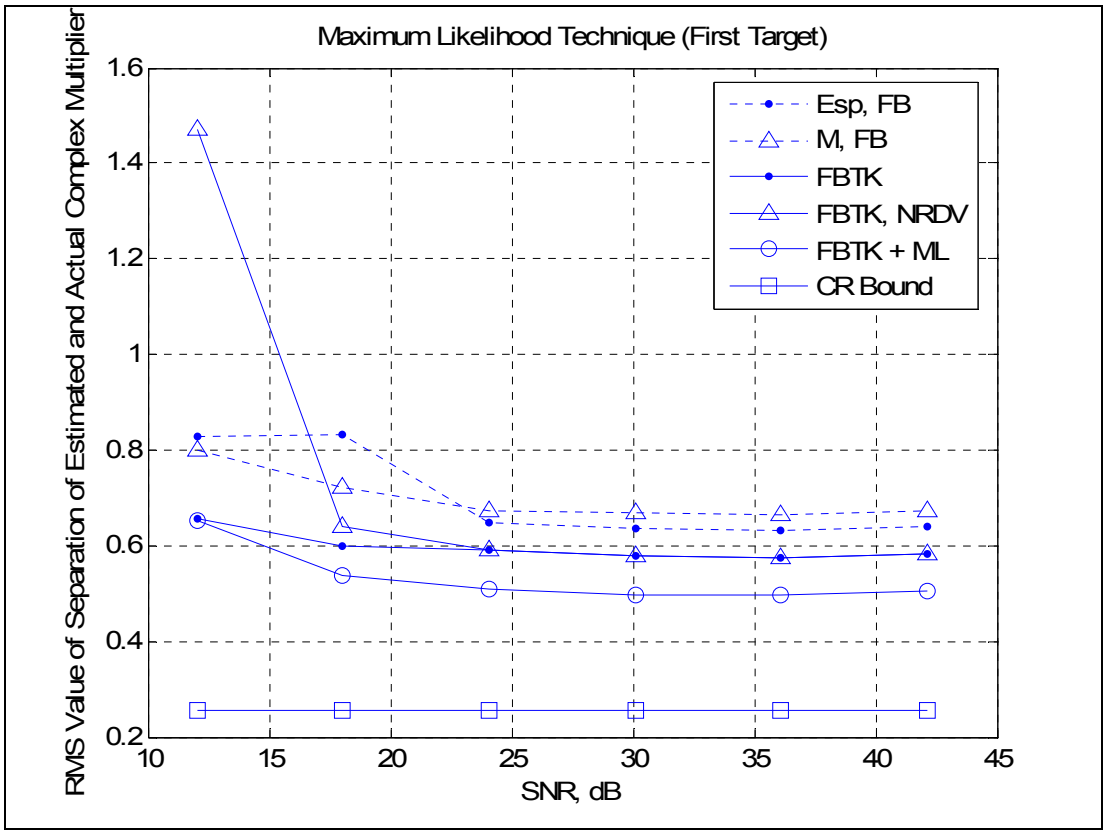

Figure 30 RMS value of separation of the first target's estimated and actual complex multiplier with SNR for selected methods (Maximum likelihood method)

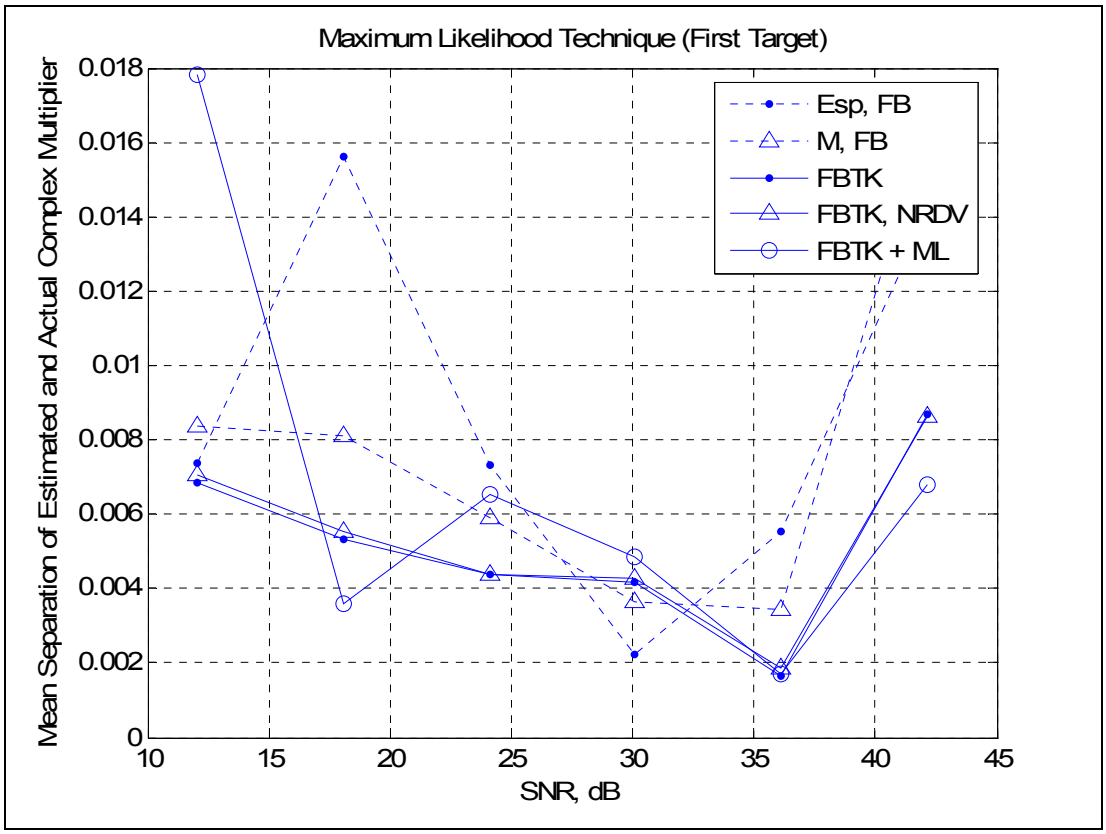

Figure 31 Bias of the first target's estimated and actual complex multiplier with SNR for selected methods (Maximum likelihood method)

9.5. Frequency Resolution for the Selected Algorithms

In order to evaluate the resolution capability of the algorithms, we have kept f_2 fixed and changed f_1: The frequency of the first target is moved towards the other target and then towards the land clutter region. The results in Figure 32 - Figure 36 show that the quality of the estimates is affected from a nearby clutter source or a nearby target in a similar fashion. We can observe this from the increase of the standard deviations and biases of the estimates at the two ends of the graphs. However, CR bound increases only when f_1 is moved towards the land clutter region. Thus the closeness of f_1 and f_2 affects the performances of the examined algorithms, whereas the CR bound is mostly determined by the distance from the clutter region.

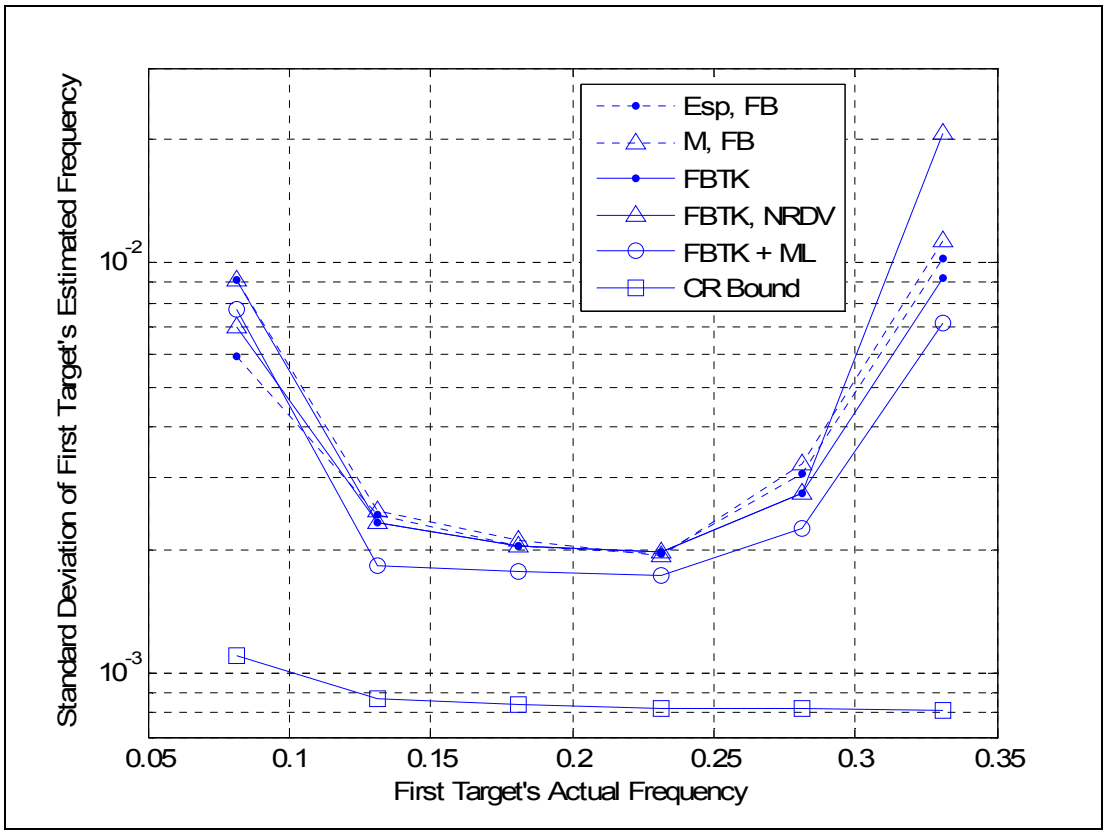

Figure 32 Standard deviation of frequency estimate of selected methods with change in Doppler frequency of the first target

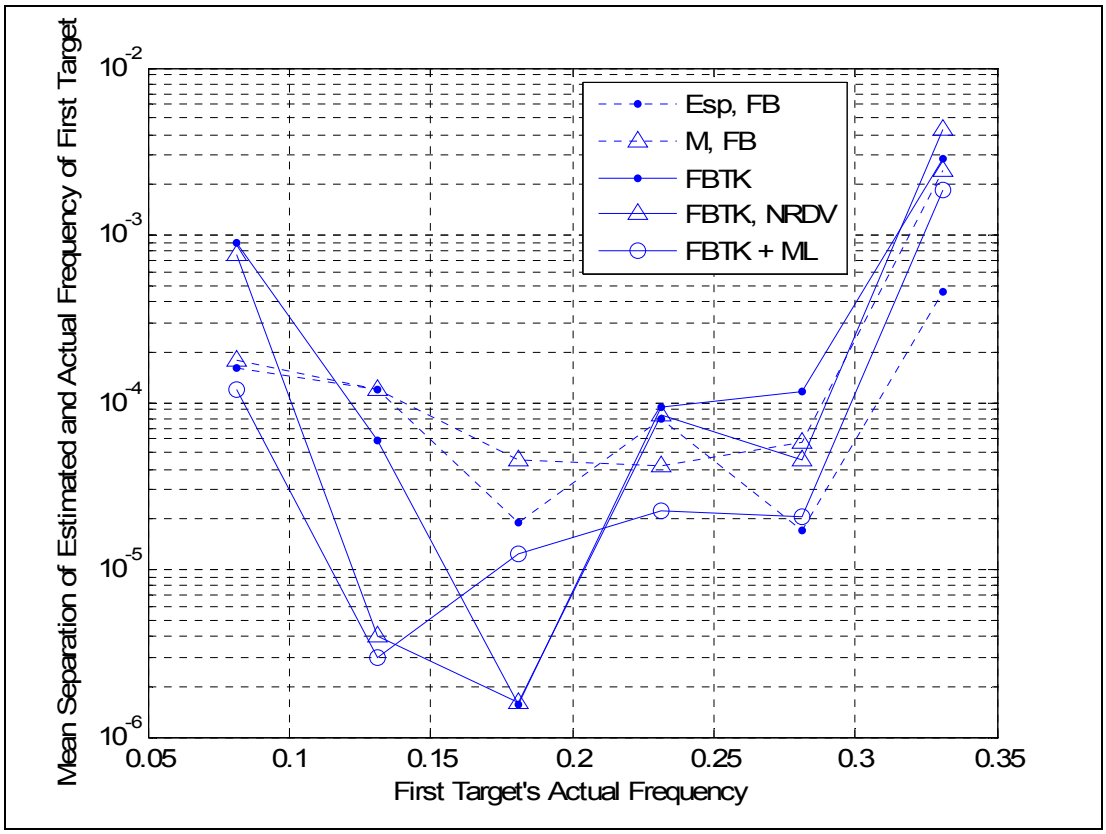

Figure 33 Bias of frequency estimate of selected methods with change in Doppler frequency of the first target

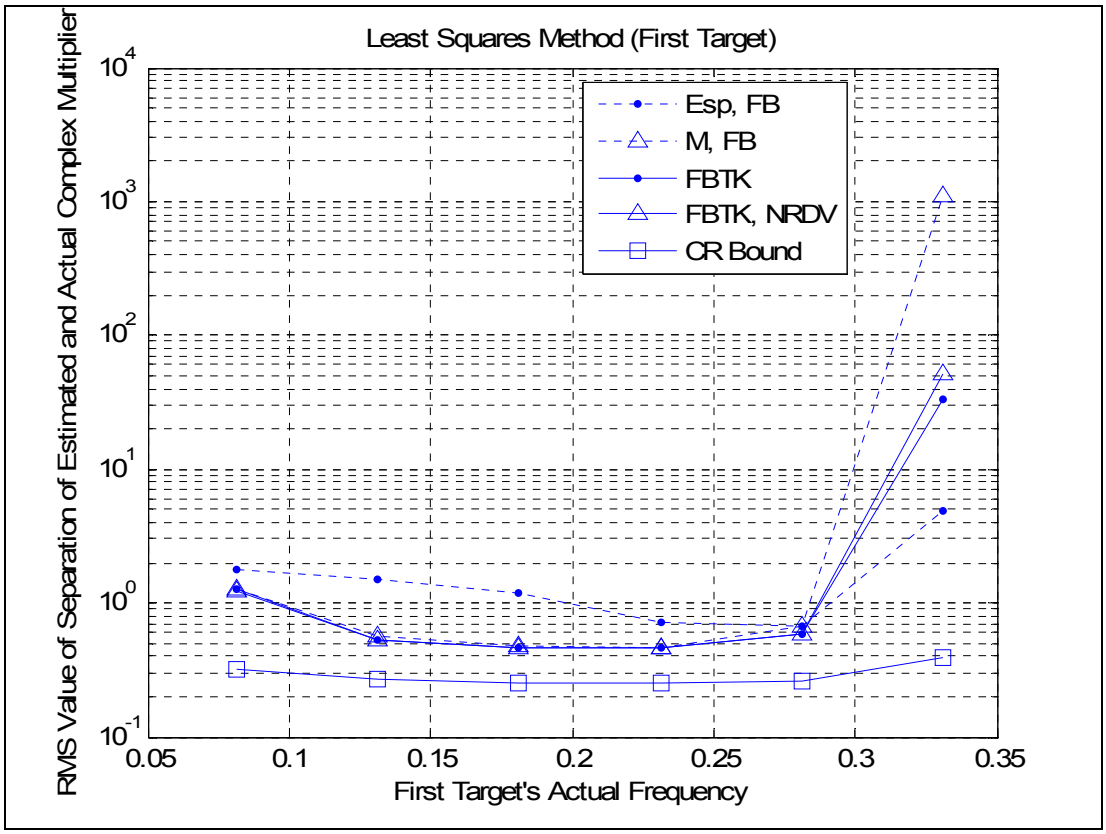

Figure 34 RMS value of separation of estimated and actual complex multiplier with change in Doppler frequency of the first target for selected methods (Least squares method)

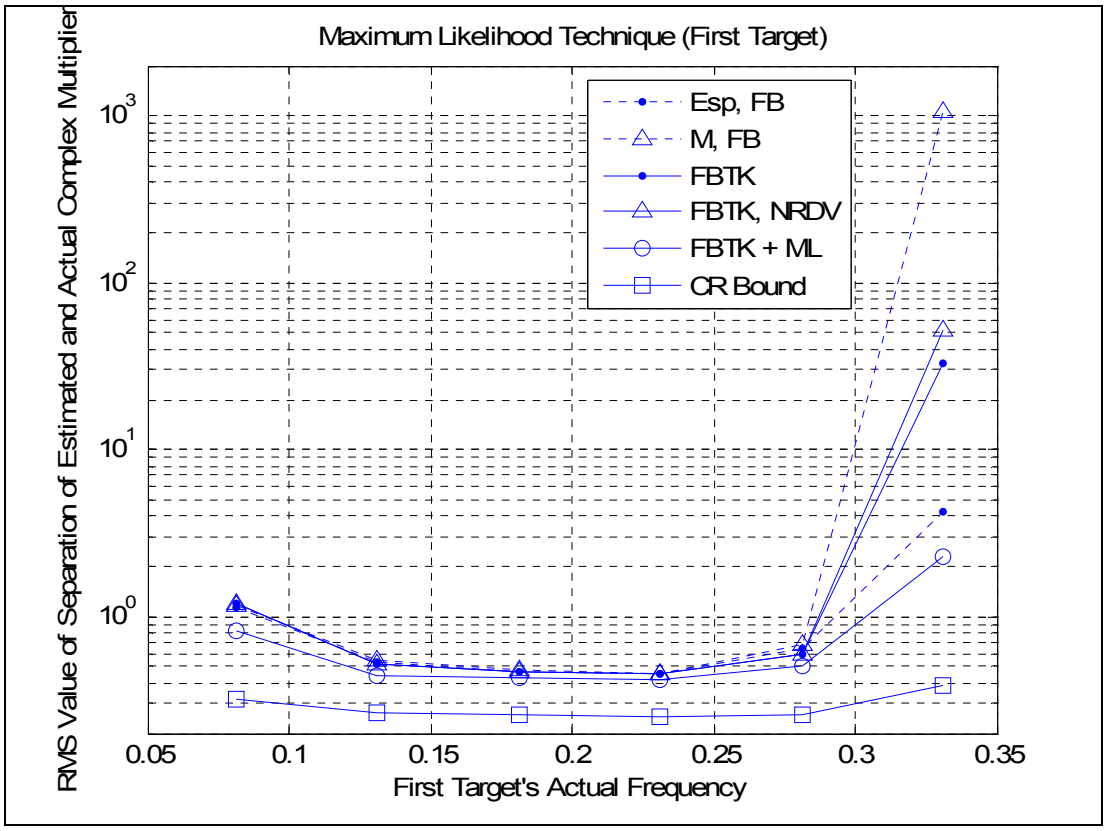

Figure 35 RMS value of separation of estimated and actual complex multiplier with change in Doppler frequency of the first target for selected methods (Maximum likelihood method)

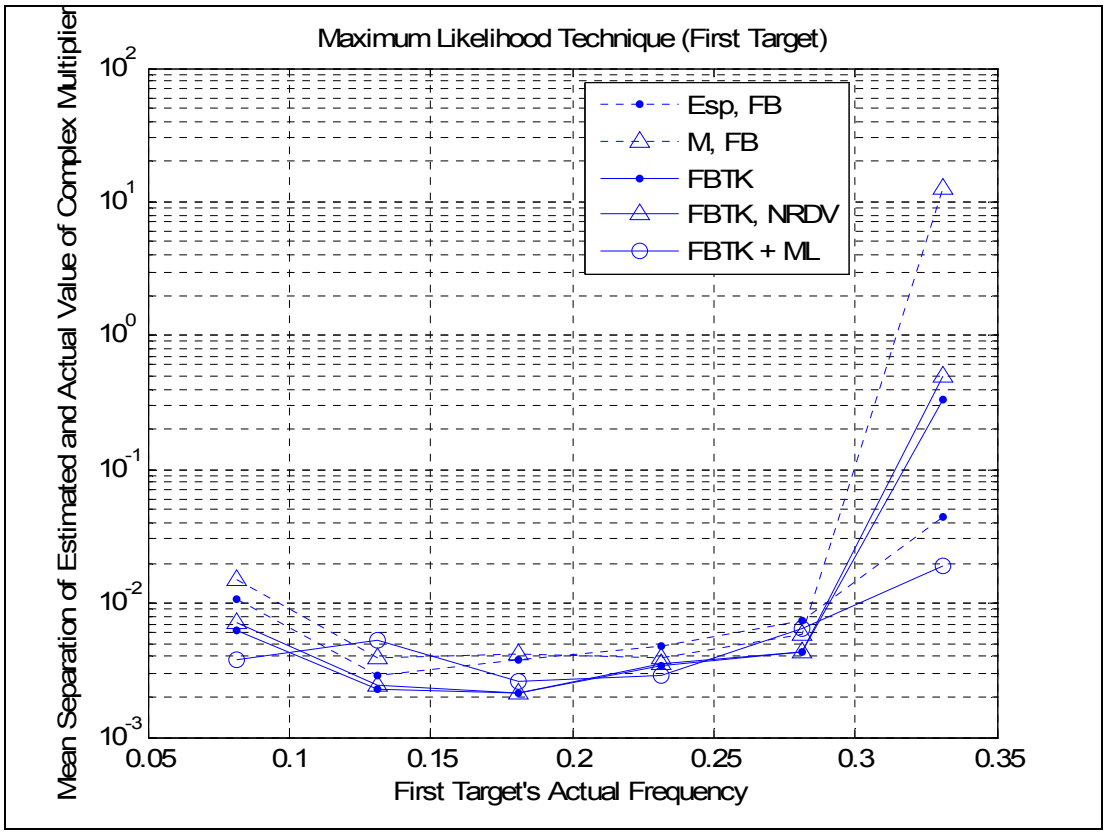

Figure 36 Bias of separation of estimated and actual complex multiplier with change in Doppler frequency of the first target for selected methods (Maximum likelihood method)

9.6. LTI MAXSIR Filter and FBTK Method

In this section, the performance of the system consisting of a MAXSIR filter (an LTI filter optimized for maximum *SCNR*; see Chapter 8) followed by a FBTK block under land clutter will be evaluated.

Figure 37 shows that due to reduced number of useable samples, the LTI MAXSIR filter with $\beta = 1/N$ (β could also be chosen same as the clutter region width) deteriorates the performance of FBTK algorithm. In the figure, 'decreasing order' means that the difference between the useable number of samples and order L is kept fixed, i.e., L is decreased with the increase in the order of the LTI MAXSIR filter.

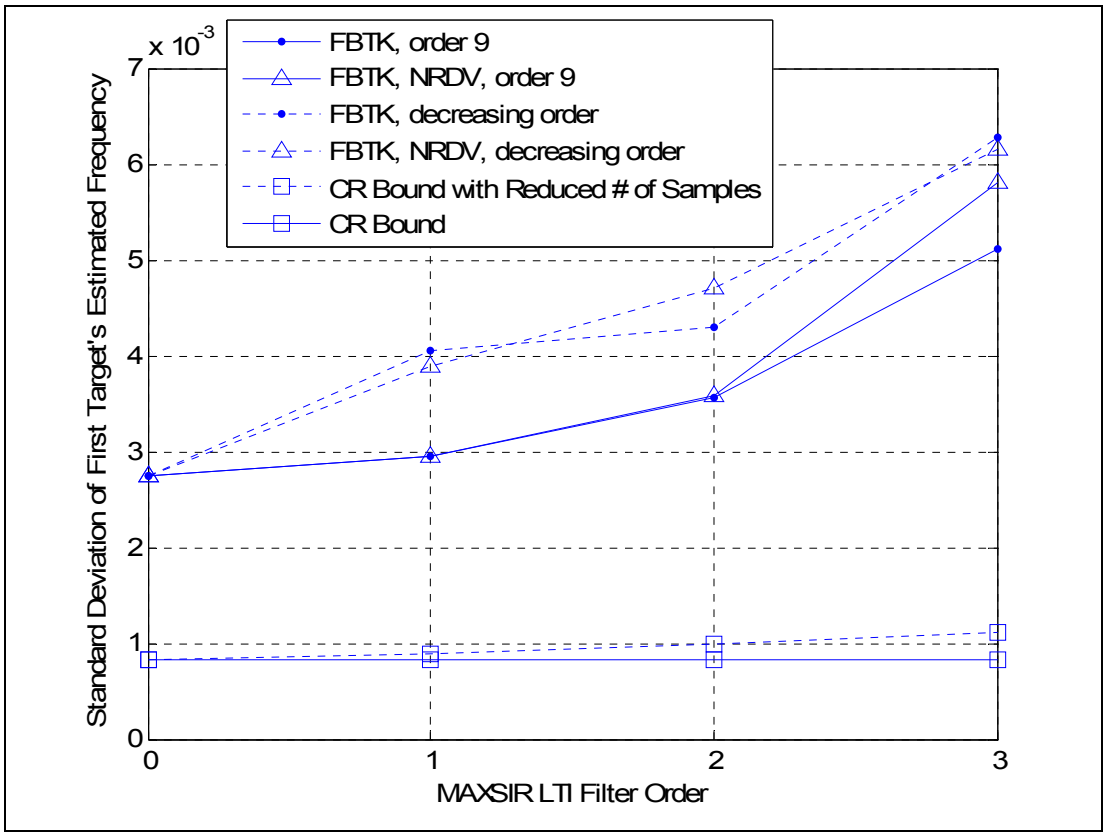

Figure 37 Standard deviation of the first target's frequency estimate of FBTK method preceded by LTI MAXSIR filter

9.7. Concluding Comments on Simulation Results

We have not performed simulations for different values of *rpm* and θ°_{2WHP}, but as *rpm* increases or θ°_{2WHP} decreases, due to reduced correlation of clutter as can be seen from equations (2.16) and (2.17), we expect spreading in the power spectrum of clutter. Larger clutter regions need to be defined and the range of detectable target frequencies will decrease.

Simulation results agree with our assertion that line spectra estimation methods can be applied in radar problem for high resolution Doppler estimation of multiple targets in the same folded range.

CHAPTER 10

FURTHER APPLICATIONS OF HIGH RESOLUTION LINE SPECTRAL ANALYSIS METHODS IN RADARS

In this chapter, we provide two further applications of the high resolution line spectral analysis tools; namely the moving clutter problem, and detection of helicopters and distinguishing them from fixed-wing targets with radars under strong clutter.

10.1. Moving Clutter

For target detection under moving clutter, we assume that an initial mean frequency where the moving clutter region is centered is provided. This is possible since for clutter detections, the same frequency values are reported consistently from burst to burst. Also clutter splits into many range cells and observed in neighboring beams. These make it possible for an outer block to supply the moving clutter center frequency which will be updated by our algorithm, by the mean value of the newly estimated moving clutter frequencies, which are identified by being in the moving clutter region. That means, around the moving clutter we define another window having a width equal to that of land clutter's window. This is called the moving clutter region and we update its location by the mean of the newly estimated moving clutter frequencies. Input to our algorithm is the initial center of this window and the output is the new center of the window.

A sample output of FBTK algorithm showing the zeros of the prediction-error filter $H(z)$ for $L=9$, whose angles will yield the frequency estimates is given in Figure 38. In the figure both land and moving clutter are present in addition to two targets at frequencies $[f_1 \quad f_2]=[0.2813 \quad 0.3563]$ and the moving clutter center

frequency f_c is taken as 0.7688. The moving clutter zeros will fall into the aforementioned moving clutter window and the mean frequency of these two zeros will be the new moving clutter window center.

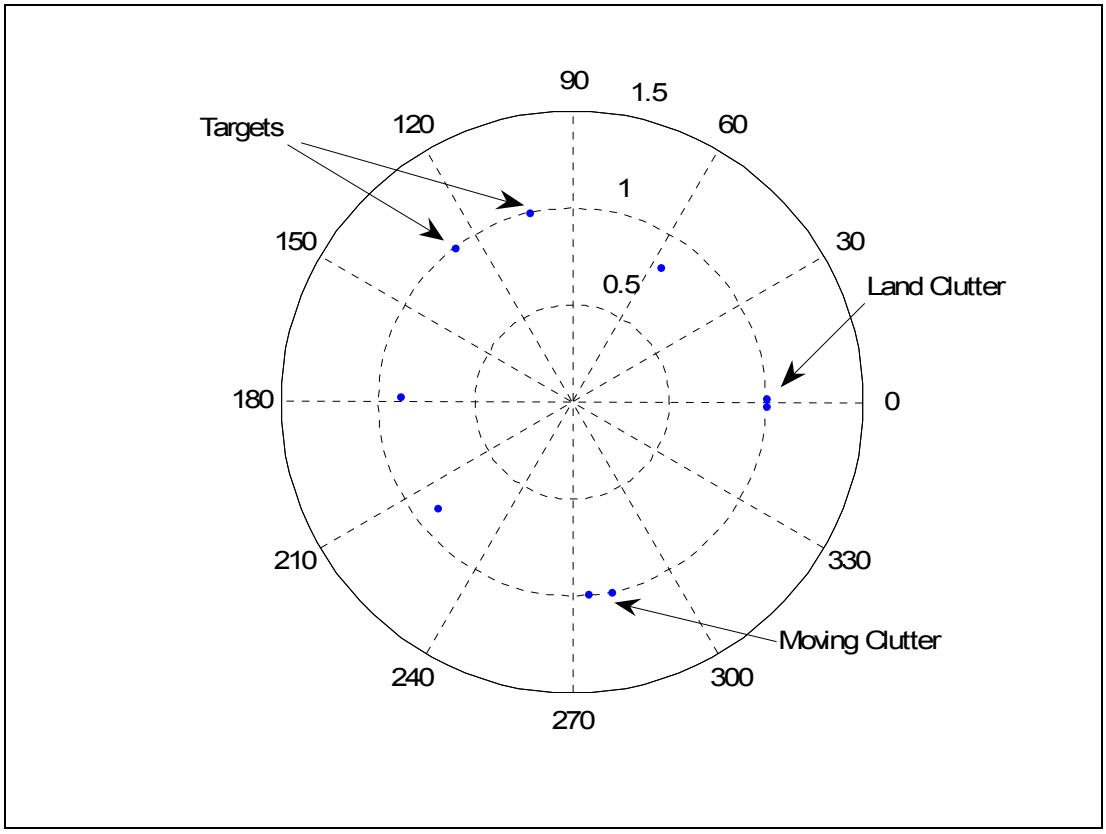

Figure 38 Zeros of prediction-error filter when two sources of clutter are present

10.2. Target Discrimination

The proposed processor can be utilized to aid distinguishing between fixed-wing and rotary-wing targets in addition to its usefulness in scenarios containing moving clutter. Appendix B contains the literature survey on rotary-wing targets in comparison with fixed-wing targets. Based on this knowledge, we will consider how

high resolution line spectra estimation algorithms can be employed for target classification purposes after presenting the mathematical model for helicopters (rotary-wing targets).

10.2.1. Modeling Helicopter Echo

The hub echo is assumed to be zero mean, Gaussian distributed, and independent from the rest of the signal model components. If i^{th} target is a helicopter, its hub's autocorrelation matrix is given by

$$\mathbf{R}_{k,l}^{hel} = \frac{\sigma_{hub}^2}{\sigma_{body}^2} e^{j2\pi f_i} \operatorname{sinc}^2\left(\frac{f_{hub}}{PRF}(k-l)\right) \tag{10.1}$$

which is used to model the helicopter hub echo $\mathbf{h}$ after defining the eigenvectors and eigenvalues of $\mathbf{R}^{hel}$ as

$$\mathbf{R}^{hel} = \mathbf{V}^{hel}\mathbf{D}^{hel}\left(\mathbf{V}^{hel}\right)^H. \tag{10.2}$$

$$\mathbf{h} = \mathbf{V}^{hel}\left(\mathbf{D}^{hel}\right)^{1/2}\mathbf{w} \tag{10.3}$$

where $\mathbf{w}$ is an N element column vector of complex white Gaussian noise.

In obtaining the CR bound for the rotary-wing target case, one just needs to add the appropriate matrices $\mathbf{R}^{hel}$ to $\mathbf{R}^{n}$ and use the resultant matrix as the new $\mathbf{R}^{n}$ in equations (3.22) - (3.27).

10.2.2. Proposed Classification Method

Line component estimation methods may be affected by the presence of the hub echo, so, further investigation is required for this point. If we assume that the effect is negligible and subtract the estimated body echoes from the received signal, one can observe that helicopter and fixed-wing targets separate out. One can check for the presence of a helicopter from the presence or absence of spreading. The remaining power around the body frequency of a rotary-wing target after subtraction may be either modeling the hub echo or may be present due to the imperfect cancellation of the actual and estimated echoes, which is again due to the presence of hub echo. In any case, classification capability of line component frequency estimation methods seems promising to further investigate.

CHAPTER 11

CONCLUSION AND FUTURE WORKS

A radar detector and Doppler processor block based on linear prediction, capable of operating under multiple-target and more than one source of clutter scenarios has been investigated. A model order detector has been suggested with its performance observed through simulations. Various simulation results on linear prediction parameters and comparison of linear prediction, MUSIC, and ESPRIT were given with results compared to the derived Cramér-Rao bounds. The effect of using LTI SIR maximizing filter prior to linear prediction was analyzed. How to use the specified radar processor for target classification has been briefly explained.

The main result of this work is that linear prediction and high resolution line spectra algorithms should be used in their forward-backward and nonwhitened versions treating each source of clutter as a group of targets with close Doppler frequencies. Other key results are:

1. Estimates obtained from the high resolution line spectra estimation algorithms can be further improved with subsequent Maximum Likelihood processing in order to obtain lower standard deviations and biases for the estimates.

2. Frequency estimates found by linear prediction cannot be improved with preprocessing the data with a whitening filter or an MAXSIR filter.

3. There is an optimum order L for the prediction-error filter used in Tufts-Kumaresan method, which is different than $3N/4$ found in the literature [1].

4. If one increases the number of samples N available to process, the order L of the prediction-error filter should be chosen accordingly. An initial increase in L may lower standard deviations of the estimates; however, further increase may deteriorate the quality of the estimates.

5. All the frequency estimation algorithms examined show similar results under varying SNR, although Tufts-Kumaresan method produces the best estimates.

6. High resolution line spectra estimation algorithms are affected from a nearby clutter source or a target with a close frequency in the same way. This is observed in the increase of the standard deviations and biases of the estimates. However; Cramér-Rao bound increases only when there is a nearby clutter source.

7. For the model we used, it is expected that results obtained using land clutter will not change if one has data corrupted with moving clutter since the only difference in their models is the center frequency of the clutter.

8. It is expected that multiple clutter sources would be treated similarly by the high resolution line spectra estimation algorithms since these algorithms do not differentiate between clutter and the targets. It is the duty of the clutter region to perform the necessary separation of targets and the clutter.

9. The proposed model order detector based on making threshold comparison of the estimated amplitudes is successful at providing the total number of targets plus clutter components.

10. A model order detector based on the closeness of the zeros of the prediction-error filter to the unit circle does not provide promising results although it will be probably beneficial to develop a model order determiner that takes as inputs to it both the amplitude of the estimates and the closeness of the corresponding zeros of the prediction-error filter to the unit circle.

11. Clutter region concept works well in separating targets from clutter. In fact, with this concept we achieve a form of whitening since clutter components which cause the noise part of the observation vector $\mathbf{x}$ to be colored is eliminated with this operation.

As a future work, the number of target plus clutter components detection procedure can be improved and a recently published modification on TK method [37] can be adapted. Research can be conducted on the applicability of the algorithms under clutter conditions that are modeled differently. Also target classification procedure can be detailed and the computational complexity of the algorithms can be investigated. Lastly, we anticipate that performance evaluation of

the algorithms on actual radar data can provide numerous insights and the methods can be improved accordingly.

REFERENCES

[1] Tufts, D. W. and Kumaresan, R., "Estimation of Frequencies of Multiple Sinusoids: Making Linear Prediction Perform Like Maximum Likelihood," IEEE Proceedings, vol. 70, no. 9, September 1982.

[2] Öztan, B. B. and Tanık, Y., "Estimation of the Parameters of Complex Exponentials under Radar Land Clutter and Single Snapshot Observation Using Modified Forward Backward Linear Prediction," IEEE Sinyal İşleme, İletişim ve Uygulamaları Kurultayı, 2008.

[3] Richards, M. A., Fundamentals of Radar Signal Processing, McGraw-Hill, 2005.

[4] Skolnik, M. I., Introduction to RADAR Systems 3rd Ed., McGraw-Hill, 2001.

[5] Banjanin, Z., Zrnic', D. S. and Cruz, J. R., "A Linear Prediction Approach to Doppler Mean Frequency Retrieval in the Presence of Ground Clutter," IEEE Trans. on Aerospace and Electronic Systems, vol. 29, no. 3, July 1993.

[6] Nathanson, F. E., Reilly, J. P. and Cohen, M. N., Radar Design Principles Signal Processing and the Environment 2nd Ed., McGraw-Hill, 1991.

[7] D'addio, E., Farina, A. and Studer, F. A., "Performance Comparison of Optimum and Conventional MTI and Doppler Processors," IEEE Trans. on Aerospace and Electronic Systems, vol. AES-20, no. 6, November 1984.

[8] Farina, A. and Protopapa, A., "New Results on Linear Prediction for Clutter Cancellation," IEEE Trans. on Aerospace and Electronic Systems, vol. 24, no. 3, May 1988.

[9] Armstrong, B. C., "A Comparison of Conventional, Adaptive and Hybrid Doppler Processing Techniques," Proc. South African Symposium on Communications and Signal Processing, 1992, pp. 127-134.

[10] Kay, S. M., Modern Spectral Estimation: Theory and Application, Prentice Hall, 1988.

[11] Therrien, C. W., Discrete Random Signals and Statistical Signal Processing, Prentice Hall, 1992.

[12] Hayes, M. H., Statistical Digital Signal Processing and Modeling, John Wiley & Sons, Inc., 1996.

[13] Rife, D. C., "Single-Tone Parameter Estimation from Discrete-Time Observations" IEEE Trans. On Information Theory, vol. IT-20, no. 5, September 1974.

[14] Rife, D. C. and Boorstyn, R. R., "Multiple Tone Parameter Estimation from Discrete-Time Observations" The Bell System Technical Journal, vol. 55, no. 9, November 1976.

[15] Van Trees, H. L., Detection, Estimation, and Modulation Theory Part I Detection, Estimation, and Linear Modulation Theory, John Wiley & Sons, Inc., 1968.

[16] Haykin, S., Currie, B. W. and Kesler, S. B., "Maximum-Entropy Spectral Analysis of Radar Clutter," Proc. IEEE, vol. 70, no. 9, September 1982.

[17] Tufts, D. W. and Kumaresan, R., "Singular Value Decomposition and Improved Frequency Estimation Using Linear Prediction," IEEE Trans. on Acoustics, Speech, and Signal Processing, vol. ASSP-30, no. 4, August 1982.

[18] Kumaresan, R., "On the Zeros of the Linear Prediction-Error Filter for Deterministic Signals," IEEE Trans. on Acoustics, Speech, and Signal Processing, vol. ASSP-31, no. 1, February 1983.

[19] California Institute of Technology, "The Moore-Penrose Pseudo Inverse," http://robotics.caltech.edu/~jwb/courses/ME115/handouts/pseudo.pdf, last date accessed: 30.06.2008.

[20] Koç, A. T., "Direction Finding With a Uniform Circular Array Via Single Snapshot Processing," Ph.D. thesis, Middle East Technical University, Ankara, Turkey, 1996.

[21] Koç, A. T. and Tanık, Y., "Direction Finding With a Uniform Circular Array Via Single Snapshot Processing," Elsevier Signal Processing 56, 1997, 17-31.

[22] Kumaresan, R. and Tufts, D. W., "Estimating the Parameters of Exponentially Damped Sinusoids and Pole-Zero Modeling in Noise," IEEE Trans. on Acoustics, Speech, and Signal Processing, vol. ASSP-30, no. 6, December 1982.

[23] Khan, R. H., "Ocean-Clutter Model for High-Frequency Radar," IEEE Journal of Oceanic Engineering, vol. 16, no. 2, April 1991.

[24] Olkin, J. A., Nowlin, W. C. and Barnum, J. R. "Detection of Ships Using OTH Radar with Short Integration Times," Proc. IEEE National Radar Conf., Syracuse, USA, May 1997, pp. 1-6.

[25] Wax, M. and Kailath, T., "Detection of Signals by Information Theoretic Criteria," IEEE Trans. on Acoustics, Speech, and Signal Processing, vol. ASSP-33, no. 2, April 1985.

[26] Oppenheim, A. V. and Schafer, R. W., Discrete-Time Signal Processing 2nd Edition, Prentice Hall, 1999.

[27] Ren, Q. S. and Willis, A. J., "Extending Music to Single Snapshot and On Line Direction Finding Applications," IEE Radar 97, no. 449, October 1997.

[28] Xie, J., Yuan, Y. and Liu, Y., "Super-Resolution Processing for HF Surface Wave Radar Based on Pre-Whitened MUSIC," IEEE Journal on Oceanic Engineering, vol. 23, no. 4, October 1998.

[29] Vaitkus, P. J., Cobbold, R. S. C. and Johnston, K. W., "A New Time-Domain Narrowband Velocity Estimation Technique for Doppler Ultrasound Flow Imaging. Part II: Comparative Performance Assessment," IEEE Trans. on Ultrasonics, Ferroelectrics, and Frequency Control, vol. 45, no. 4, July 1998.

[30] Ivkovic, D. S., Simic, S., Dukic, M. L. and Eric, M. M., "Software Model of the Signal Processing Unit in the Conventional Radar," IEEE EUROCON, November 2005.

[31] Wang, J. and Kirlin, R. L., "Improvement of High Frequency Ocean Surveillance Radar Using Subspace Methods Based on Sea Clutter Suppression," Proc. Sensor Array and Multichannel Signal Processing Workshop, August 2002, pp. 557-560.

[32] Shahapurkar, N. and Ramalingam, C. S., "Threshold Performance of MUSIC When Using the Forward-Backward Data Matrix," IEEE Signal Proc. Letters, vol. 13, no. 2, February 2006.

[33] Shah, A. A. and Tufts, D. W., "Determination of the Dimension of a Signal Subspace from Short Data Records," IEEE Trans. on Signal Processing, vol. 42, no. 9, September 1994.

[34] Wildman, P., "STAT 2005 Homepage Chapter 6 Lessons," http://wind.cc.whecn.edu/~pwildman/statnew/chapter_6_lessons.htm, Casper College, Spring 2002, last date accessed: 27.06.2008.

[35] McGraw-Hill, Confidence Intervals and Sample Size, http://highered.mcgraw-hill.com/sites/dl/free/0072549076/79745/ch07.pdf, May 2003, last date accessed: 27.06.2008.

[36] Maddock, J., Bristow, P. A., Holin, H. and Zhang, X., "boost Math Toolkit," http://freespace.virgin.net/boost.regex/toolkit/html/index.html, September 2007, last date accessed: 27.06.2008.

[37] So, H.-C. and Leung, C.-T., "A Simple Improvement to Tufts-Kumaresan Method for Multiple Sinusoidal Frequency Estimation," IEICE Trans. Fundamentals, vol. E88-A, no. 1, January 2005.

[38] Proakis, J. G., Digital Communications 4th Edition, McGraw-Hill, 2001.

[39] Wikipedia The Free Encyclopedia, "Newton's Method in Optimization," http://en.wikipedia.org/wiki/Newton%27s_method_in_optimization, May 2008, last date accessed: 28.06.2008.

[40] Tikkinen, J. M., Helander, E. E., and Visa, A., "Joint Utilization of Incoherently and Coherently Integrated Radar Signal in Helicopter Categorization," *IEEE*, 0-7803-8882-8/05, 2005.

[41] Feng X., Yan J., Huang P., and Xiao Z., "Detection of Hovering Helicopter," *ICSP'02 Proceedings*, 0-7803-7488-6/02, IEEE 2002.

[42] Yoon, S.-H., Kim, B., and Kim, Y.-S., "Helicopter Classification Using Time-Frequency Analysis," *Electronics Letters,* vol. 36, no. 22, 26th October 2000.

[43] Ziyue T., Yongliang W., and Zhiwen W., "STAP Scheme to Detection of Hovering Helicopter," *Proceedings of ICSP2000*, 0-7803-5747-7/00, IEEE 2000.

[44] Gini, F. and Farina, A., "Matched Subspace CFAR Detection of Hovering Helicopters," *IEEE Trans. Aerospace and Electronic Systems,* vol. 35, no. 4, October 1999.

[45] Kulpa, K., Czekala, Z., Misiurewicz, J., and Falkiewicz, J., "Parametric Detection of the Helicopter Hub Echo," *IEEE*, 0-7803-4977-6/99, 1999.

[46] Rotander, C E and Sydow, H von, "Classification of Helicopters by the L/N-Quoutient," *IEE, Radar 97,* Publication No. 449, 14 – 16 October 1997.

[47] Misiurewicz, J., Kulpa, K., and Czekala, Z., "Analysis of Recorded Helicopter Echo," *IEE, Radar 97,* Publication No. 449, 14 – 16 October 1997.

[48] Bullard, B. D. and Dowdy, P. C., "Pulse Doppler Signature of a Rotary-Wing Aircraft," *IEEE*, CH2952-0/91/0000-0160, 1991.

[49] Misiurewicz, J., Kulpa, K., and Czekala, Z., "Analysis of Radar Echo from a Helicopter Rotor Hub," Warsaw, Poland.

[50] Abatzoglou, "Helicopter Recognition Radar Processor," *United States Patent, No.: US 7,079,072 B1,* Date: Jul. 18, 2006.

[51] Nagel, “Radar Process for Classifying or Identifying Helicopters,” *United States Patent, No.: US 7,046,192 B2,* Date: May 16, 2006.

[52] Hommel et al., “Target Classification Method,” *United States Patent, No.: US 6,573,861 B1,* Date: Jun. 3, 2003.

[53] Shi et al., “Radar Detection and Classification of Helicopters,” *United States Patent, No.: 5,689,268,* Date: Nov. 18, 1997.

[54] Abatzoglou, “Helicopter Recognition Radar Processor,” *United States Patent, No.: 5,376,940,* Date: Dec. 27, 1994.

[55] Ludloff et al., “Method for Detecting and Classifying Helicopters,” *United States Patent, No.: 5,231,402,* Date: Jul. 27, 1993.

APPENDIX A

IMPLEMENTATION OF MAXIMUM LIKELIHOOD TECHNIQUE

Equations (3.9) and (3.10) can be solved using the steepest descent method [38] in which case the specified equations without equating to zero provide the necessary gradient information. If one uses an algorithm that requires real variables, entries of the gradient are given by

$$\begin{aligned}
\frac{\partial \ln(p)}{\partial (a_k)_{real}} &= 2\,\mathrm{Re}\left\{-\mathbf{V}_{:,k}^H \mathbf{Q}\mathbf{x}\right\} + 2\,\mathrm{Re}\left\{\sum_{l=1}^{M} \mathbf{V}_{:,k}^H \mathbf{Q} a_l \mathbf{V}_{:,l}\right\}, \quad k = 1,\ldots,M \\
\frac{\partial \ln(p)}{\partial (a_k)_{imaginary}} &= 2\,\mathrm{Re}\left\{j\mathbf{V}_{:,k}^H \mathbf{Q}\mathbf{x}\right\} + 2\,\mathrm{Re}\left\{-j\sum_{l=1}^{M} \mathbf{V}_{:,k}^H \mathbf{Q} a_l \mathbf{V}_{:,l}\right\}, \quad k = 1,\ldots,M \\
\frac{\partial \ln(p)}{\partial \omega_p} &= 2\,\mathrm{Re}\left\{\sum_{i=1}^{M} a_i^* a_p \mathbf{V}_{:,i}^H \mathbf{Q}\mathbf{V}'_{:,p}\right\} - 2\,\mathrm{Re}\left\{a_p \mathbf{x}^H \mathbf{Q}\mathbf{V}'_{:,p}\right\}, \quad p = 1,\ldots,M
\end{aligned} \tag{A.1}$$

In the steepest descent algorithm, estimates for any generic variable z is updated as

$$z_{new} = z_{old} - \mu \left.\frac{\partial \ln(p)}{\partial z}\right|_{z=z_{old}} \tag{A.2}$$

where μ is a properly chosen step size parameter that should guarantee convergence.

Another possibility may be to use Newton–Raphson method [39] with the update equation

$$\mathbf{z}_{new} = \mathbf{z}_{old} - \gamma \left[\mathbf{H}_{\ln(p)}(\mathbf{z}_{old})\right]^{-1} \nabla_{\ln(p)}(\mathbf{z}_{old}) \tag{A.3}$$

which requires the Hessian matrix $\mathbf{H}_{\ln(p)}$ in addition to gradient information $\nabla_{\ln(p)}$. $\mathbf{H}_{\ln(p)}$ is the matrix of second-order partial derivatives of the cost function $\ln(p)$ (− sign is omitted for short notation) with the $(i,j)^{\text{th}}$ element given by [12]

$$\left\{\mathbf{H}_{\ln(p)}(\mathbf{z})\right\}_{i,j} = \frac{\partial^2 \ln\left(p(\mathbf{z})\right)}{\partial \mathbf{z}_i \partial \mathbf{z}_j}. \tag{A.4}$$

The necessary equations corresponding to our model required to form the Hessian matrix are

$$\begin{aligned}
&\frac{\partial^2 \ln(p)}{\partial a_k \partial a_t} = \mathbf{V}_{:,k}^H \mathbf{Q} \mathbf{V}_{:,t} \\
&\frac{\partial^2 \ln(p)}{\partial \omega_k^2} = -2\,\mathrm{Re}\left\{a_k \mathbf{x}^H \mathbf{Q} \mathbf{V}_{:,k}^{''}\right\} + 2\,\mathrm{Re}\left\{\sum_{l=1}^{M} a_l^* a_k \mathbf{V}_{:,l}^H \mathbf{Q} \mathbf{V}_{:,k}^{''}\right\} \\
&\frac{\partial^2 \ln(p)}{\partial \omega_k \partial \omega_t} = 2\,\mathrm{Re}\left\{a_t^* a_k \left(\mathbf{V}_{:,t}^{'}\right)^H \mathbf{Q} \mathbf{V}_{:,k}^{'}\right\}, \text{ valid for } k \neq t \\
&\frac{\partial^2 \ln(p)}{\partial \omega_k \partial a_k} = -\left(\mathbf{V}_{:,k}^{'}\right)^H \mathbf{Q}\mathbf{x} + a_k \mathbf{V}_{:,k}^H \mathbf{Q} \mathbf{V}_{:,k}^{'} + \sum_{l=1}^{M} a_l \left(\mathbf{V}_{:,k}^{'}\right)^H \mathbf{Q} \mathbf{V}_{:,l} \\
&\frac{\partial^2 \ln(p)}{\partial \omega_k \partial a_t} = a_k \mathbf{V}_{:,t}^H \mathbf{Q} \mathbf{V}_{:,k}^{'}, \text{ valid for } k \neq t
\end{aligned} \tag{A.5}$$

where $\mathbf{V}_{:,k}^{''}$ is

$$\mathbf{V}_{:,k}^{''} = \begin{bmatrix} 0 & -e^{j\omega_k} & \cdots & -(N-1)^2 e^{j(N-1)\omega_p} \end{bmatrix}^T. \tag{A.6}$$

If one requires the corresponding equations for algorithms accepting real variables, they are given as

$$\begin{aligned}
&\frac{\partial^2 \ln(p)}{\partial (a_k)_{real} \partial (a_p)_{real}} = 2\,\mathrm{Re}\left\{\mathbf{V}_{:,k}^H \mathbf{Q} \mathbf{V}_{:,p}\right\} \\
&\frac{\partial^2 \ln(p)}{\partial (a_k)_{imaginary} \partial (a_p)_{imaginary}} = 2\,\mathrm{Re}\left\{\mathbf{V}_{:,k}^H \mathbf{Q} \mathbf{V}_{:,p}\right\} \\
&\frac{\partial^2 \ln(p)}{\partial (a_k)_{real} \partial (a_p)_{imaginary}} = 2\,\mathrm{Re}\left\{j\mathbf{V}_{:,k}^H \mathbf{Q} \mathbf{V}_{:,p}\right\} \\
&\frac{\partial^2 \ln(p)}{\partial \omega_k^2} = -2\,\mathrm{Re}\left\{a_k \mathbf{x}^H \mathbf{Q} \mathbf{V}_{:,k}^{''}\right\} + 2\,\mathrm{Re}\left\{\sum_{l=1}^{M} a_l^* a_k \mathbf{V}_{:,l}^H \mathbf{Q} \mathbf{V}_{:,k}^{''}\right\} \\
&\frac{\partial^2 \ln(p)}{\partial \omega_k \partial \omega_p} = 2\,\mathrm{Re}\left\{a_p^* a_k \left(\mathbf{V}_{:,p}^{'}\right)^H \mathbf{Q} \mathbf{V}_{:,k}^{'}\right\}, \text{ valid for } k \neq p \\
&\frac{\partial^2 \ln(p)}{\partial \omega_k \partial (a_k)_{real}} = -2\,\mathrm{Re}\left\{\left(\mathbf{V}_{:,k}^{'}\right)^H \mathbf{Q}\mathbf{x}\right\} + 4(a_k)_{real}\,\mathrm{Re}\left\{\mathbf{V}_{:,k}^H \mathbf{Q} \mathbf{V}_{:,k}^{'}\right\} + 2\,\mathrm{Re}\left\{\left(\mathbf{V}_{:,k}^{'}\right)^H \mathbf{Q} a_k \mathbf{V}_{:,k}\right\}
\end{aligned}$$

$$\frac{\partial^2 \ln(p)}{\partial \omega_k \partial (a_p)_{real}} = 2\,\mathrm{Re}\left\{a_k \mathbf{V}_{:,p}^H \mathbf{Q} \mathbf{V}_{:,k}^{'}\right\},\ \text{valid for } k \neq p$$

$$\frac{\partial^2 \ln(p)}{\partial \omega_k \partial (a_k)_{imaginary}} = 2\,\mathrm{Re}\left\{j\left(\mathbf{V}_{:,k}^{'}\right)^H \mathbf{Q}\mathbf{x}\right\} + 4(a_k)_{imaginary}\,\mathrm{Re}\left\{\mathbf{V}_{:,k}^H \mathbf{Q} \mathbf{V}_{:,k}^{'}\right\} + \cdots \quad \text{(A.7)}$$

$$\cdots 2\,\mathrm{Re}\left\{-j\left(\mathbf{V}_{:,k}^{'}\right)^H \mathbf{Q} a_k \mathbf{V}_{:,k}\right\}$$

$$\frac{\partial^2 \ln(p)}{\partial \omega_k \partial (a_p)_{imaginary}} = 2\,\mathrm{Re}\left\{-j a_k \mathbf{V}_{:,p}^H \mathbf{Q} \mathbf{V}_{:,k}^{'}\right\},\ \text{valid for } k \neq p$$

What we have used in solving the minimization problem (3.6) is the MATLAB function *fminunc* with gradient and Hessian information provided by us. Another alternative we tried is to minimize equation (3.18) without providing gradient or Hessian information to the same MATLAB function. One can refer to MATLAB help for further details.

APPENDIX B

LITERATURE ON HELICOPTER ECHO AND DETECTION AND CLASSIFICATION

In this part, a summary of the references [40] - [55] will be presented. If *SNR* and time-on-target $(N \bullet PRI)$ values are appropriately selected, helicopter radar echo possesses some characteristic features. Additionally, *PRF* , which is the data sampling rate for a pulse Doppler radar, must be high enough (10s of kHz) for representing the helicopter echo without aliasing (an unambiguous velocity of at least 500 m/s is necessary). Helicopter backscattering results from several reflectors including fuselage, main rotor blades, tail rotor, rotor hub, and reflections caused by the interaction & interference of these components etc.

B.1. Body (Fuselage, Skin)

Fuselage echo resembles that of a fixed-wing aircraft with radar cross-section (*RCS*) of a few square meters (Note that *RCS* changes with radar frequency and target orientation). Since rotary-wing targets have other components contributing to the echo signal, spectral width of their echoes are expected to be larger than those of fixed-wing targets. Fuselage echo may overlap with the spectrum of clutter in the case of hovering; otherwise, it has a Doppler frequency depending on radial velocity relative to the radar. The effect of undesired ground clutter is not present when the helicopter is not a hovering one.

B.2. Main Rotor

The main rotor consists of several blades rotating at a rate of 200 ~ 350 rpm. The rotation speed of the main rotor remains nearly constant during the flight and the maximum velocity of the tips of the main rotor blades varies only slightly between

different types of helicopters (blade end linear velocity is about 180 – 230 m/s). The approaching tip of the main rotor blade has the highest velocity component, whereas it is the opposite for the receding tip of the main rotor blade.

The echo of the periodically rotating blades of the main rotor consists of successive intense temporal flashes (caused when consecutive rotor blades are perpendicular to the direction of radar beam yielding the maximum RCS) with evenly distributed two-sided Doppler signature around the fuselage line (both amplitude and phase modulation are caused in radar echo). For even number of rotor blades, the spectrum will be symmetrical since the backscattered signals of coming and going blades will be simultaneous. For the odd number case with short integration times the spectrum is slightly asymmetrical. Flash duration depends on the length of the blades, rotor rate, and radar wavelength, while the flash interval depends on the rotor rate and the rotor blade number. Power reflected by the blades is typically less than 1% of the total reflected power.

At X-band 230m/s rotor tip speed results in approximately 15 kHz of Doppler shift, indicating a minimum PRF sampling rate of 30 kHz. Maximum forward flight speeds of helicopters are limited approximately to 100 m/s due to retreating blade stall. Consequently, maximum Doppler shift of an advancing blade tip of a helicopter in forward flight can increase up to 22 kHz necessitating a minimum radar PRF of 44 kHz.

Since echo components of main and tail rotors are distributed over a broad spectral range, for the cases when Doppler filter bank is employed, one may sometimes observe that output signals from majority of the individual filters (> 75%) are above the threshold. Neglecting those corresponding to the fuselage, outputs that are above the threshold exhibit very little amplitude spread indicating presence of a helicopter.

Rotor blade echo consisting of very short spikes is not very promising for a surveillance radar since it may go unnoticed as common time-on-target values are much smaller than spike repetition rate. In other words integration time long enough for registering two or more successive main rotor flashes is required. As a rule of thumb 100s of ms to a second of observation time is required to detect the rotor blade flashes successfully. Helicopter classification can be based on an estimate of the

quotient of the number of rotor blades and their length; however, this requires high SNR or Signal to Clutter Ratio (SCR).

B.3. Tail Rotor

The tail rotor has smaller diameter and higher rotation rate (50 – 110 rps). Its echo also consists of spikes, but the spikes are smaller and more frequent. The echo of the tail rotor remains often invisible because of being hidden by the fuselage. If horizontal polarization is used in transmission and reception, effect of modulation caused by the vertically rotating tail rotor can be neglected in the received signal.

B.4. Hub

Hub is the mechanical joint that serves many functions in addition to connecting the blades to the engine shaft: power transfer, blade attack angle steering, and damping of blade vibrations to name a few. The origin of the triangular shaped spectral area centered on the fuselage line component is the hub. At X-band it occupies a ±2 kHz bandwidth (considering 99% power). The RCS of the hub is in the range of 0.25 m^2, lower than the fuselage echo by 5 – 20 dB. Taking hub return power equal to one tenth of target skin return is a feasible approach. Since the RCS of the hub of a helicopter is very small, a technique based on using the echoes of hub is feasible for a helicopter target in close range which is actually what we are interested in. Hub detection is also suitable for the scenarios with relatively short time-on-target values (10s of ms). In fact spectral signature of the rotor hub has a higher probability of occurrence than the blade flash.

Analyzed portion of the signal should contain no spikes, namely, the rotor flashes, as it would interfere with the detection of a helicopter based on its hub spectrum.

In determining the radar echo strength the transmitted power is multiplied by the square of the radar antenna pattern for mechanically scanned antennas in the time domain. This is equivalent to convolution operation in the frequency domain which, therefore, widens the fuselage spectrum covering the weak hub echo. The use of further time windowing lowers the frequency resolution more. Taking into account the typical width of the hub spectrum for different wavelengths, the Fourier analysis

technique can only be used when time-on-target is sufficiently long (tens of milliseconds for an S-band radar), (frequency resolution=k/observation time=k/time-on-target, k is chosen depending on the window function used).

Extraction of the fuselage echo from the received signal makes hub detection easier, since with this operation hub could be detected in frequency domain as a spectral power density increase in the area around the fuselage Doppler frequency. Also at this step signal power test could also be sufficient. The same fuselage echo extraction procedure can also be applied for schemes utilizing blade flashes.

Comparison of ideal rotary-wing (helicopter) and fixed-wing target spectra is given in Figure 39 and Figure 40.

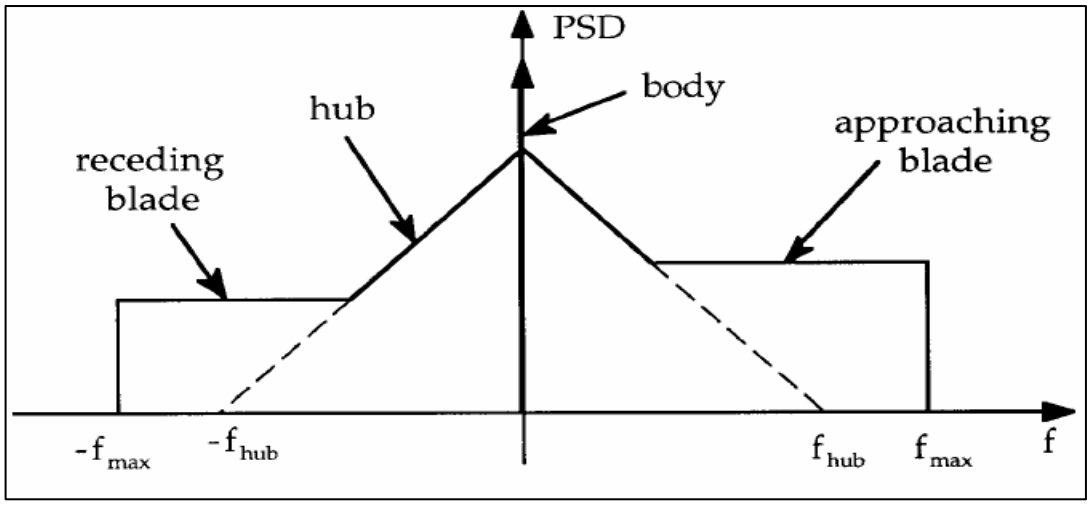

Figure 39 Helicopter spectrum (For the hovering or zero radial velocity case, $f_{body}=0$, otherwise $f_{body}\neq 0$)

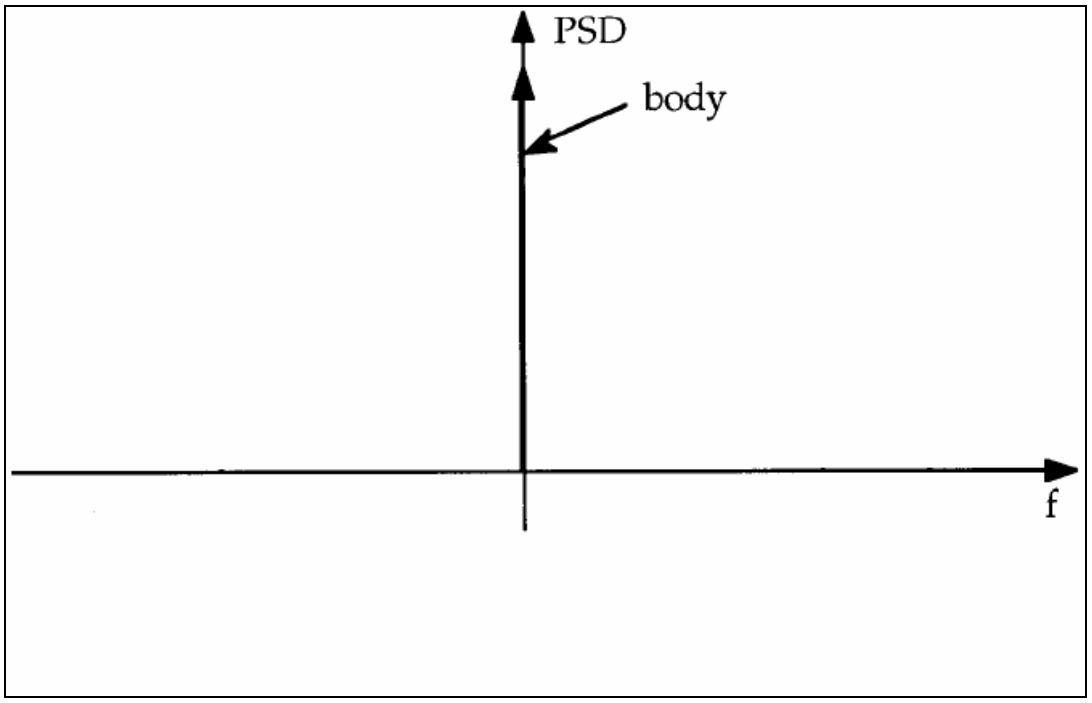

Figure 40 Fixed-wing spectrum (For targets with zero radial velocity $f_{body}=0$, otherwise $f_{body}\neq 0$)

B.5. Some of the Other Available Techniques

STAP scheme detection, time-frequency analysis, maximizing hub to remaining signal plus noise components power ratio, Neyman–Pearson criterion combined with principal vector usage approximation for detection based on hub and matched subspace approach to CFAR detection of hovering helicopters had been proposed in the literature. Time-frequency records, aspect angle analysis & distance profiles of helicopters and database comparisons could also be utilized for classification purposes.

Joint utilization of radar and infrared sensor is one of the feasible ways to get additional information from the target. However, one should keep in mind that information from various sensors differs in its reliability. Acoustic signal based helicopter signal extraction is also an alternative.

Besides the methods presented, it is discussed in the literature that basing the decision on multiple bursts may lower false target reports.